EERC Publication ER10-06

Iowa DOT Intelligent Compaction Research and Implementation – Phase I

November 2010

Final Report

EERC
EARTHWORKS ENGINEERING
RESEARCH CENTER





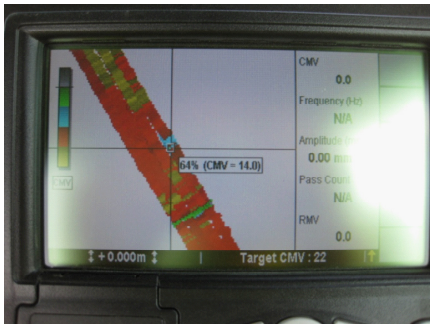

IOWA STATE UNIVERSITY
Institute for Transportation

Sponsored by
Iowa Department of Transportation
(InTrans Project 09-354)

About the EERC

The mission of the Earthworks Engineering Research Center at Iowa State University is to be the nation's premier institution for developing fundamental knowledge of earth mechanics, and creating innovative technologies, sensors, and systems to enable rapid, high quality, environmentally friendly, and economical construction of roadways, aviation runways, railroad embankments, dams, structural foundations, fortifications constructed from earth materials, and related geotechnical applications.

Iowa State University Disclaimer Notice

The contents of this report reflect the views of the authors, who are responsible for the facts and the accuracy of the information presented herein. The opinions, findings and conclusions expressed in this publication are those of the authors and not necessarily those of the sponsors.

The sponsors assume no liability for the contents or use of the information contained in this document. This report does not constitute a standard, specification, or regulation.

The sponsors do not endorse products or manufacturers. Trademarks or manufacturers' names appear in this report only because they are considered essential to the objective of the document.

Iowa State University Non-discrimination Statement

Iowa State University does not discriminate on the basis of race, color, age, religion, national origin, sexual orientation, gender identity, sex, marital status, disability, or status as a U.S. veteran. Inquiries can be directed to the Director of Equal Opportunity and Diversity, (515) 294-7612.

Iowa Department of Transportation Statements

Federal and state laws prohibit employment and/or public accommodation discrimination on the basis of age, color, creed, disability, gender identity, national origin, pregnancy, race, religion, sex, sexual orientation or veteran's status. If you believe you have been discriminated against, please contact the Iowa Civil Rights Commission at 800-457-4416 or Iowa Department of Transportation's affirmative action officer. If you need accommodations because of a disability to access the Iowa Department of Transportation's services, contact the agency's affirmative action officer at 800-262-0003.

The preparation of this (report, document, etc.) was financed in part through funds provided by the Iowa Department of Transportation through its "Agreement for the Management of Research Conducted by Iowa State University for the Iowa Department of Transportation," and its amendments.

The opinions, findings, and conclusions expressed in this publication are those of the authors and not necessarily those of the Iowa Department of Transportation.

Technical Report Documentation Page

1. Report No. ER10-06	2. Government Accession No.	3. Recipient's Catalog No.	
4. Title and Subtitle Iowa DOT Intelligent Compaction Research and Implementation – Phase I		5. Report Date November, 2010	
		6. Performing Organization Code	
7. Author(s) White, D.J., Vennapusa, P., Gieselman, H.		8. Performing Organization Report No.	
9. Performing Organization Name and Address Institute for Transportation Earthworks Engineering Research Center Iowa State University 2711 South Loop Drive, Suite 4700 Ames, IA 50010-8664		10. Work Unit No. (TRAIS)	
		11. Contract or Grant No.	
12. Sponsoring Organization Name and Address Iowa Department of Transportation Research and Technology Bureau 800 Lincoln Way Ames, Iowa 50010		13. Type of Report and Period Covered	
		14. Sponsoring Agency Code	
15. Supplementary Notes Visit www.eerc.iastate.edu for color PDF files of this and other research reports.			

16. Abstract

The Iowa Department of Transportation Intelligent Compaction Research and Implementation was initiated in summer 2009. Three field demonstration projects were conducted in Iowa as part of Phase I of this research program to evaluate three different IC measurement technologies: (1) machine drive power (MDP) measurement technology on Caterpillar CP56 padfoot roller, (2) continuous compaction value (CCV) technology on Sakai SW880 dual vibratory smooth drum asphalt roller, and (3) compaction meter value (CMV) technology on Volvo SD116DX smooth drum vibratory roller. The main objectives of the project include:

(1) evaluating the effectiveness of the IC measurement values (IC-MVs) in assessing the compaction quality of cohesive subgrade materials, granular base/subbase materials, and HMA materials,
(2) developing project specific correlations between IC-MVs and various conventionally used in-situ point measurements in earthwork quality control (QC) and quality assurance (QA) practice and HMA construction,
(3) evaluating the advantages of using the IC technology for production compaction operations,
(4) obtaining data to evaluate future IC specifications, and
(5) developing content for future educational and training materials for Iowa DOT and contractor personnel for effective implementation of the technology in to earthwork and HMA construction practice.

This research report presents results obtained from the three demonstration projects along with an overview of the different IC technologies and various QC/QA test methods. Statistical regression analysis was performed to evaluate correlations between IC-MVs and various in-situ test measurements (e.g., dry unit weight, moisture content, modulus, California bearing ratio, temperature (for HMA)). Comparatively, modulus was better correlated with IC-MVs compared to dry unit weight. Geostatistical analysis methods were used to assess "uniformity" of the spatially referenced IC measurements. Results from this study were used to develop special provision specifications as part of Phase II research program.

17. Key Words Intelligent compaction, quality control, quality assurance, specifications		18. Distribution Statement No restrictions.	
19. Security Classification (of this report) Unclassified.	20. Security Classification (of this page) Unclassified.	21. No. of Pages	22. Price NA

IOWA DOT INTELLIGENT COMPACTION RESEARCH AND IMPLEMENTATION – PHASE I

Final Report ER10-06

US30 Colo, IA — July 6 to 7, 2009
US218 Coralville, IA — August 21 to September 3, 2009
I29 Monona County, IA — August 31 to September 2, 2009 & September 10, 2009

Principal Investigator

David J. White, Ph.D.
Associate Professor and Director

Research Associates

Pavana KR. Vennapusa, Ph.D.
Research Assistant Professor

Heath Gieselman, M.S.
Assistant Scientist III

Earthworks Engineering Research Center (EERC)
Department of Civil Construction and Environmental Engineering
Iowa State University
2711 South Loop Drive, Suite 4600
Ames, IA 50010-8664
Phone: 515-294-7910

November 2010

TABLE OF CONTENTS

LIST OF FIGURES

LIST OF TABLES

ACKNOWLEDGMENTS

This study is funded by Iowa Department of Transportation. Caterpillar Inc., Sakai America, and Volvo, and Trimble provided support with IC rollers for the project. Sandra Larson, Mark Dunn, Ed Engle, and many others with Iowa DOT, and contractor personnel assisted with the coordination and execution of the field projects and participated in field demonstrations. All their assistance and interest is greatly appreciated. Bradley Fleming, Rachel Goldsmith, Stephen Quist, Luke Johanson, Alex Johnson, and Alexander Wolfe of Earthworks Engineering Research Center at Iowa State University provided support with field and laboratory testing along with the Iowa State University Geotechnical Mobile Lab. Their assistance and efforts are greatly appreciated.

LIST OF SYMBOLS

a	Theoretical vibration amplitude (eccentric moment divided by the drum mass)
A_{Ω}	Acceleration at fundamental frequency
$A_{X\Omega}$	Acceleration at X-order harmonic
A’	Machine acceleration
b	Machine internal loss coefficient used in MDP calculation
b_0	Intercept in a linear regression equation
b_1, b_2, b_3	Regression coefficients
C	Semivariogram scale
C_0	Semivariogram nugget
$C+C_0$	Semivariogram sill
CBR	California bearing ratio
CCV	Continuous compaction value
CMV	Compaction meter value
COV	Coefficient of variation (calculated as the ratio of mean and standard deviation)
DPI	Dynamic cone penetration index
d_0	Measured settlement under plate
D_{10}	Particle size corresponding to 10% passing
D_{30}	Particle size corresponding to 30% passing
D_{60}	Particle size corresponding to 60% passing
E	Elastic modulus
$E_{LWD\text{-}Z3}$	Elastic modulus determined from 300-mm plate Zorn light weight deflectometer
$E_{FWD\text{-}K3}$	Elastic modulus determined from 300-mm plate KUAB falling weight deflectometer
f	Vibration frequency
F	Shape factor
g	Acceleration of gravity
G_s	Specific gravity
GPS	Global positioning system
h	Separation distance
IC-MV	Intelligent compaction measurement value
LL	Liquid limit
m	Machine internal loss coefficient used in MDP calculation
MDP	Caterpillar Machine drive power
MDP_{40}	See description in text
n	Number of test measurements
p	Number of regression parameters
P_g	Gross power needed to move the machine
PL	Plastic limit
PI	Plasticity index
r	Radius of the plate
R	Semivariogram range
R’	Radius of the roller drum
R^2	Coefficient of determination
RMV	Resonant meter value

T	Temperature
T_{FWD}	Temperature measurements from the thermal camera mounted on the FWD
T_{TC}	Temperature measurements from the FLIR thermal camera
v	Roller velocity
w	Moisture content determined from Humboldt nuclear gauge
w_{opt}	Optimum moisture content
W	Roller weight
α	Slope angle (roller pitch from a sensor)
μ	Statistical mean
σ	Statistical standard deviation
σ_0	Applied stress
η	Poisson's ratio
γ_d	Dry unit weight determined from Humboldt nuclear gauge (NG)
γ_{dmax}	Maximum dry unit weight
$\gamma(h)$	Semivariogram

EXECUTIVE SUMMARY

The *Iowa Department of Transportation (DOT) Intelligent Compaction Research and Implementation* was initiated in summer 2009. Three field demonstration projects were conducted in Iowa as part of Phase I of this research program to evaluate three different IC measurement technologies: (1) machine drive power (MDP_{40}) measurement technology on Caterpillar CP56 padfoot roller, (2) continuous compaction value (CCV) technology on Sakai SW880 dual vibratory smooth drum asphalt roller, and (3) compaction meter value (CMV) technology on Volvo SD116DX smooth drum vibratory roller. Goals of the field demonstration projects are as follows:

1. Evaluate the effectiveness of the IC measurement values (IC-MVs) in assessing the compaction quality of cohesive subgrade materials, granular base/subbase materials, and HMA materials,
2. Develop project specific correlations between IC-MVs and various conventionally used in-situ point measurements (point-MVs) in earthwork quality control (QC) and quality assurance (QA) practice and HMA construction,
3. Evaluate the advantages of using the technology for production compaction operations,
4. Obtain data to evaluate future IC specifications,
5. Develop content for future educational and training materials for Iowa DOT and contractor personnel for effective implementation of the technology in to earthwork and HMA construction practice.

This report presents an overview of the three IC measurement technologies and various in-situ testing methods used in the field demonstration projects, and documents the results and analysis from each demonstration project. Statistical regression analysis was performed to evaluate correlations between IC-MVs and various in-situ test measurements (e.g., dry unit weight (γ_d), moisture content (w), light weight deflectometer modulus ($E_{LWD\text{-}Z3}$), falling weight deflectometer modulus ($E_{FWD\text{-}K3}$), California bearing ratio (CBR), temperature (for HMA)). Geostatistical analysis methods were used to assess "uniformity" of the spatially referenced IC measurements. Results from this study were used to develop special provision specifications as part of Phase II research program. The results and findings from this report should be of significant interest to the pavement, geotechnical, and construction engineering community and are anticipated to serve as a good knowledge base for implementation of IC technologies and various new in-situ QC/QA testing methods into earthwork and HMA construction practice.

Some significant findings from each demonstration project are as follows:

US30 Colo, Iowa – Cohesive Fill Compaction Demonstration Project

Caterpillar IC padfoot roller with MDP_{40} measurement system was used on this project. The project involved construction and testing on one calibration test strip, two spatial areas, and one production test bed with multiple lifts wherein IC-MVs and in-situ point-MVs were obtained. Data obtained from each test bed was analyzed separately to develop correlations. In the end, data obtained from all the test beds were combined to develop site wide correlations

over a wide measurement range. Following are some of the key findings from the analysis presented above.

- The moisture content of the subgrade materials was generally wet of optimum (about 5% wet of w_{opt}) and the relative compaction of the materials varied on average (per test bed) from 90% to 97% of standard Proctor γ_{dmax}. The material was in wet conditions due to frequent rain events at the time of project demonstration.
- MDP_{40} IC-MV compaction curves are affected by roller "off-tracking", i.e., roller operator not maintaining the same track as the previous pass.
- Spatial visualization of MDP_{40} IC-MV maps from multiple lifts in a production area (TB3) indicated that a "soft" zone with relatively low MDP_{40} values (< 70) on lift 1 reflected through the successive lifts 2, 3, 4, and 5 with similarly low MDP_{40} values in that zone. Geostatistical semivariogram analysis on MDP_{40} measurements on lifts 1 to 5 indicated that the variability reduced and the spatial continuity improved from lifts 1 to 5 as demonstrated by a decrease in the sill and an increase in the range values.
- Regression analysis results indicated better correlations between MDP_{40} and $E_{LWD\text{-}Z3}$ and CBR_{300} point-MVs compared to γ_d measurements. Combining data from all test beds, MDP_{40} vs. $E_{LWD\text{-}Z3}$ and CBR_{300} yielded a non-linear power relationship with $R^2 > 0.50$. MDP vs. γ_d did not yield a statistically significant relationship. MDP_{40} measurements were somewhat sensitive to moisture content (MDP_{40} decreased with increasing *w*). Correlation between MDP_{40} and *w* yielded a linear relationship with $R^2 = 0.20$.
- Multivariate non-linear regression analysis was performed to assess the influence of including a moisture content parameter in predicting MDP_{40} from $E_{LWD\text{-}Z3}$ measurements. This analysis showed $R^2 = 0.71$, which is a slight improvement over the simple regression model without the moisture content parameter ($R^2 = 0.63$). Similar analysis was performed to predict MDP_{40} from CBR_{300} measurements, but it did not show any improvement in the R^2 value. MDP-γ_d dataset combined with moisture content did not show a statistically significant relationship.

IA218 Coralville, Iowa – HMA Overlay Construction Demonstration Project

Sakai dual drum IC roller equipped with Sakai CCV IC-MV measurement system was used on this project. The project involved compaction of HMA overlay over the existing PCC layer. The Sakai IC roller was used for HMA break down rolling along with another Sakai conventional break down roller. Main objectives of testing and data analysis on this project were to: (1) evaluate the impact of using real-time pass coverage information to the roller operator on the uniformity of the pass coverage achieved during compaction; (2) develop correlations between CCV IC-MVs and asphalt density (RC) and modulus ($E_{FWD\text{-}K3}$) point-MVs; and (3) evaluate the influence of temperature measurements on the correlations. Objective (1) was achieved by conducting a blind study on day 1 where the IC monitoring system was switched on but the on-board monitor was closed for viewing by the operator, and by allowing the operator to use the on-board monitor on days 2 and 3 to aid in uniform pass coverage. Objective (2) was achieved by obtaining spatially referenced (with GPS measurements) RC and $E_{FWD\text{-}K3}$ point-MVs at 50 test locations and pairing them with spatially nearest CCV IC-MVs to develop correlations. Objective (3) was achieved by obtaining temperature measurements at each in-situ point-MV

location and conducting statistical analysis. Following are the key findings from the results and data analysis from this project:

- Univariate statistics (mean and standard deviation) of pass count information on each day did not reveal any differences between day 1 (blind study) and days 2 or 3. Geostatistical semivariogram analysis of pass count information revealed quantitative evidence of improved uniformity in pass coverage on day 3 compared to on day 1.
- The temperature of HMA on the shoulder lane was on average about 19^{o}F warmer than the temperature of the HMA on the mainline. The RC of the HMA layer was on average about 6% lower on the shoulder compared to the mainline. These differences in temperature and RC measurements are attributed to greater HMA layer thickness on the shoulder lane than on the mainline.
- $E_{FWD\text{-}K3}$ point-MVs and CCV IC-MVs obtained over a stretch of about 1.3 km showed that the measurements on the shoulder lane were lower than on the mainline. This is likely because of potentially weaker support conditions under the shoulder lane compared to the mainline.
- Correlation between CCV and $E_{FWD\text{-}K3}$ showed a relatively strong linear regression relationship with $R^2 = 0.8$ compared to correlation between CCV and RC with $R^2 = 0.4$. This should be expected as CCV is a result of drum response under loading which is a measure of material stiffness and not necessarily related to the density of the material. The regression relationships are influenced by differences in underlying support conditions as it was clearly reflected with data groupings (with separate groups for shoulder lane and mainline measurements) in the correlations. Data analysis indicated that the CCV, RC, and $E_{FWD\text{-}K3}$ measurements are influenced by temperature.

I-29 Monona County, Iowa – Pavement Foundation Layer Construction Demonstration Project

Experimental test results and field observations from a demonstration project conducted on I-29 in Monona County, using Volvo IC vibratory smooth drum roller equipped with CMV measurement system are presented above. The project involved construction of three calibration test beds and eight production area test beds. Data from calibration test beds was used to develop CMV and point-MV compaction curves and correlation analysis. Data obtained from the production areas were used to assess the influence of amplitude and underlying layer support conditions on the CMV measurements and the correlations between CMV and point-MVs. Multiple pass data obtained from the calibration test strips was used to assess the repeatability of the CMV IC-MVs. Following are some of the key findings from this project:

- Data from calibration strips indicated that the CMV, $E_{LWD\text{-}Z3}$, CBR, and γ_d measurements on the recycled HMA subbase layer were relatively higher than on the subgrade layer. The CMV and $E_{LWD\text{-}Z3}$ values on the RPCC base layer were relatively higher than on the subbase layer. The γ_d measurements were slightly lower on the RPCC base layer than on the recycled HMA subbase layer.
- The average CMV values did not change much with increasing pass number on the subgrade (varied from 2 to 3) and recycled HMA subbase layers (varied from 6 to 8), but showed a slight increase (from about 17 to 20) on the RPCC base layer.

- The average $E_{LWD\text{-}Z3}$ values on the subgrade and subbase layers increased from pass 0 to 2 and then remained constant up to the final compaction pass. The average $E_{LWD\text{-}Z3}$ on the base layer increased from pass 0 to 1, remained constant up to pass 4, and then increased up to pass 10. The average γ_d on all three layers increased from pass 0 to 1 and then generally remained at the same level up to the compaction pass.
- Correlations between CMV IC-MVs and point-MVs on calibration test strips generally showed weak correlations ($R^2 < 0.4$). Primary reason for such weak correlations is the narrow range over which the measurements were obtained in each calibration test strip. Correlations developed by combining data from multiple test beds yielded non-linear exponential relationships between CMV and $E_{LWD\text{-}Z3}$ with $R^2 = 0.66$ and 0.86 for low and high amplitude settings, respectively. Relatively weak regression relationships with $R^2 < 0.2$ was observed between CMV and CBR. No statistically significant relationship was found between CMV and γ_d.
- Comparison of CMV IC-MV production area maps with in-situ point MVs obtained at selected locations generally indicate that relatively low, medium, and high CMV locations match with relatively low, medium, and high $E_{LWD\text{-}Z3}$ point-MVs and in some cases with CBR point-MVs. CMV maps obtained on special backfill subbase and the overlaid RPCC base layers indicate that "soft" and "stiff" zones in the subbase layer maps are reflected on the RPCC base layer maps.
- CMV maps were able to effectively delineate "soft" and "stiff" zones effectively. This was verified in a case of subbase layer over a concrete box culvert where CMV and in-situ point-MVs ($E_{LWD\text{-}Z3}$, CBR, and γ_d) were all relatively higher compared to measurements along the edge of the culvert with "soft" conditions.
- CMV measurements on the subgrade, subbase, and base layers were on average about 1.1 to 1.5 times greater in high amplitude setting (i.e., $a = 2.00$ mm) than in low amplitude setting (i.e., $a = 1.50$ mm). This is likely due to potential differences in the magnitude of stresses applied on the materials by the roller drum under different amplitude settings (Vennapusa et al. 2010b).
- CMV measurement error was evaluated conducting a statistical repeatability analysis. The CMV measurement error was about ≤ 1.1 for low amplitude settings at a nominal operation speed of about 4 km/h.

CHAPTER 1: INTRODUCTION

Intelligent compaction (IC) or continuous compaction control (CCC) technologies with global position system (GPS) documentation offer 100 percent coverage information with real-time data visualization of compaction data, which is a significant improvement over traditional quality control/ assurance (QC/QA) procedures involving tests at discrete point locations. Several roller manufacturers have developed IC technologies applicable to earthwork and hot mix asphalt (HMA) materials. To date, results from research and demonstration projects have shown promise in application of the IC technologies for earthwork and asphalt construction, although results are somewhat limited. A few pilot specifications have been developed by state agencies in the U.S. (e.g., Mn/DOT 2007a, 2007b) and a few specifications exist from European countries (e.g., ZTVE-StB 1994, RVS 8S.02.6 1999, ATB Väg 2004, ISSMGE 2005). A review of these specifications (see White et al. 2008) indicated a weakness in that they are technology and material specific, and there are no widely accepted specifications in the U.S. Recent findings from three national level annual workshops organized by the Earthworks Engineering Research Center (EERC) and the Iowa Department of Transportation (DOT) (see White 2008, White and Vennapusa 2009, 2010) indicated the following major obstacles for successful implementation of the IC technologies: (a) lack of experience and proper education/training materials, (b) correlations on a wide-range of materials between IC values and traditionally used QC/QA testing tools, (c) poor database and documentation of existing data/case histories, (d) standard protocols for data analysis/management, and (e) standardized specifications inclusive of various IC technologies.

The *Iowa Department of Transportation Intelligent Compaction Research and Implementation* project was initiated in summer 2009 to make advancements in addressing the obstacles described above. The project is divided into three phases. Phase I of this research project involves conducting field demonstration projects with various IC measurement technologies on three projects with earthwork and HMA construction. Phase II of this research project involves evaluation of some pilot IC specifications on earthwork and HMA construction projects in Iowa. Phase III involves revision of pilot IC specifications and development of education and training materials for Iowa DOT.

Three demonstration projects were conducted in Iowa as part of Phase I to evaluate three different IC measurement technologies:

1. Machine drive power (MDP) measurement technology on Caterpillar CP56 padfoot roller — US30 cohesive embankment subgrade.
2. Continuous compaction value (CCV) technology on Sakai SW880 dual vibratory smooth drum asphalt roller — US218 HMA overlay.
3. Compaction meter value (CMV) technology on Volvo SD116DX smooth drum vibratory roller — I-29 pavement foundation layers.

The goals of the field demonstration projects were as follows:

1. Evaluate the effectiveness of the IC measurement values (IC-MVs) in assessing the compaction quality of cohesive subgrade, granular base/subbase, and HMA materials.

2. Develop project specific correlations between IC-MVs and various conventionally used in-situ point measurements (point-MVs) in earthwork quality control (QC) and quality assurance (QA) practice and HMA construction.
3. Evaluate the advantages of using the technology for production compaction operations,
4. Obtain data to evaluate future IC specifications.
5. Develop content for future educational and training materials for Iowa DOT and contractor personnel for effective implementation of the technology in to earthwork and HMA construction practice.

This report presents a brief overview of the three IC measurement technologies (i.e., MDP, CCV, and CMV) and various in-situ testing methods used in the field demonstration projects, and documents the results and analysis from each demonstration project. Information from this report can be utilized for developing future education and training materials. Statistical regression analysis was performed to evaluate correlations between IC-MV and various in-situ test measurements (e.g., dry unit weight, moisture content, modulus, California bearing ratio (CBR), temperature (only for HMA)). Dry unit weight and moisture content measurements were obtained using nuclear gauge, modulus measurements were obtained using Zorn light weight deflectometer (LWD) and Kuab falling weight deflectometer (FWD), CBR was determined using dynamic cone penetrometer (DCP), temperature of HMA was measured using a hand-held thermal imaging camera and an infrared sensor mounted on the FWD. Geostatistical semivariogram analysis was performed on spatially referenced IC-MVs to assess the spatial nature of the measurements and quantify "non-uniformity" of compacted fill materials.

CHAPTER 2: OVERVIEW OF INTELLIGENT COMPACTION TECHNOLOGIES

Three IC rollers were used as part of the field demonstration projects. A Caterpillar CP56 padfoot roller equipped with Caterpillar's machine drive power (MDP) measurement system was used on the US30 project. A Volvo SD116DX vibratory smooth drum roller equipped with Trimble's compaction meter value (CMV) measurement system was used on the I-29 project. A Sakai SW880 dual drum vibratory smooth drum asphalt roller equipped with Sakai compaction control value (CCV) was used for break down rolling on the US218 project. A digital display unit employing proprietary software is mounted on each of these rollers for on-board visualization of roller position, IC-MVs, pass coverage information, amplitude/frequency settings, speed, etc. Some key features of these IC rollers are summarized in Table 1. Pictures of the IC rollers and on-board display units on each of these rollers are provided in Figure 1. A brief description of the IC-MVs is provided in the following discussion.

Table 1. Key features of the IC rollers used on the project

Feature	Caterpillar CP56	Sakai SW880	Volvo SD116DX
Drum Type	Padfoot	Dual smooth drum	Smooth drum
Frequency (f)	30 Hz	42, 50, and 67 Hz	34 Hz (low amp setting) 30 Hz (high amp setting)
Amplitude (a) Settings	Static, 0.90 mm (low), and 1.80 mm (high)	0.30 mm (low), 0.60 mm (high)	1.45 mm (low), 1.85 mm (high)
IC-MV	MDP_{40} (shown as CCV in the output)	CCV	CMV, RMV
Display Software	AccuGrade™	Aithon MT-R™	Trimble® CB430/ Sitevision ™ office
Output Documentation	Date/Time, Location (Northing/Easting/ Elevation of left and right ends of the roller drum), Speed, CCV, Frequency, Amplitude (theoretical), Direction (forward/ backward), Vibration (On/Off)	Date/Time, Location (Northing/Easting/ Elevation), CCV, Temperature, Frequency, Direction (forward/backward), Vibration (On/Off), GPS Quality	Date/Time, Location (Northing/Easting/ Elevation of left and right ends of the roller drum), Speed, CMV, RMV, Frequency, Amplitude (theoretical), Direction (forward/ backward), Vibration (On/Off)
Automatic Feedback Control (AFC)[a]	No	No	No

[a]AFC mode involves automatic adjustment of vibration amplitude and/or frequency during compaction.

Figure 1. Caterpillar CP56 (top) padfoot roller with onboard AccuGrade display unit used on US30 project, Sakai SW880 (middle) dual smooth drum roller with onboard Aithon MT display unit used on US218 project, and Volvo SD116DX (bottom) roller with onboard Trimble CB430 display unit used on I29 project

Machine Drive Power (MDP) Value

Machine drive power (MDP) technology relates mechanical performance of the roller during compaction to the properties of the compacted soil. Detailed background information on the MDP system is provided by White et al. (2005). MDP is calculated using Eq. 1.

$$MDP = P_g - Wv\left(\mathrm{Sin}\alpha + \frac{A'}{g}\right) - (mv + b) \quad (1)$$

where MDP = machine drive power (kJ/s), P_g = gross power needed to move the machine (kJ/s), W = roller weight (kN), A' = machine acceleration (m/s^2), g = acceleration of gravity (m/s^2), α = slope angle (roller pitch from a sensor), v = roller velocity (m/s), and m (kJ/m) and b (kJ/s) = machine internal loss coefficients specific to a particular machine (White et al. 2005). MDP is a relative value referencing the material properties of the calibration surface, which is generally a hard compacted surface (MDP = 0 kJ/s). Positive MDP values therefore indicate material that is less compact than the calibration surface, while negative MDP values indicate material that is more compacted than the calibration surface (i.e. less roller drum sinkage). The MDP values obtained from the machine were recalculated to range between 1 and 150 using Eq. 2 (referred to as MDP_{40}). The calibration surface with MDP = 0 kJ/s was scaled to MDP_{40} = 150 and a soft surface with MDP = 54.23 kJ/s (40000 lb-ft/s) was scaled to MDP_{40} = 1.

$$MDP_{40} = 150 - 2.75(MDP) \quad (2)$$

Compaction Meter Value (CMV) and Resonant Meter Value (RMV)

CMV is a dimensionless compaction parameter developed by Geodynamik that depends on roller dimensions, (i.e., drum diameter and weight) and roller operation parameters (e.g., frequency, amplitude, speed), and is determined using the dynamic roller response (Sandström 1994). The concept of development of different harmonic components of drum vibration with increasing ground stiffness is illustrated in Figure 2. It is calculated using Eq. 3, where C is a constant (300), $A_{2\Omega}$ = the acceleration of the first harmonic component of the vibration, A_{Ω} = the acceleration of the fundamental component of the vibration (Sandström and Pettersson 2004). Correlation studies relating CMV to soil dry unit weight, strength, and stiffness are documented in the literature (e.g., Floss et al. 1983, Samaras et al. 1991, Brandl and Adam 1997, Thompson and White 2008, White and Thompson 2008).

$$CMV = C \cdot \frac{A_{2\Omega}}{A_{\Omega}} \quad (3)$$

RMV provides an indication of the drum behavior (e.g. continuous contact, partial uplift, double jump, rocking motion, and chaotic motion) and is calculated using Eq. 4, where $A_{0.5\Omega}$ = subharmonic acceleration amplitude caused by jumping (the drum skips every other cycle). It is important to note that the drum behavior affects the CMV measurements (Brandl and Adam

1997) and therefore must be interpreted in conjunction with the RMV measurements (Vennapusa et al. 2010a). More discussion on effect of drum behavior on CMV measurements is provided later in this report.

$$RMV = C \cdot \frac{A_{0.5\Omega}}{A_{\Omega}} \tag{4}$$

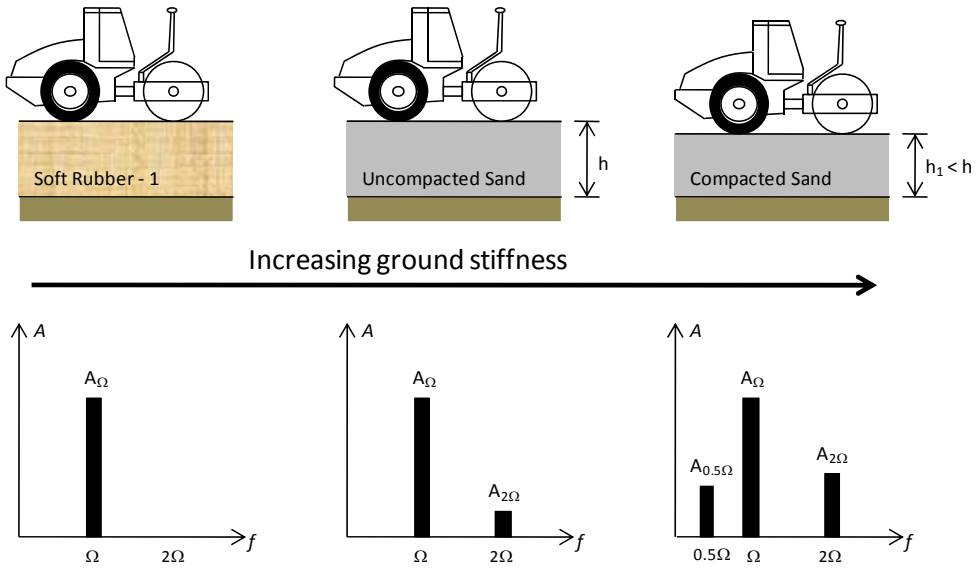

Figure 2. Illustration of changes in drum harmonics with increasing ground stiffness (modified from Thurner and Sandström 1980)

Roller-Integrated Compaction Control Value (CCV)

Sakai *Compaction Control Value* (CCV) is a vibratory-based technology which makes use of an accelerometer mounted to the roller drum to create a record of machine-ground interaction with the aid of GPS. Research conducted by Sakai (Scherocman et al. 2007) found that as the ground stiffness increases and the roller drum starts to enter into a "jumping" motion, vibration accelerations at various frequency components are developed as illustrated in Figure 3.

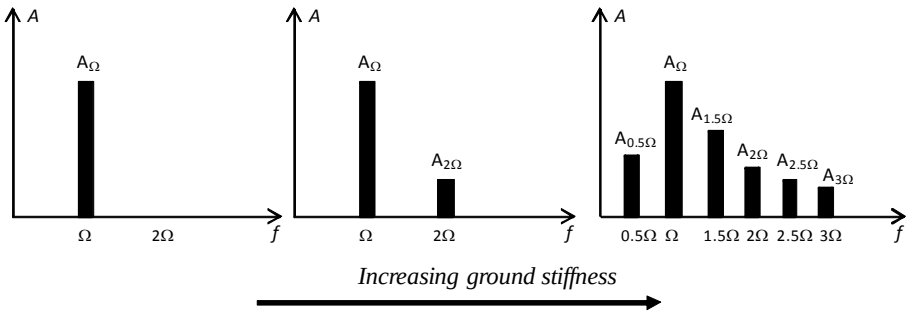

Figure 3. Changes in amplitude spectrum with increasing ground stiffness (modified from Scherocman et al. 2007)

The CCV is calculated using the acceleration data from first subharmonic (0.5Ω), fundamental (Ω), and higher-order harmonics (1.5Ω, 2Ω, 2.5Ω, 3Ω) as presented in Eq. 5.

$$CCV = \left[\frac{A_{0.5\Omega} + A_{1.5\Omega} + A_{2\Omega} + A_{2.5\Omega} + A_{3\Omega}}{A_{0.5\Omega} + A_{\Omega}} \right] \times 100 \quad (5)$$

The vibration acceleration signal from the accelerometer is transformed through the Fast Fourier Transform (FFT) method and then filtered through band pass filters to detect the acceleration amplitude spectrum (Scherocman et al. 2007). CCV measurements on the SW880 model are made using the accelerometer mounted on the front drum of the roller.

CHAPTER 3: EXPERIMENTAL TESTING METHODS

In-situ Testing Methods

Five different in-situ testing methods were used in this research study to evaluate the in-situ soil and asphalt compaction properties (Figure 4): (a) calibrated Humboldt nuclear gauge (NG); (b) dynamic cone penetrometer (DCP); (c) Zorn light weight deflectometer (LWD) setup with 300 mm plate diameter; (d) KUAB falling weight deflectometer (FWD) setup with 300 mm diameter four-segmented plate, and (e) FLIR thermal camera to measure temperature. Brief descriptions of these test devices/methods are provided below.

Nuclear Moisture-Density Gauge

A calibrated nuclear moisture-density gauge (NG) device was used on all three projects. The device was used to provide rapid measurements of soil dry unit weight (γ_d) and moisture content (w) for cohesive and granular materials, and total density and estimates of binder content for HMA. For tests performed on subgrade, subbase, and base materials, a flat surface was prepared in accordance with ASTM D6938-10 "Standard Test Method for In-Place Density and Water Content of Soil and Soil-Aggregate by Nuclear Methods (Shallow Depth)". Generally, two measurements of moisture and dry unit weight were obtained at a particular location and an average of the two measurements is reported. Measurements were obtained by inserting the measuring probe penetration depths to depth equal to the compaction layer thickness or 300 mm, whichever is greater.

For testing on HMA surface, silica sand was spread on the surface to fill surface voids and the measurements were obtained using back scattering method (Humboldt 2006).

Light Weight Deflectometer

LWD testing was performed following manufacturer recommendations (Zorn 2003) and the $E_{LWD\text{-}Z3}$ values were determined using Eq. 6, where E = elastic modulus (MPa), d_0 = measured settlement (mm), η = Poisson's ratio, σ_0 = applied stress (MPa), r = radius of the plate (mm), F = shape factor depending on stress distribution (assumed as 8/3 for subbase and base materials and $\pi/2$ for subgrade materials; see Vennapusa and White 2009).

$$E = \frac{(1-\eta^2)\sigma_0 r}{d_0} \times F \tag{6}$$

Falling Weight Deflectometer

FWD testing was performed by applying one seating drop using a nominal applied contact stress of about 390 kPa followed by three test drops each at a nominal applied contact stress of about 390 kPa, 590 kPa and 800 kPa. The actual applied force was recorded using a load cell. A composite modulus value ($E_{FWD\text{-}K3}$) was calculated using measured deflection at the center of the plate using Eq. 6. Shape factor F = 2 was assumed in the calculations as the plate used for testing was a segmented plate (assumed to produce uniform contact stress distribution).

Dynamic Cone Penetrometer

DCP tests were performed to determine dynamic cone penetration index (DPI) and calculate CBR in accordance with ASTM D6951-03 "Standard Test Method for Use of the Dynamic Cone Penetrometer in Shallow Pavement Applications" using Eqs. 7 and 8. The DCP test results are presented in this report as CBR point values or CBR depth profiles. When the data is presented as point values, the data represents a weighted average CBR of the compaction layer depth or depth indicated in the subscript (e.g., CBR_{300} indicates weighted average CBR to a depth of 300 mm and CBR indicates weighted average CBR to the depth equal to the thickness of the compaction layer).

$$CBR = \frac{292}{DPI^{1.12}} \quad \text{for all soils except CL soils with CBR} < 10 \tag{7}$$

$$CBR = \frac{1}{(0.017019 \cdot DCP)^2} \quad \text{for CL soils with CBR} < 10 \tag{8}$$

Figure 4. In-situ testing methods used on the project: (a) Humboldt nuclear gauge, (b) dynamic cone penetrometer, (c) Zorn light weight deflectometer, (d) KUAB falling weight deflectometer, (e) FLIR thermal imaging camera

Weather Data

The Iowa State University Geotechnical mobile laboratory (Figure 5) is equipped with Davis Vantage Pro weather station with a Weatherlink datalogger system. Weather data was monitored on US30 project by recording air temperature, wind speed, and rain fall every 30 minutes by the datalogger.

Figure 5. Iowa state university geotechnical mobile laboratory

Laboratory Testing Methods

ASTM standard test methods followed in determining the soil index properties for materials obtained from US30 and I-29 projects are as follows.

- Particle size analysis – ASTM D422-63 "Standard Test Methods for Particle-Size Analysis of Soils".
- Atterberg limits – ASTM D4318-05 "Standard Test Methods for Liquid Limit, Plastic Limit, and Plasticity Index of Soils".
- Soil classification according to USCS – ASTM D2487-00 "Standard Practice for Classification of Soils for Engineering Purposes (Unified Soil Classification System)".
- Soil classification according to AASHTO system – ASTM D3282-09 "Standard Practice for Classification of Soils and Soil-Aggregate Mixtures for Highway Construction Purposes"
- Standard Proctor testing – ASMT D698-07e1 "Standard Test Methods for Laboratory Compaction Characteristics of Soil Using Standard Effort (12 400 ft-lbf/ft^3 (600 kN-m/m^3))".
- Modified Proctor testing – ASTM D1557-02 "Standard Test Methods for Laboratory Compaction Characteristics of Soil Using Modified Effort (56,000 ft-lbf/ft^3 (2,700 kN-m/m^3))".
- Relative density testing – ASTM D4523-00 "Standard Test Methods for Maximum Index Density and Unit Weight of Soils Using a Vibratory Table" and ASTM D4254 "Standard Test Methods for Minimum Index Density and Unit Weight of Soils and Calculation of Relative Density".

CHAPTER 4: DATA ANALYSIS METHODS

Simple linear and non-linear regression analysis was performed to develop correlations between IC-MVs and in-situ point-MVs. Geostatistical semivariogram analysis was performed on spatially referenced IC-MVs to assess the spatial nature of the measurements and quantify "uniformity" of compacted fill materials. A brief overview of these analysis methods is provided below.

Regression Analysis

Simple regression relationships between IC-MVs and in-situ point-MVs were developed by spatially pairing the data obtained from the test beds. The analysis was performed by considering point-MVs as "true" independent variables and IC-MVs as dependent variables using the models shown in Eqs. 9 to 11, where b_0 = intercept and b_1 = regression parameter.

$$\text{Linear model: } IC\text{–}MV = b_0 + b_1 \cdot Point\,MV \tag{9}$$

$$\text{Non-linear power model: } IC\text{–}MV = b_0 \cdot (Point\,MV)^{b_1} \tag{10}$$

$$\text{Non-linear exponential model: } IC\text{–}MV = e^{(b_1 * Point\,MV)} \tag{11}$$

Statistical significance of the independent variable was assessed based on *p*- and *t*-values. The selected criteria for identifying the significance of a parameter included: *p*-value < 0.05 = significant, < 0.10 = possibly significant, > 0.10 = not significant, and *t*-value < -2 or > +2 = significant. The best fit model is determined based on the strength of the regression relationships assessed by the coefficient of determination (i.e., R^2) values.

Geostatistical Analysis

Vennapusa et al. (2010a) demonstrated the use of geostatistical semivariogram analysis in combination with conventional statistical analysis to evaluate non-uniformity in QC/QA during earthwork construction using spatially referenced IC-MVs. A semivariogram is a plot of the average squared differences between data values as a function of separation distance, and is a common tool used in geostatistical studies to describe spatial variation. A typical semivariogram plot is presented in Figure 6. The semivariogram $\gamma(h)$ is defined as one-half of the average squared differences between data values that are separated at a distance *h* (Isaaks and Srivastava 1989). If this calculation is repeated for many different values of *h* (as the sample data will support) the result can be graphically presented as experimental semivariogram shown as circles in Figure 6. More details on experimental semivariogram calculation procedure are available elsewhere in the literature (e.g., Clark and Harper 2002, Isaaks and Srivastava 1989).

To obtain an algebraic expression for the relationship between separation distance and experimental semivariogram, a theoretical model is fit to the data. Some commonly used models include linear, spherical, exponential, and Gaussian models. A spherical model was used for data analysis in this report. Arithmetic expression of the spherical model and the spherical variogram are shown in Figure 6. Three parameters are used to construct a theoretical semivariogram: sill ($C+C_0$), range (R), and nugget (C_0). These parameters are briefly described in Figure 6. More discussion on the theoretical models can be found elsewhere in the literature

(e.g., Clark and Harper 2002, Isaaks and Srivastava 1989). For the results presented in this section, the sill, range, and nugget values during theoretical model fitting were determined by checking the models for "goodness" using the modified Cressie goodness fit method (see Clark and Harper 2002) and cross-validation process (see Isaaks and Srivastava 1989). From a theoretical semivariogram model, a low "sill" and longer "range of influence" represent best conditions for uniformity, while the opposite represents an increasingly non-uniform condition.

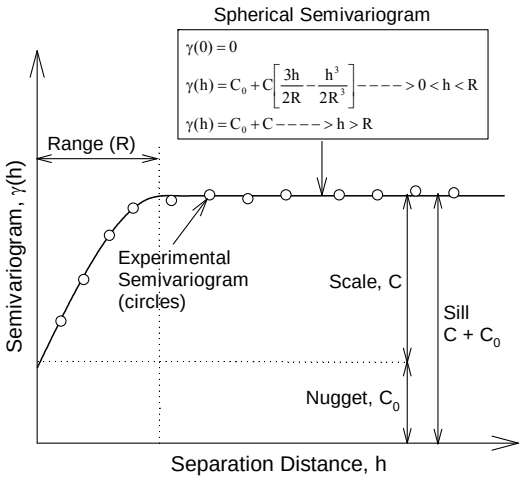

Range, R: As the separation distance between pairs increase, the corresponding semivariogram value will also generally increase. Eventually, however, an increase in the distance no longer causes a corresponding increase in the semivariogram, i.e., where the semivariogram reaches a plateau. The distance at which the semivariogram reaches this plateau is called as range. Longer range values suggest greater spatial continuity or relatively larger (more spatially coherent) "hot spots".

Sill, $C+C_0$: The plateau that the semivariogram reaches at the range is called the sill. A semivariogram generally has a sill that is approximately equal to the variance of the data.

Nugget, C_0: Though the value of the semivariogram at h = 0 is strictly zero several factors, such as sampling error and very short scale variability, may cause sample values separated by extremely short distances to be quite dissimilar. This causes a discontinuity at the origin of the semivariogram and is described as nugget effect. (Isaaks and Srivastava, 1989)

Figure 6. Description of a typical experimental and spherical semivariogram and its parameters

CHAPTER 5: DEMONSTRATION PROJECT 1 — US30 COLO, IOWA

Project Description

This project was about 6.8 miles long and was located on US30 between Colo and State Center, Iowa (Sta. 2506+50 to 2889+00; Iowa DOT project number NHSX-30-5(209)--3H-85). The project location map is shown in Figure 7. It involved adding two lanes to the existing highway to make it a four-lane divided highway. Grading work typically included construction of embankment and subgrade layers with "select clay" subgrade treatment in the top 0.76 m (2.5 ft) of the final subgrade elevation. Soil survey sheets in the project plans indicate the soils on-site consist of dark clays at the surface underlain sandy to silty clay soils derived from glacial deposits. Fill materials were obtained from on-site borrow and cut areas along the project alignment. Project specifications require that the moisture content of the material be within ± 2% of standard Proctor optimum moisture content.

The ISU research team was present on the project site from July 5 to July 8, 2009. Four test beds were constructed and tested during this period. No testing was conducted on July 8th due to heavy rainfall on July 7th night (Figure 8). Compaction on the test beds was mostly achieved using CP56 padfoot IC roller equipped with MDP_{40} IC-MV measurement system. Compaction was also achieved using pull behind sheepsfoot rollers in some areas. In-situ LWD, DCP, and NG tests were conducted on the test beds to develop correlations with MDP_{40} measurements. The materials on-site were generally wet due to frequent rain at the time of construction.

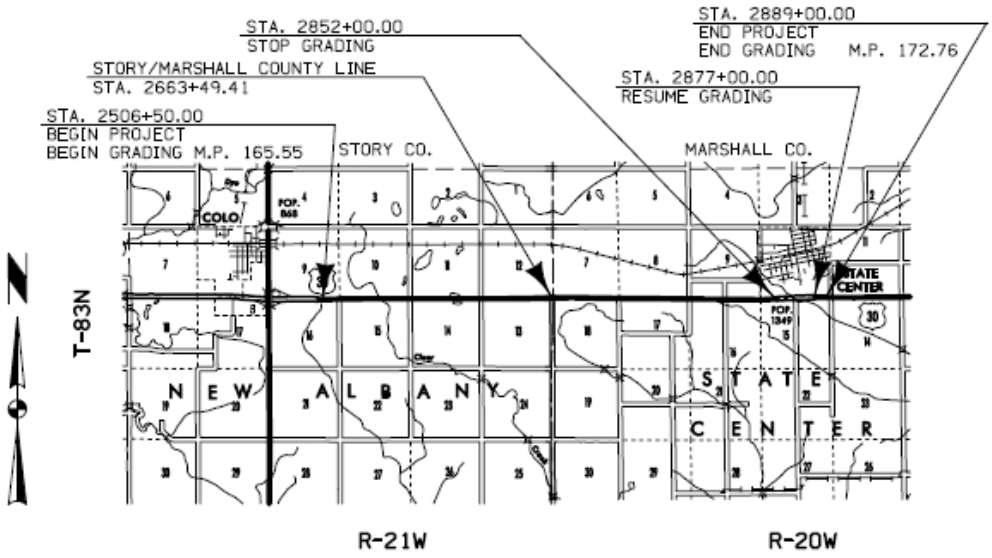

Figure 7. Project location map – US30 demonstration project

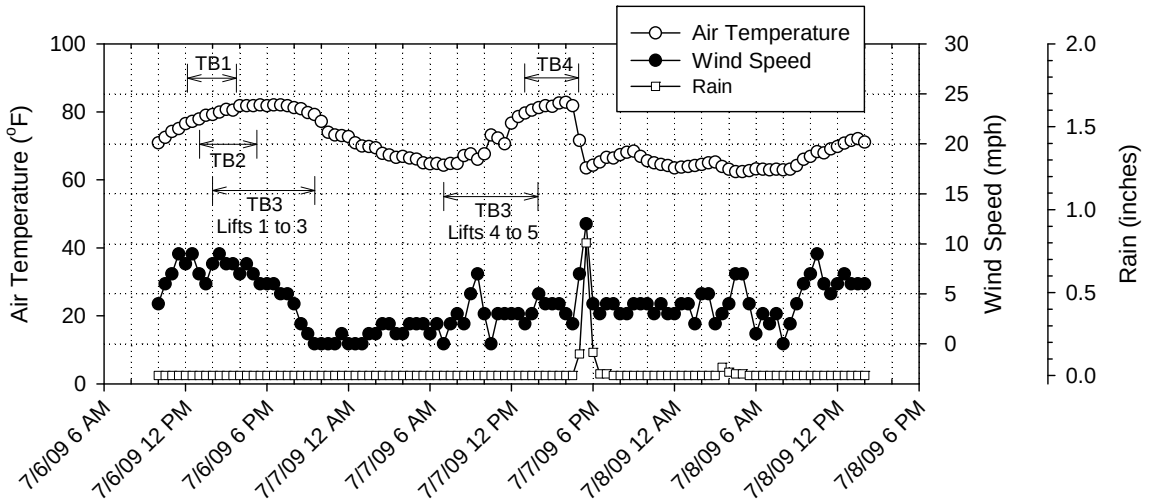

Figure 8. Air temperature, wind speed, and rain fall data on US30 project

Experimental Testing

Four test beds were constructed as part of the field investigation. Approximate location of test beds are shown in Figure 9. A summary of test bed conditions, number of roller passes using the IC roller, and in-situ test measurements obtained is provided in Table 2. Test bed (TB) 1 involved compaction of a one-dimensional test strip using eight roller passes and obtaining in-situ point-MVs. TBs 2 and 4 consisted of mapping a spatial area and obtaining in-situ point-MVs at locations selected based on the on-board IC-MV display map. Test bed 3 consisted of compaction of five lifts of fill material in 6 to 11 roller lanes, and obtaining in-situ point-MVs on each lift.

A summary of soil index properties of the two fill materials obtained from the project is presented in Table 3. Figure 10 and Figure 11 presents laboratory standard Proctor test results for the fill materials in comparison with in-situ moisture (w) and dry unit weight (γ_d) measurements obtained from TBs 1 and 4, and TBs 2 and 3, respectively. In-situ w -γ_d measurements indicate that the materials were generally wet of standard Proctor optimum moisture content (w_{opt}) in all test beds. The average in-situ w of the TBs 1 and 4 material was about 17.8% (i.e., 5.4% wet of w_{opt}) and the average relative compaction (RC) of the material was about 95% of the standard Proctor γ_{dmax}. The average in-situ w of the TBs 2 and 3 material was about 17.4% (i.e., 4.4% wet of w_{opt}) and the average relative compaction (RC) of the material was about 94% of the standard Proctor γ_{dmax}. Photographs of subgrade and embankment construction operations are provided in Figure 12.

Correlations between MDP_{40} IC-MVs and in-situ point-MVs were developed for each test bed by matching the GPS referenced in-situ point-MV locations with the spatially nearest GPS referenced IC-MVs. Roller GPS measurements on test beds 1, 2, and 3 (lift 1) were apparently recorded in a wrong data transformation setting (GPS northing values are recorded as negative). Due to this error, in-situ point-MV locations on those test beds could not be directly matched

with the IC-MVs. As an alternate, the point-MV locations were approximated using reference points taken along the edge of the test beds to identify the spatially nearest IC-MV.

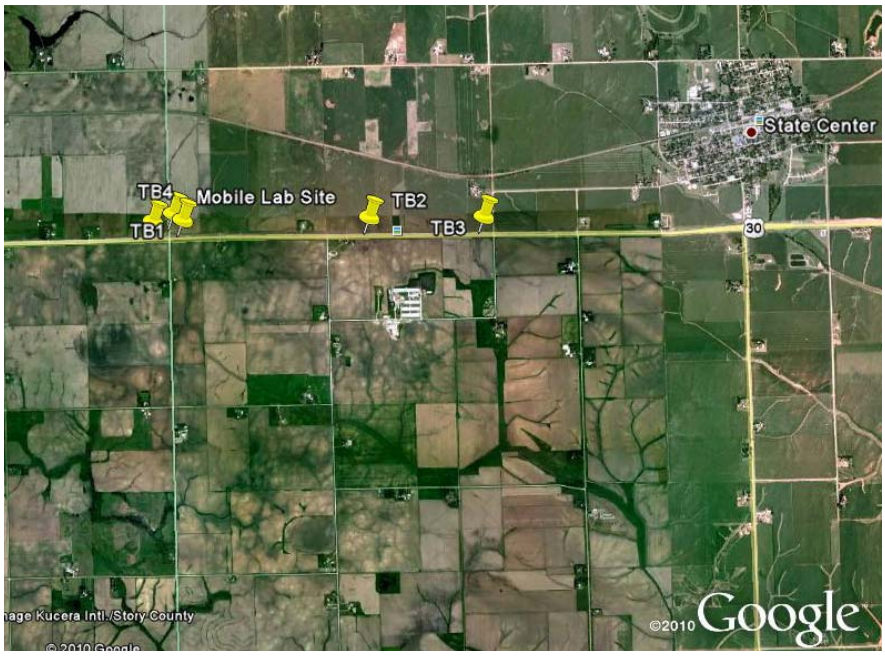

Figure 9. Approximate location of test beds – US30 project

Table 2. Summary of test beds and in-situ testing – US30 project

TB	Approx. Location	Date	Lift	Pass*	In-situ Point-MVs	Comments
1	Near Sta. 2685	07/06	—	1-8	CBR, $E_{LWD\text{-}Z3}$, w, and γ_d after pass 8	Test strip compacted using eight roller passes in one roller lane.
2	Between Sta. 2750 and 2760	07/06	—	1-2**	CBR, $E_{LWD\text{-}Z3}$, w, and γ_d after pass 2	Spatial area mapped in eight roller lanes followed by in-situ testing.
3	Between Sta. 2775 and 2780	07/06 to 07/07	1 2 3 4 5	1 (Map)** 1-12 1-10 1-4** 1-4**	CBR, $E_{LWD\text{-}Z3}$, w, and γ_d after mapping	Spatial area maps obtained on lifts 1 to 5 placed on existing subgrade. Each lift compacted in 6 to 11 roller lanes followed by in-situ testing after final pass on each lift.
4	Between Sta. 2673 and 2683 (west of Story/Marshall county line)	07/07	1	1-2**	CBR, $E_{LWD\text{-}Z3}$, w, and γ_d after pass 2	Spatial area mapped in three roller lanes followed by in-situ testing

*all compaction passes were made in static mode at 6 km/h nominal speed.
**compaction was achieved using Contractor's pull behind sheepsfoot roller prior to IC roller passes.

Table 3. Summary of soil index properties – US30 project

Parameter	TBs 1 and 4 Subgrade Material	TBs 2 and 3 Subgrade Material
Standard Proctor Test Results		
γ_{dmax} (kN/m^3)	18.60	18.47
γ_{dmax} (pcf)	118.4	117.6
w_{opt}	12.4	13.0
Gravel Content (%) (> 4.75mm)	2	2
Sand Content (%) (4.75mm – 75μm)	50	41
Silt Content (%) (75μm – 2μm)	35	45
Clay Content (%) (< 2μm)	13	12
Liquid Limit, LL (%)	22	25
Plastic Limit, PL (%)	12	19
Plasticity Index, PI (%)	10	6
AASHTO Classification	A-4	A-4
USCS Classification	SC	CL-ML
Specific Gravity, G_s (Assumed)	2.70	2.70

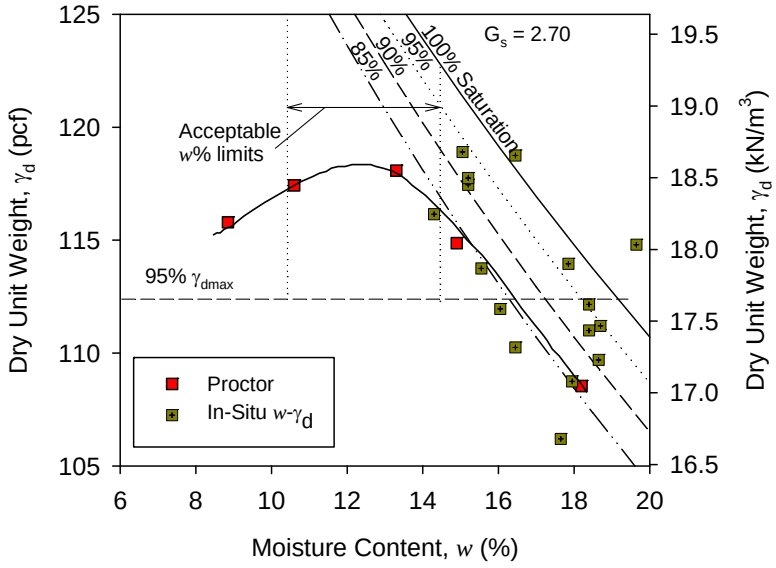

Figure 10. In-situ moisture-density measurements in comparison with laboratory standard Proctor test data – US30 TBs 1 and 4 subgrade material

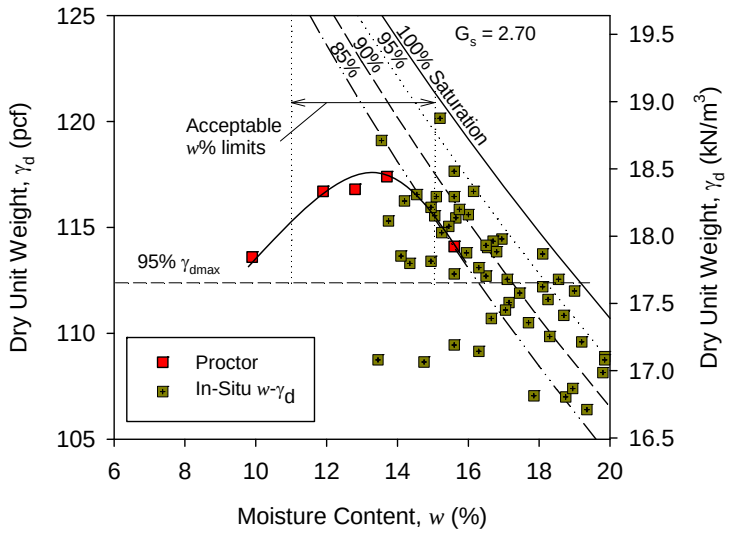

Figure 11. In-situ moisture-density measurements in comparison with laboratory standard Proctor test data – US30 TBs 2 and 3 subgrade material

Figure 12. Photographs of in-situ soil conditions, construction operations, and in-situ testing

In-Situ Test Results

Test Bed 1 – Calibration Test Strip

TB1 involved obtaining MDP_{40} measurements over a 50 m long one-dimensional test strip for nine roller passes. In-situ point-MVs ($E_{LWD\text{-}Z3}$, γ_d, w, CBR) were obtained after nine roller passes at seven test locations. Compaction was performed by operating the roller in forward and reverse gears in static mode at a nominal velocity of about 6 km/h.

Average MDP_{40} (averaged per pass) with increasing pass is shown in Figure 13. The average MDP_{40} values did not show a consistent trend with increasing pass due to roller "off-tracking" during compaction operation as illustrated in Figure 14. Off-tracking refers to roller operator not maintaining a consistent travel path during each pass. A similar case where IC-MV compaction curves were affected by roller "off-tracking" was documented in a field study by Newman and White (2008). MDP_{40} plots in comparison with in-situ point-MVs after pass 9 are provided in Figure 15. DCP-CBR profiles at each point location are shown in Figure 16. A summary of MDP_{40} and in-situ point-MV statistics (mean (μ), standard deviation (σ), and coefficient of variation (COV)) are presented in Table 4. The average w of the material was about 17.7% (i.e., 5.3% wet of w_{opt}) and the average RC of the material was about 93% of the standard Proctor γ_{dmax}. Regression analysis between MDP_{40} measurements and in-situ point-MVs is presented in Figure 17. Correlation analysis between $E_{LWD\text{-}Z3}$ and MDP_{40} yielded a strong linear relationship with $R^2 = 0.95$. Relationships between MDP_{40} and other point-MVs yielded relatively weak correlations with $R^2 \leq 0.1$.

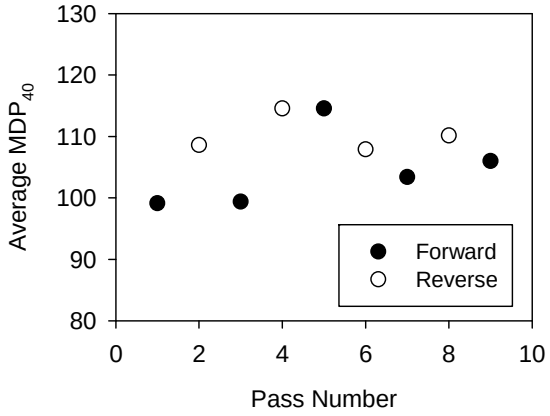

Figure 13. MDP_{40} compaction growth with increasing pass – TB1

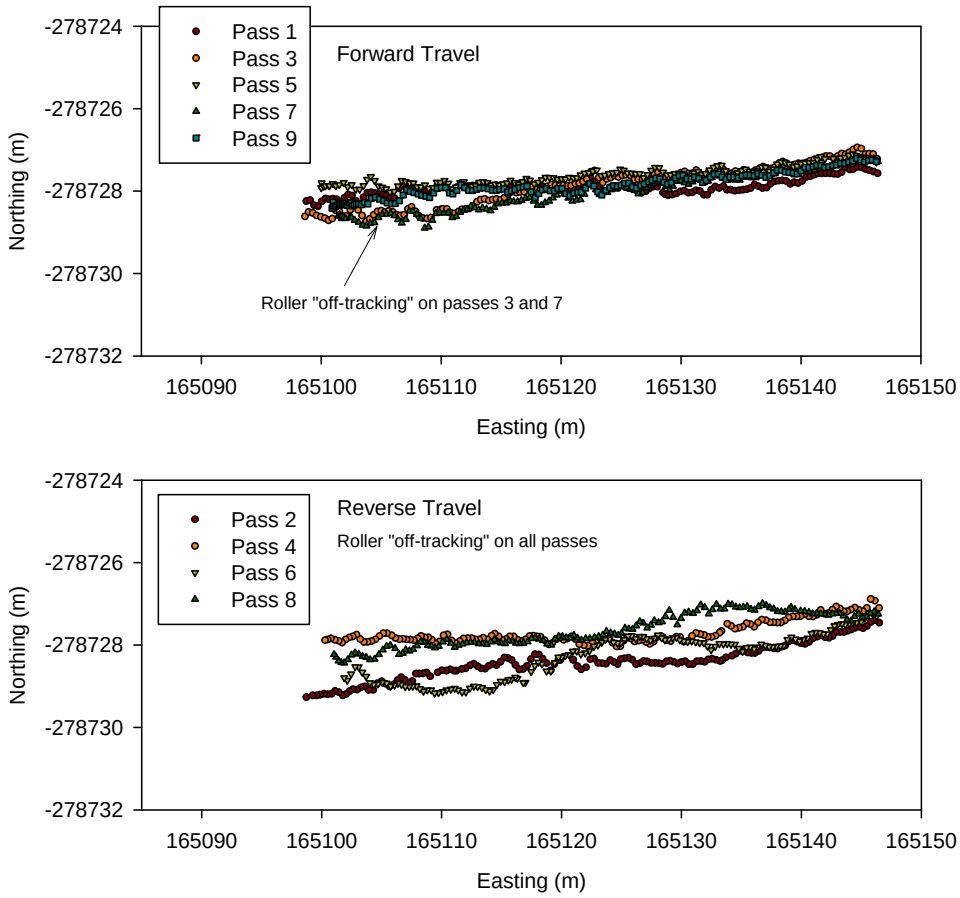

Figure 14. GPS northing and easting coordinates for forward and reverse travel

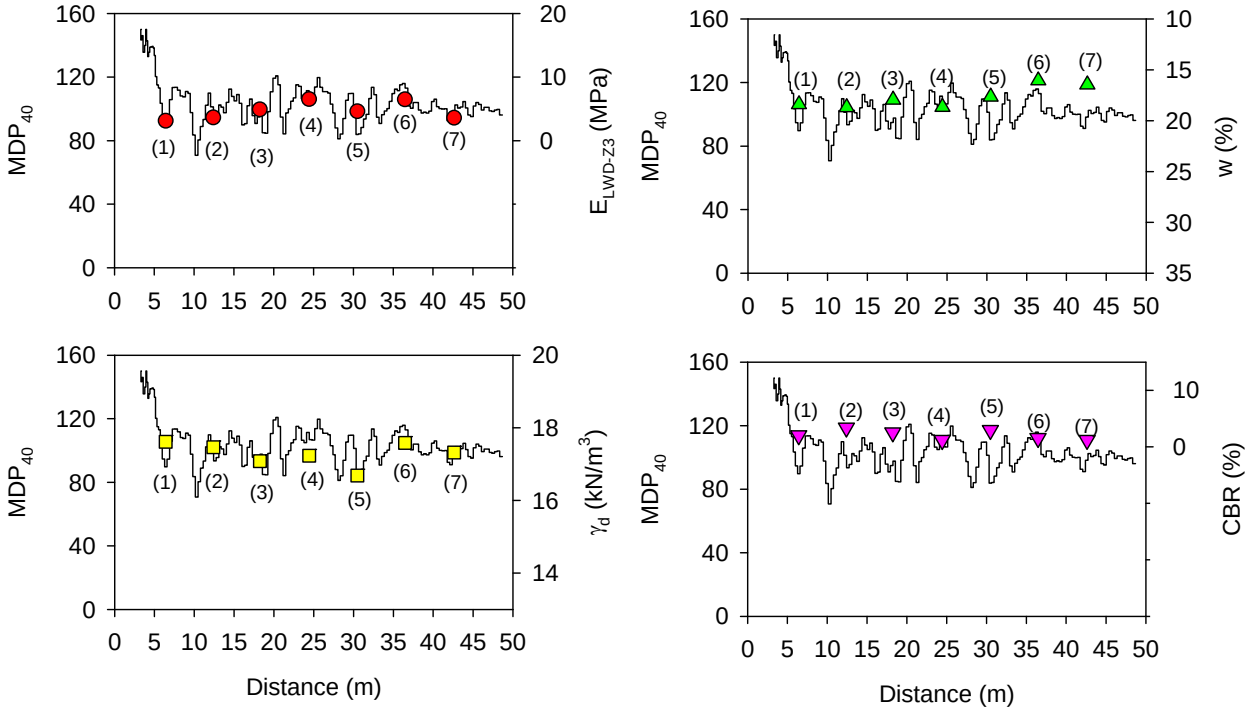

Figure 15. MDP_{40} and in-situ point measurements after final compaction pass – TB1

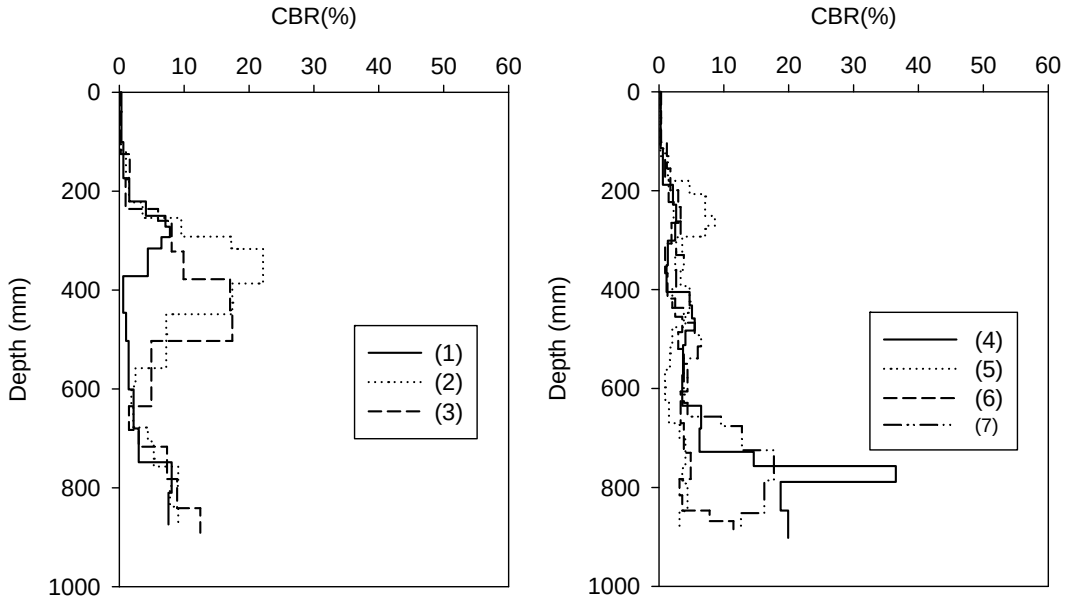

Figure 16. DCP-CBR profiles after final compaction pass – TB1

Table 4. Summary statistics of in-situ test results – TB1

Measurement Value	n	μ	σ	COV(%)
MDP_{40} (full test strip – pass 9)	152	106.0	15.4	15
MDP_{40} (at in-situ point test locations – pass 9)	7	100.0	10.0	10
Dry unit weight, γ_d (kN/m^3)	7	17.28	0.33	2
Dry unit weight, γ_d (pcf)	7	110.0	2.1	2
Relative compaction RC (%)	7	92.9	1.8	2
Moisture content, *w* (%)	7	17.7	1.1	6
Modulus, $E_{LWD\text{-}Z3}$ (MPa)	7	4.7	1.4	29
CBR_{300} (%)	7	2	1	41

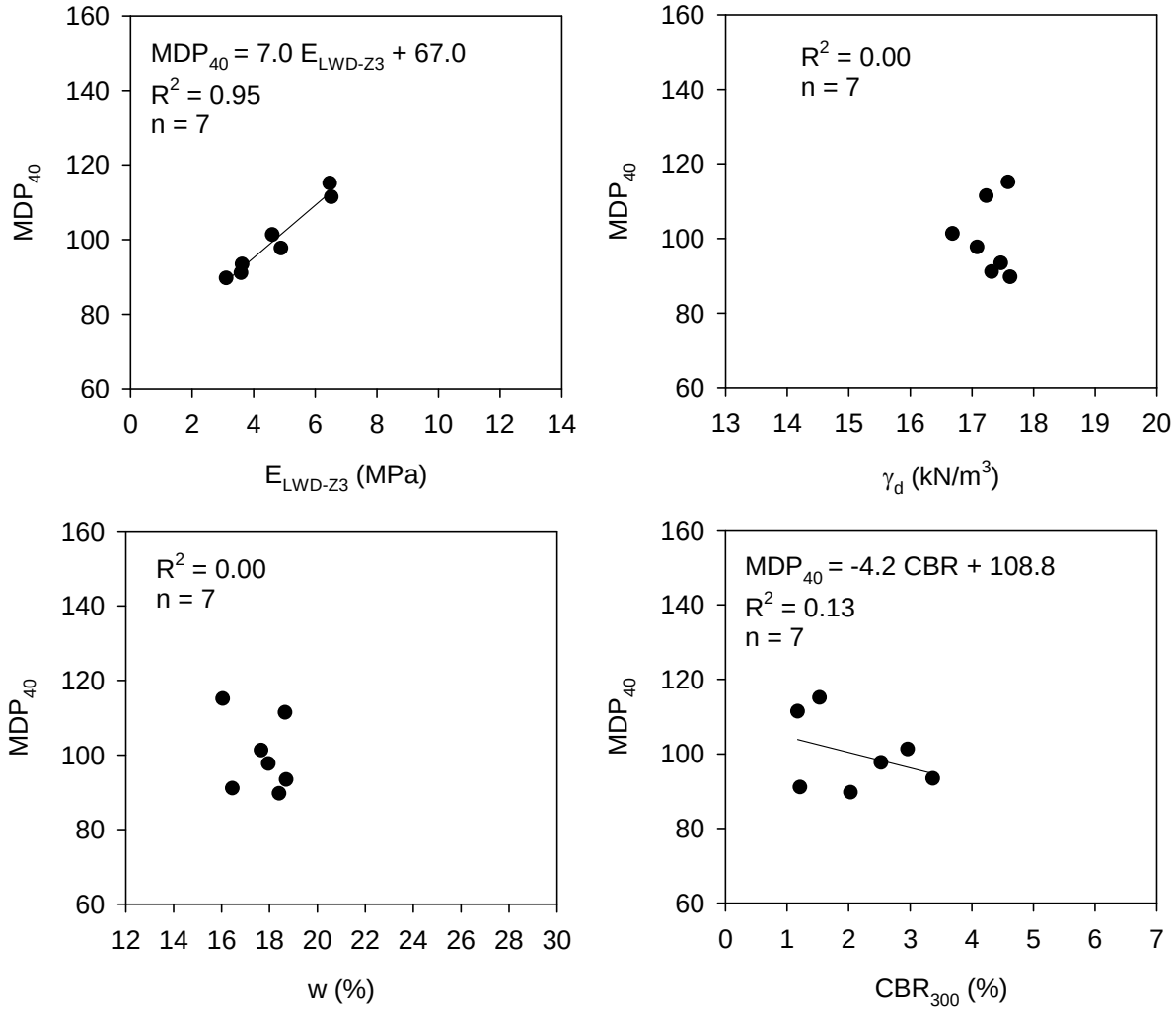

Figure 17. Correlations between MDP_{40} and in-situ point measurements – TB1

TBs 2 and 4 – Spatial Mapping and In-Situ Testing

TB2 involved mapping a compacted subgrade area with plan dimensions of about 36 m x 25 m. Mapping was performed in eight roller lanes. On-board display IC-MV map showed variations in MDP_{40} measurements in the north-south direction. Seven test locations as shown in Figure 18 were selected to obtain in-situ point-MVs ($E_{LWD\text{-}Z3}$, γ_d, w, and CBR). DCP-CBR profiles and other in-situ point-MVs obtained at each test location are provided in Figure 19. Summary statistics of MDP_{40} and in-situ point-MVs are provided in Table 5. The average w of the material was about 18.8% (i.e., 5.8% wet of w_{opt}) and the average percent RC of the material was about 92% of the standard Proctor γ_{dmax}.

Regression analysis between MDP_{40} measurements and in-situ point-MVs is presented in Figure 20. Correlation analysis between $E_{LWD\text{-}Z3}$ and MDP_{40} yielded a strong linear relationship with $R^2 = 0.82$. Correlation analysis between CBR_{300} and MDP_{40} also yielded a strong linear relationship with $R^2 = 0.77$. Correlations between γ_d and w point-MVs and MDP_{40} did not show statistically significant relationships.

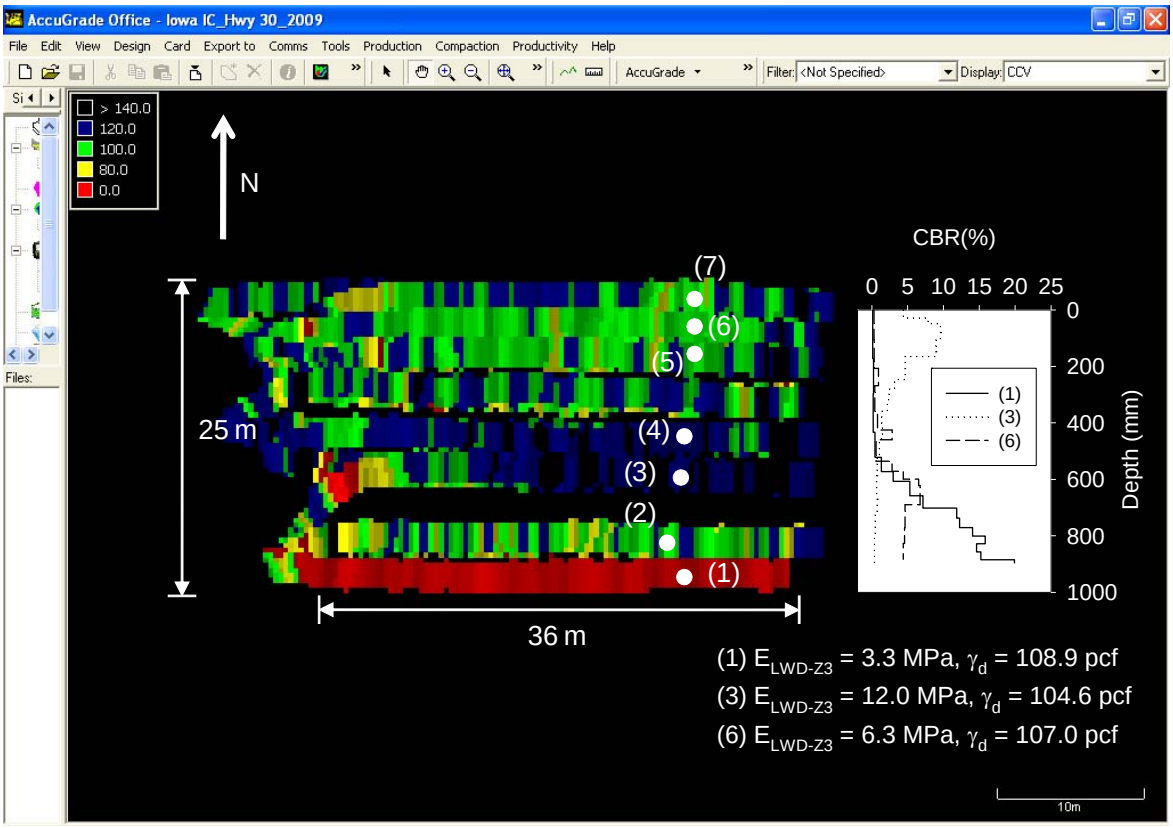

Figure 18. MDP_{40} final pass map – TB2

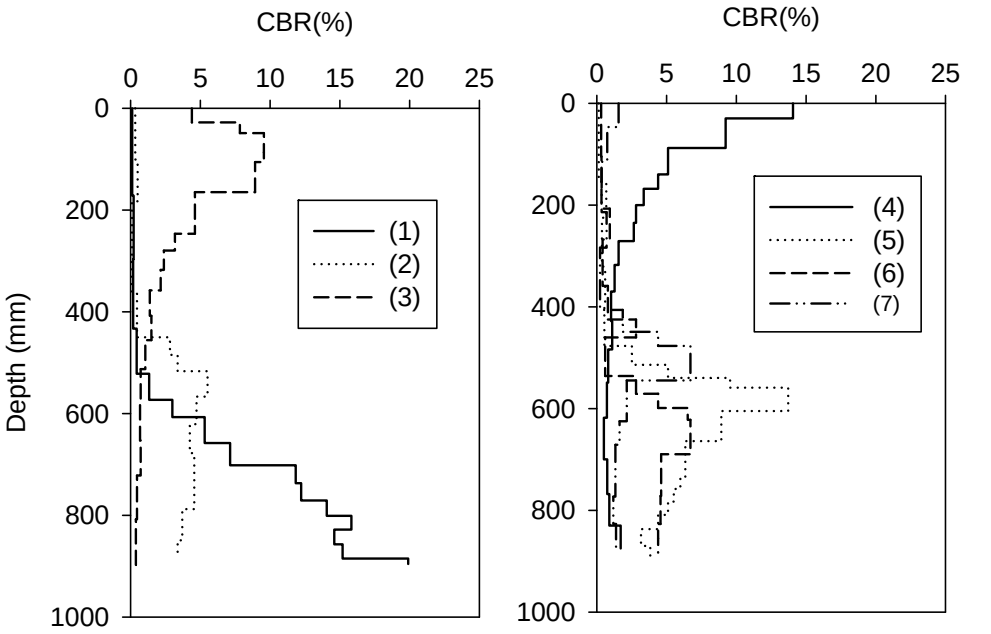

(1) $E_{LWD\text{-}Z3}$ = 3.3 MPa, γ_d = 17.11 kN/m^3 (108.9 pcf), w = 19.9%, CBR_{300} < 1
(2) $E_{LWD\text{-}Z3}$ = 6.0 MPa, γ_d = 18.14 kN/m^3 (115.5 pcf), w = 15.7%, CBR_{300} < 1
(3) $E_{LWD\text{-}Z3}$ = 12.0 MPa, γ_d = 16.43 kN/m^3 (104.6 pcf), w = 20.1%, CBR_{300} = 6
(4) $E_{LWD\text{-}Z3}$ = 12.4 MPa, γ_d = 16.21 kN/m^3 (103.2 pcf), w = 19.5%, CBR_{300} = 5
(5) $E_{LWD\text{-}Z3}$ = 4.8 MPa, γ_d = 16.81 kN/m^3 (107.0 pcf), w = 18.8%, CBR_{300} < 1
(6) $E_{LWD\text{-}Z3}$ = 6.3 MPa, γ_d = 16.80 kN/m^3 (107.0 pcf), w = 20.4%, CBR_{300} < 1
(7) $E_{LWD\text{-}Z3}$ = 4.9 MPa, γ_d = 17.51 kN/m^3 (111.5 pcf), w = 17.2%, CBR_{300} < 1

Figure 19. DCP-CBR profiles, and moisture and density measurements on TB2

Table 5. Summary statistics of in-situ test results – TB2

Measurement Value	**n**	**μ**	**σ**	**COV(%)**
MDP_{40} (full test area – pass 2)	1515	110.0	21.6	20
MDP_{40} (at in-situ point test locations – pass 2)	7	104.1	19.7	19
Dry unit weight, γ_d (kN/m^3)	7	17.00	0.66	4
Dry unit weight, γ_d (pcf)	7	108.2	4.2	4
Relative compaction RC (%)	7	92.0	3.5	4
Moisture content, *w* (%)	7	18.8	1.7	9
Modulus, $E_{LWD\text{-}Z3}$ (MPa)	7	7.1	3.6	51
CBR_{300} (%)	7	1.9	2.6	137

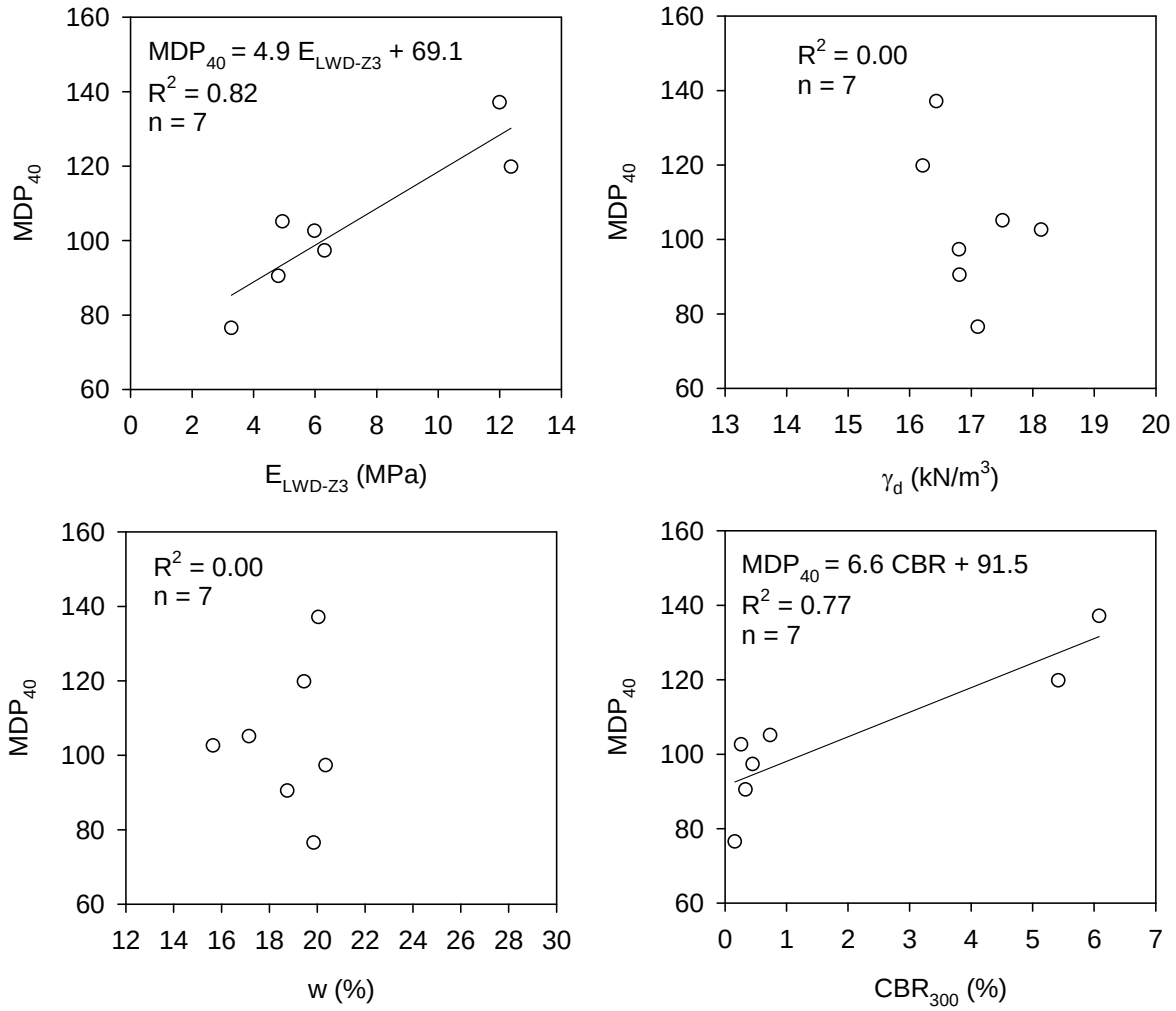

Figure 20. Correlations between MDP_{40} and in-situ point measurements – TB2

TB4 involved mapping a compacted subgrade area with plan dimensions of about 7 m x 283 m in two roller passes (Figure 21). Mapping was performed in three roller lanes. Eleven test locations as shown in Figure 21 were selected to obtain in-situ point-MVs ($E_{LWD\text{-}Z3}$, γ_d, w, and DCP-CBR). MDP_{40} plots in comparison with in-situ point-MVs after pass 2 separately for each roller lane are provided in Figure 22 and Figure 23. Summary statistics of MDP_{40} and in-situ point-MVs are provided in Table 6. The average w of the material was about 17.9% (i.e., 4.9% wet of w_{opt}), and the average percent RC of the material was about 96% of the standard Proctor γ_{dmax}.

Regression analysis between MDP_{40} measurements and in-situ point-MVs is presented in Figure 24. Correlation analysis between $E_{LWD\text{-}Z3}$ and MDP_{40} yielded a linear relationship with $R^2 = 0.61$. Correlation analysis between CBR and γ_d point-MVs and MDP_{40} also yielded linear relationships with $R^2 = 0.45$ and 0.31, respectively. MDP_{40} measurements on this test bed were sensitive to moisture content (MDP_{40} decreased with increasing w). Correlation between MDP_{40} and w yielded a non-linear power relationship with $R^2 = 0.45$.

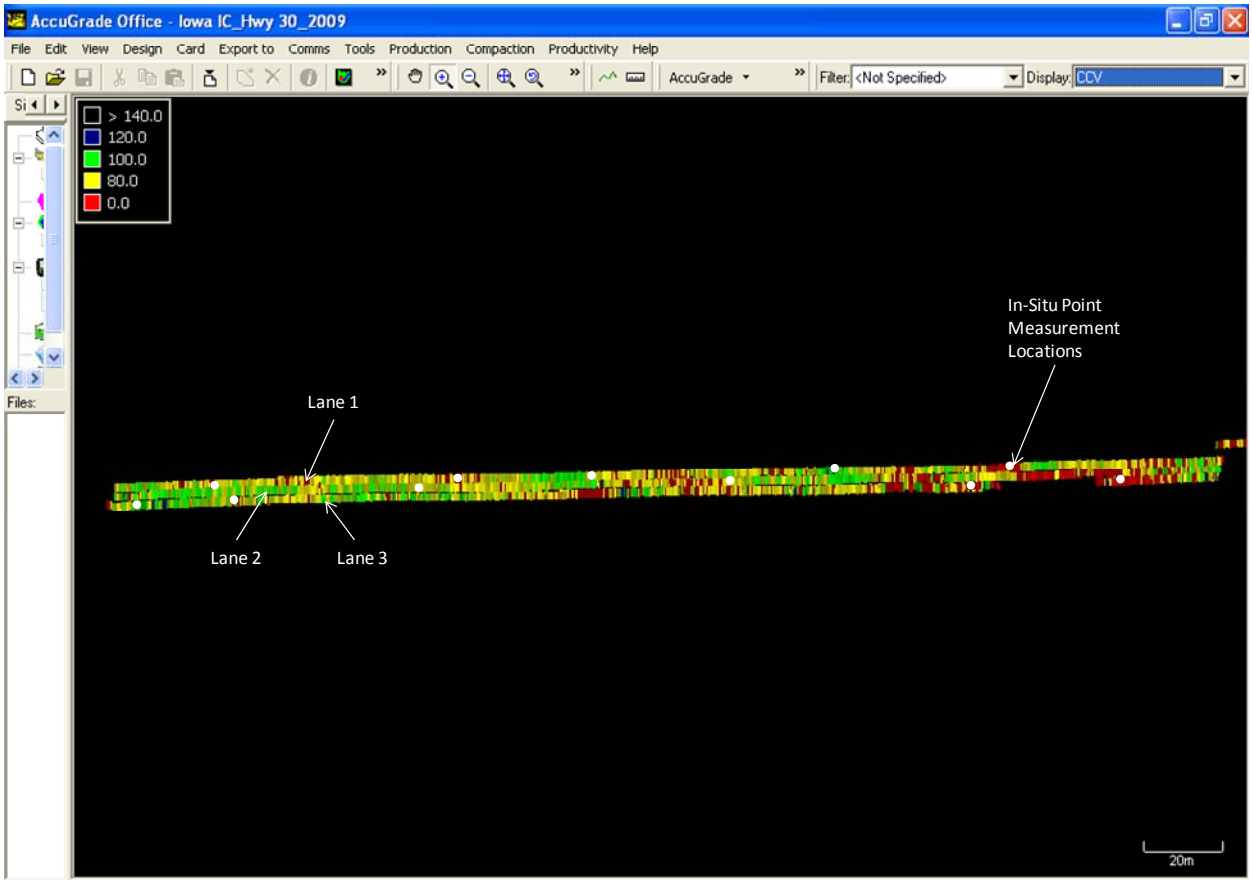

Figure 21. MDP_{40} map and in-situ test locations on TB4

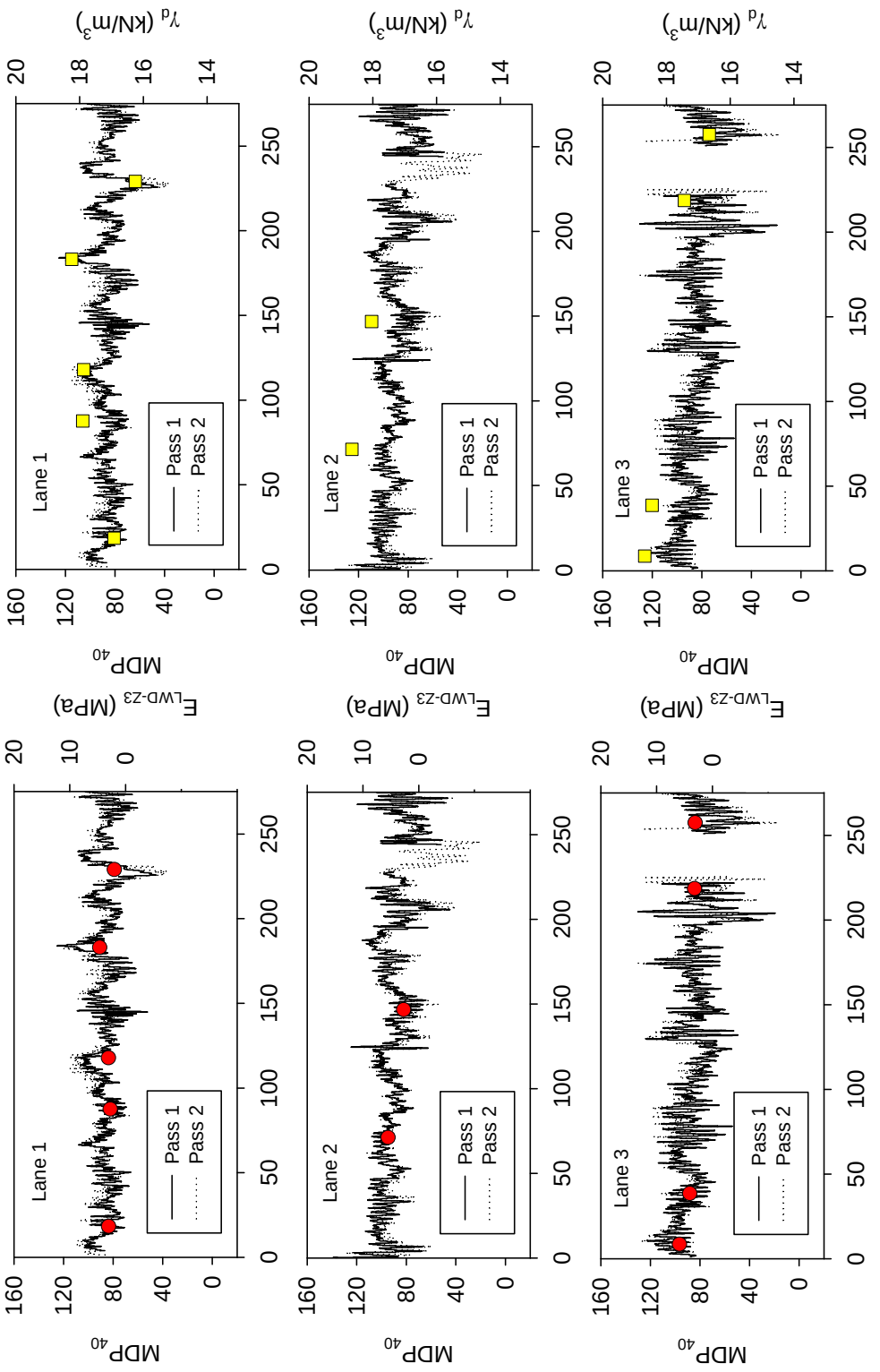

Figure 22. MDP_{40} measurements for passes 1 and 2, and in-situ point measurements ($E_{LWD\text{-}Z3}$ and dry density) after pass 2 – TB4

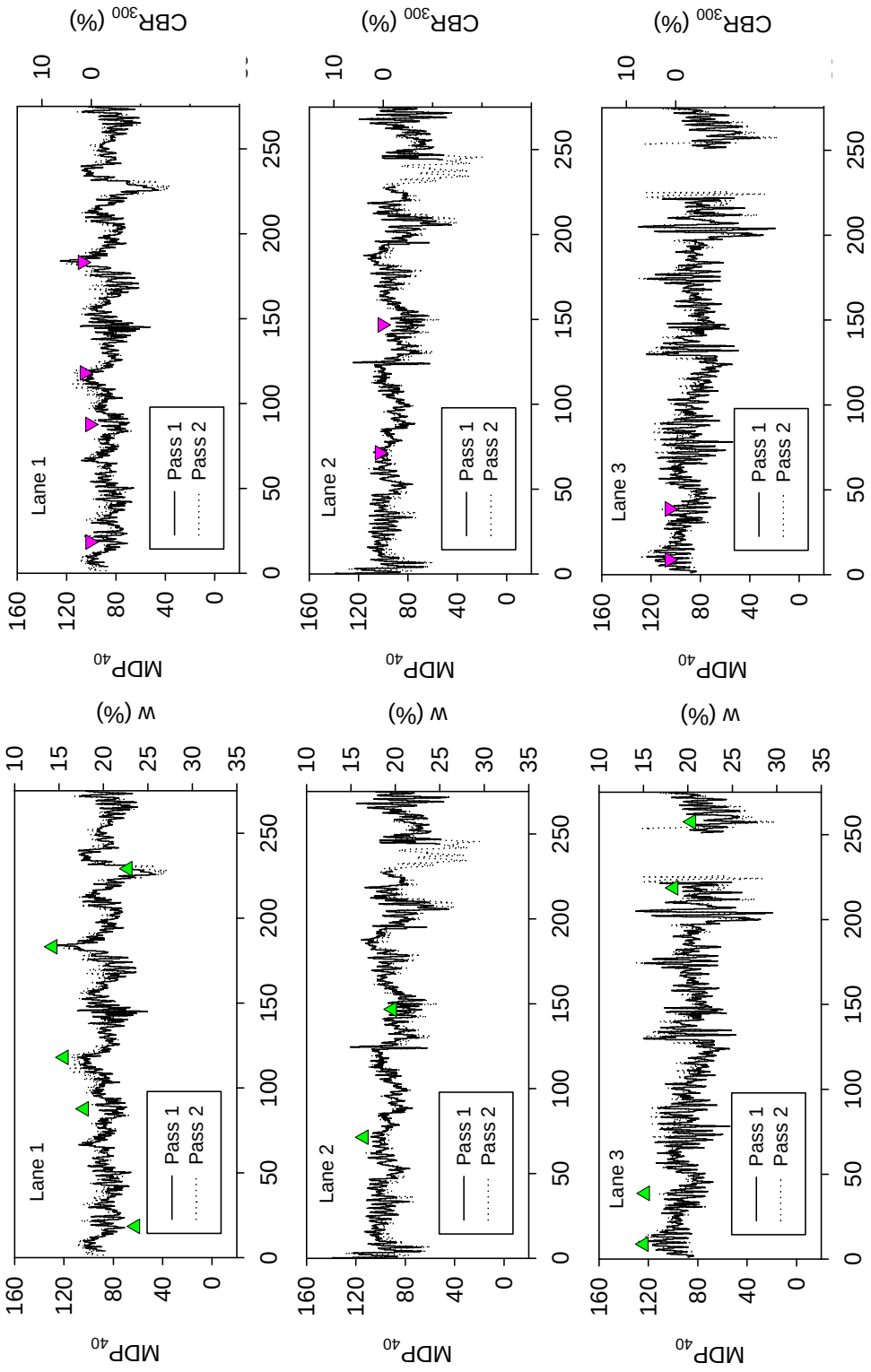

Figure 23. MDP_{40} measurements for passes 1 and 2, and in-situ point measurements (moisture content and CBR) after pass 2 – TB4

Table 6. Summary statistics of in-situ test results – TB4

Measurement Value	n	μ	σ	COV(%)
MDP_{40} (full test area – pass 2)	2420	89.7	14.5	16
MDP_{40} (at in-situ point test locations – pass 2)	12	88.0	9.0	10
Dry unit weight, γ_d (kN/m^3)	12	17.80	0.81	5
Dry unit weight, γ_d (pcf)	12	113.3	5.2	5
Relative compaction RC (%)	12	96.3	4.4	5
Moisture content, *w* (%)	12	17.9	3.1	18
Modulus, E_{LWD-Z3} (MPa)	12	3.7	1.2	33
CBR_{300} (%)	8	0.9	0.6	67

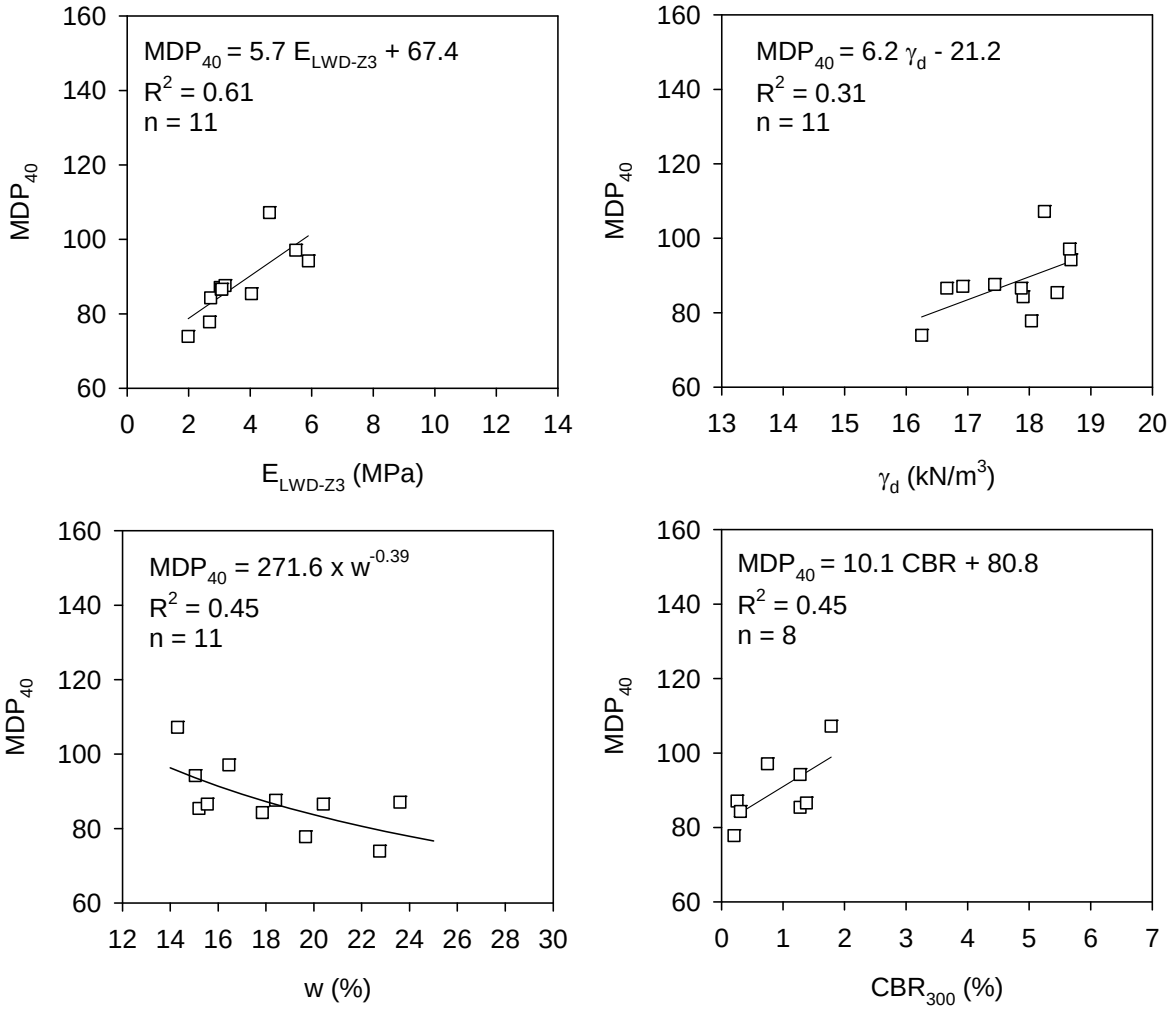

Figure 24. Correlations between MDP_{40} and in-situ point measurements – TB4

TB3 – Five Lifts of Embankment Fill

TB3 consisted of placing and compacting five lifts of embankment fill material in a production area. The area slopes down from the south west quadrant to the north east quadrant of the test bed. Lift 1 consisted of native subgrade material which was relatively wet. The area was mapped using one roller pass using the IC roller. Lifts 2 and 5 consisted of a 150 mm to 300 mm thick layers of new fill material placed and compacted in each layer. Compaction on lifts 2 and 3 was achieved using the IC roller. On lifts 4 and 5, pull behind sheepsfoot roller was first used for compaction and followed by four to six IC roller passes. MDP_{40}, percent target MDP_{40}, pass count, and elevation maps of each lift are presented in Figure 25 to Figure 29. Percent target MDP_{40} was determined using an arbitrary target $MDP_{40} = 140$. Viewing percent target MDP_{40} maps can be useful for pass/fail QA analysis. Monitoring the elevation maps during construction can be a useful QC method to control lift thickness.

A three-dimensional view of MDP_{40} maps of lifts 2 to 5 is presented in Figure 30. Lift 1 MDP_{40} map could not be presented in the three-dimensional view along with other lifts due to incorrect settings in the roller GPS as noted earlier in this report. In-situ point-MVs ($E_{LWD\text{-}Z3}$, γ_d, w, and DCP-CBR) were obtained after the final IC roller pass from 3 locations on lift 1, 22 locations on lift 2, 14 locations on lift 3, 17 locations on lift 4, and 12 locations from lift 5.

MDP_{40} map on lift 1 indicated a soft zone (with $MDP_{40} < 70$) in the north east quadrant of the test bed that reflected through the successive lifts 2, 3, 4, and 5 with similarly low MDP_{40} values in that quadrant. Visually, the maps indicate that the MDP_{40} values are relatively more uniform on lift 5 compared to the values on the underlying lifts. To quantitatively assess the change in the uniformity of MDP_{40} values on each lift, geostatistical semivariograms of MDP_{40} are presented in Figure 31. Theoretical spherical variograms are fit to the experimental variogram data from each lift. As indicated earlier, a lower "sill" and longer "range" represent best conditions for uniformity while the opposite represents an increasingly non-uniform condition. The sill values decreased from about 300 MDP_{40}^2 on lift 2 to 200 MDP_{40}^2on lift 3 indicating an increase in uniformity. The sill values remained at around 200 MDP_{40}^2 on lifts 4 and 5. The range values decreased from about 25 m on lift 2 to about 12 m on lift 3, and then continued to increase up to about 19 m on lift 5. This increase in range values from lift 3 to 5 demonstrates an increase in uniformity.

MDP_{40} plots in comparison with in-situ point-MVs for lift 2 are presented in Figure 33 to Figure 36. Similar plots for lifts 3 to 5 are presented in Figure 37 to Figure 48. Summary statistics of MDP_{40} and in-situ point-MVs for each lift are provided in Table 7. The average MDP_{40} and in-situ point-MVs on lifts 1 to 5 is shown in Figure 49. The average MDP_{40}, $E_{LWD\text{-}Z3}$, and CBR_{300} measurement values increased from lift 1 to 3 and then decreased from lift 3 to 5. The dry density measurements on the other hand increased consistently from lifts 1 to 5. The average moisture content of the material was lower on lift 3 (average $w = 16.4$, 4% wet of w_{opt}) than on other lifts.

Regression analysis between MDP_{40} measurements and in-situ point-MVs is presented in Figure 50. Correlation analysis between $E_{LWD\text{-}Z3}$ and CBR_{300} point-MVs and MDP_{40} values yielded power relationships with $R^2 = 0.41$ and 0.59, respectively. Correlation analysis between γ_d

measurements and MDP_{40} yielded a relatively weak linear relationship with $R^2 = 0.11$. MDP_{40} measurements on this test bed were sensitive to moisture content (MDP_{40} decreased with increasing *w*). Correlation between MDP_{40} and *w* yielded a linear relationship with $R^2 = 0.20$.

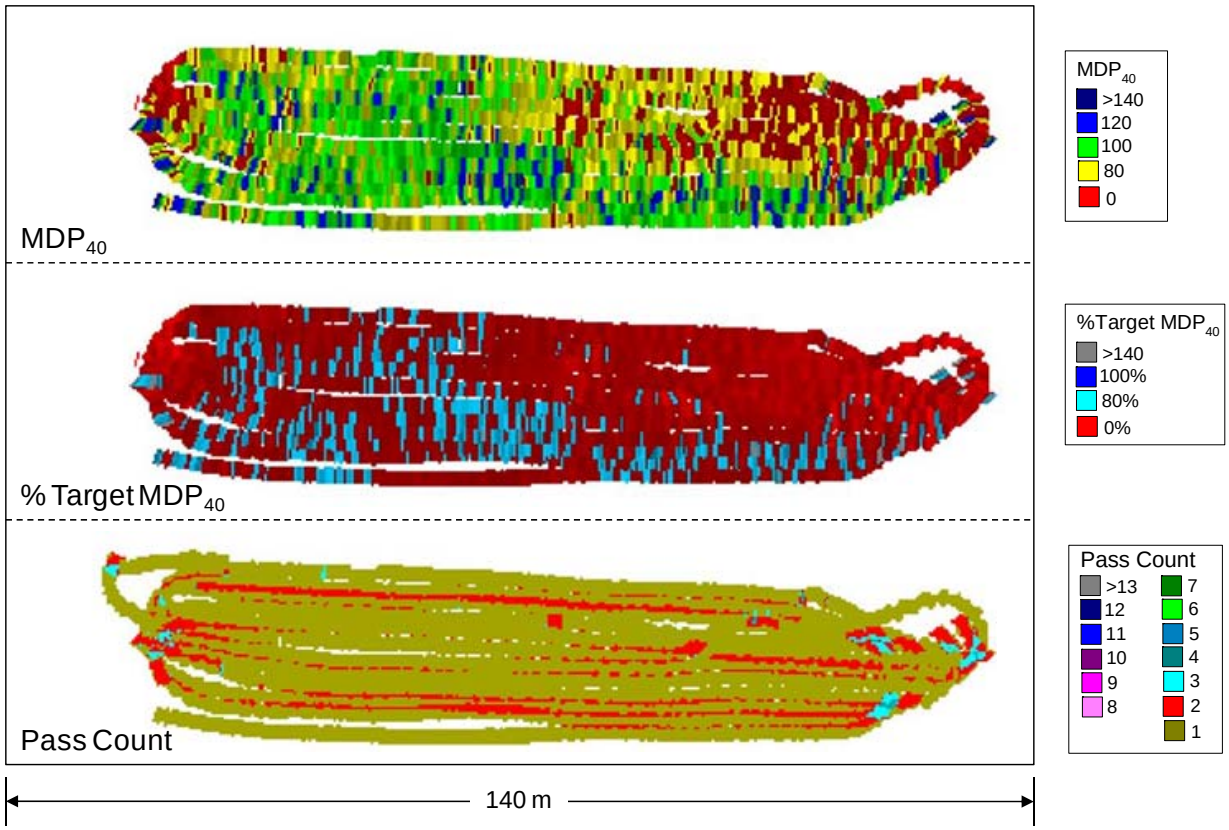

Figure 25. MDP_{40}, percent target MDP_{40} (assuming target MDP_{40} = 140), and pass count maps on lift 1 – TB3

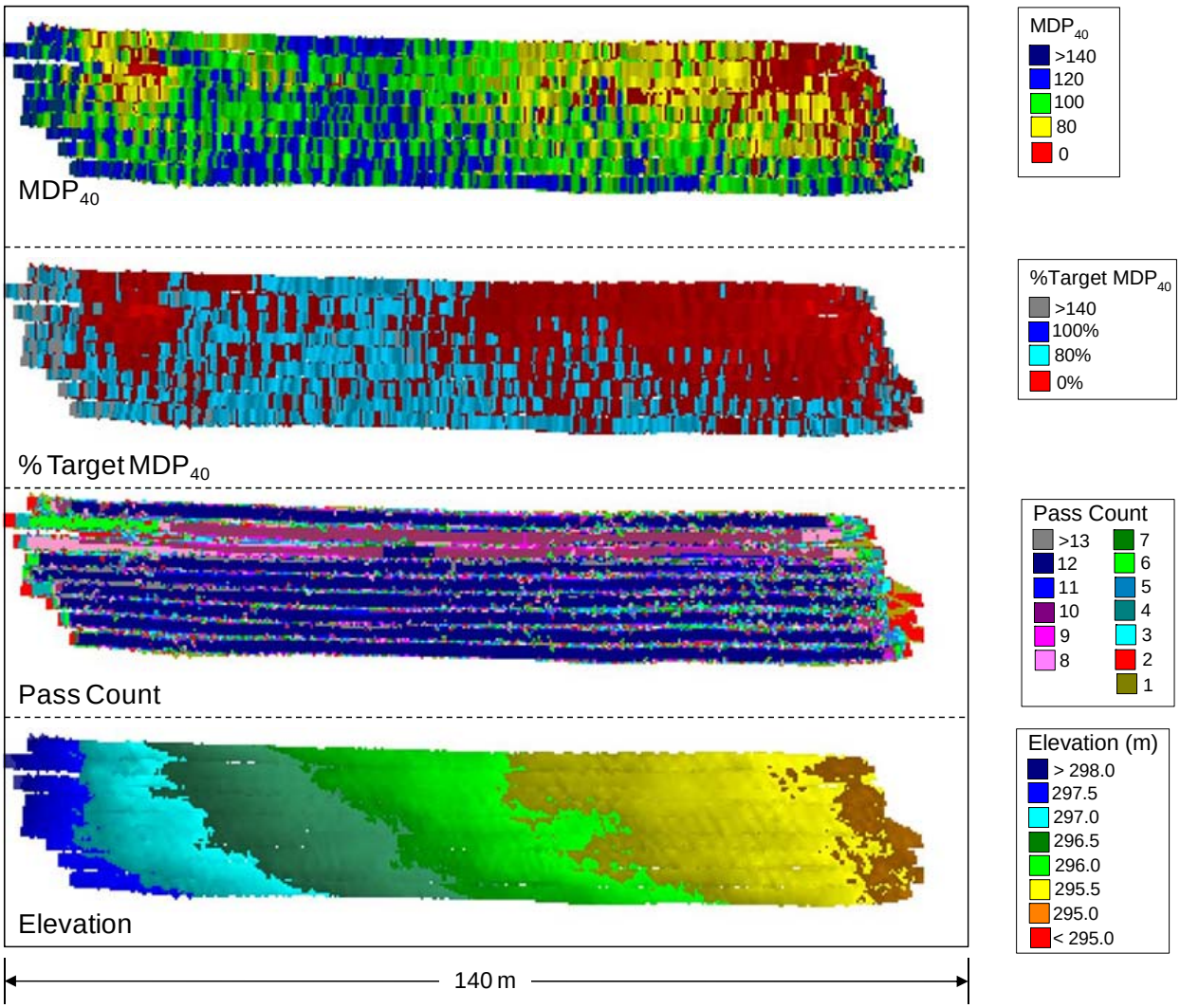

Figure 26. MDP_{40}, percent target MDP_{40} (assuming target MDP_{40} = 140), pass count, and elevation maps on lift 2 – TB3

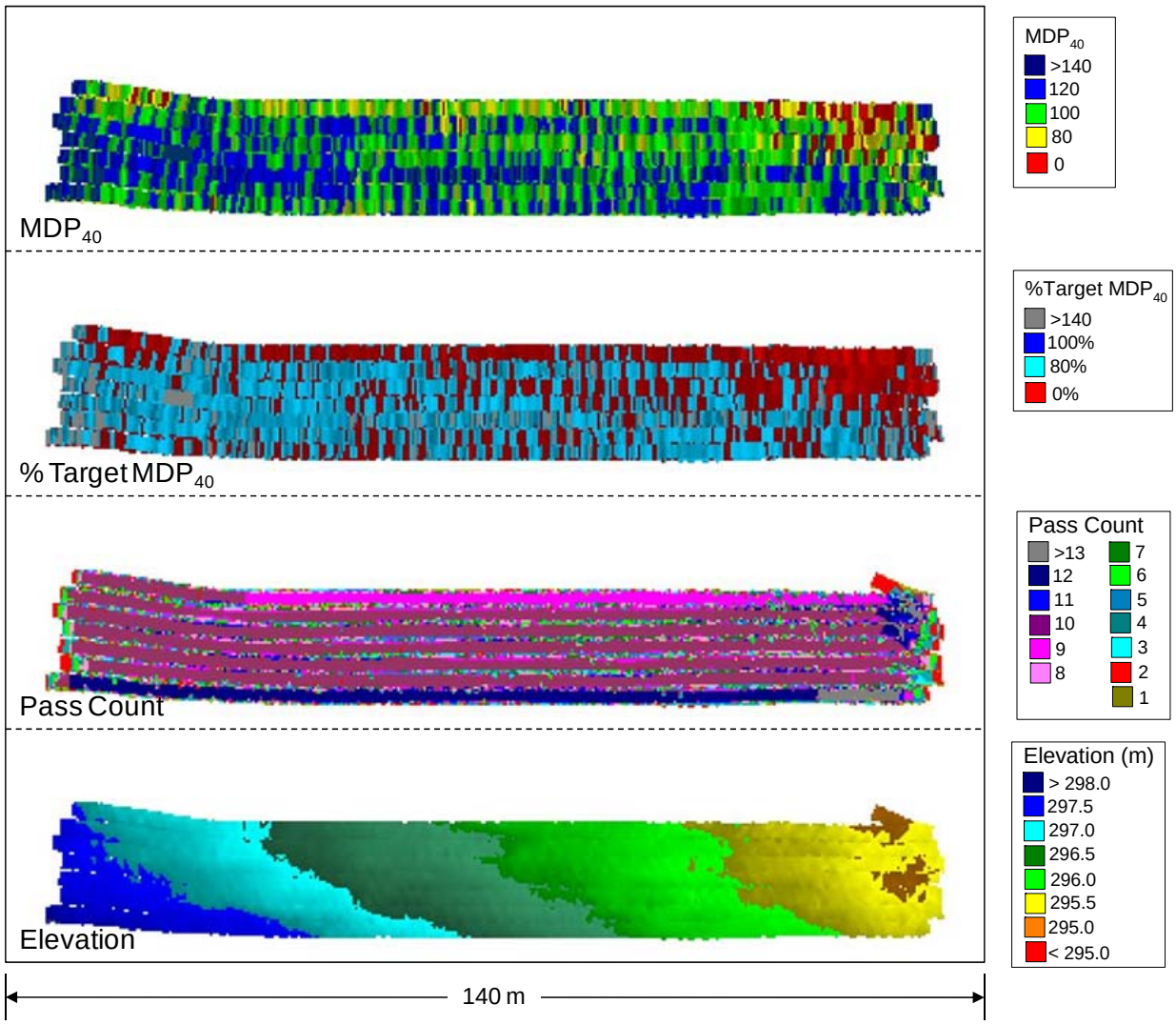

Figure 27. MDP_{40}, percent target MDP_{40} (assuming target MDP_{40} = 140), pass count, and elevation maps on lift 3 – TB3

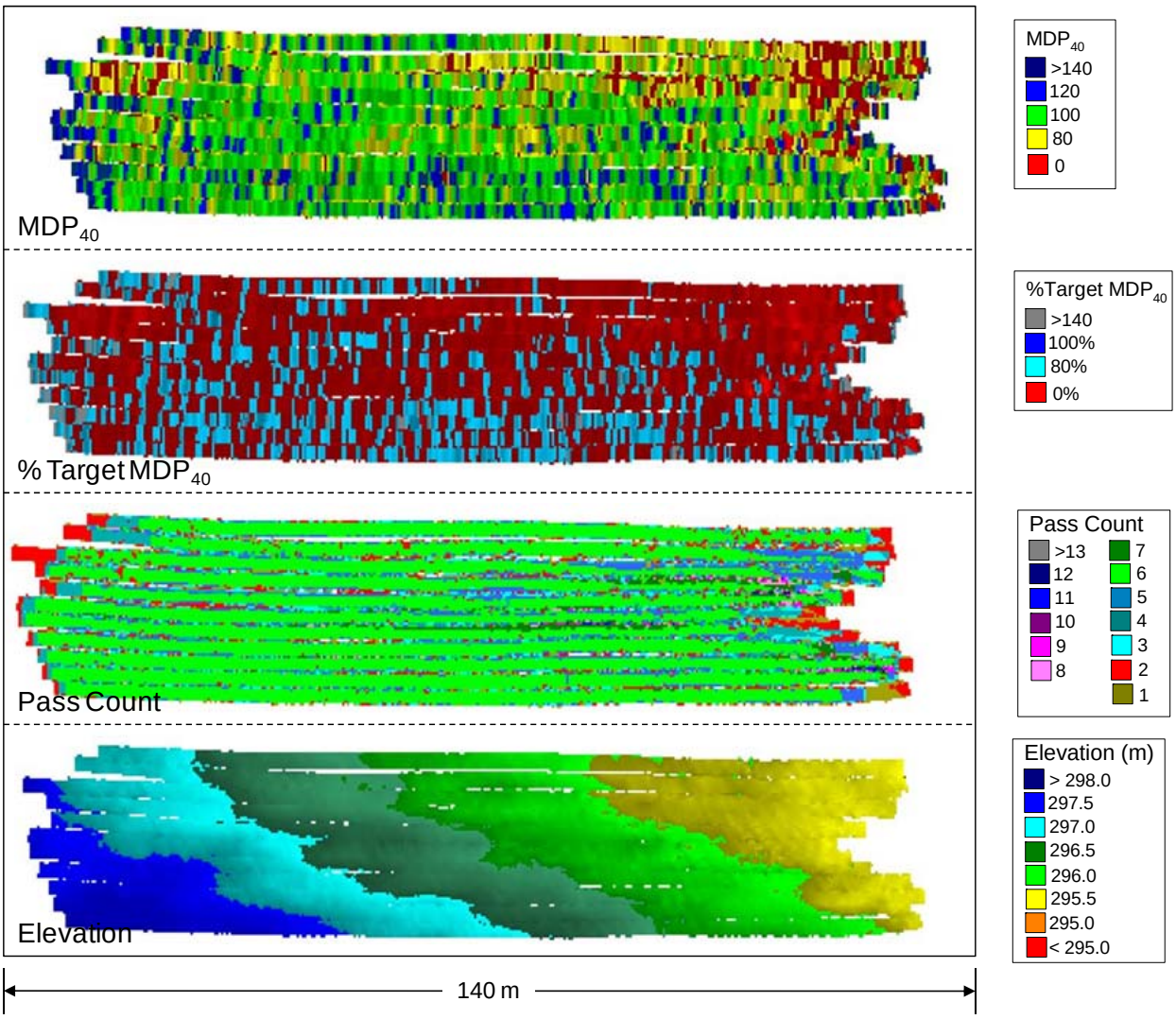

Figure 28. MDP_{40}, percent target MDP_{40} (assuming target MDP_{40} = 140), pass count, and elevation maps on lift 4 – TB3 (compaction was performed using pull behind sheepsfoot roller prior to IC roller passes)

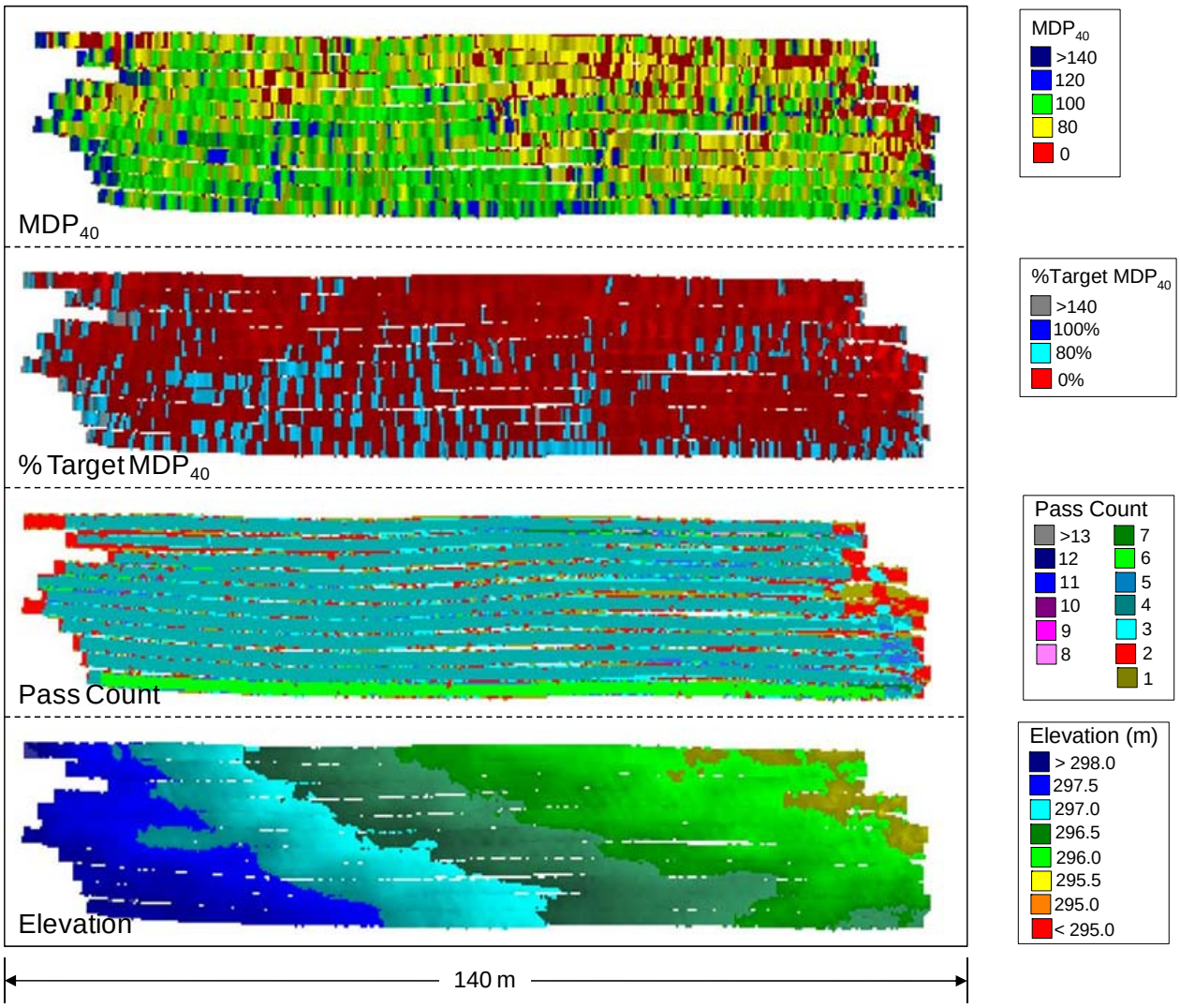

Figure 29. MDP_{40}, percent target MDP_{40} (assuming target MDP_{40} = 140), pass count, and elevation maps on lift 5 – TB3 (compaction was performed using pull behind sheepsfoot roller prior to IC roller passes)

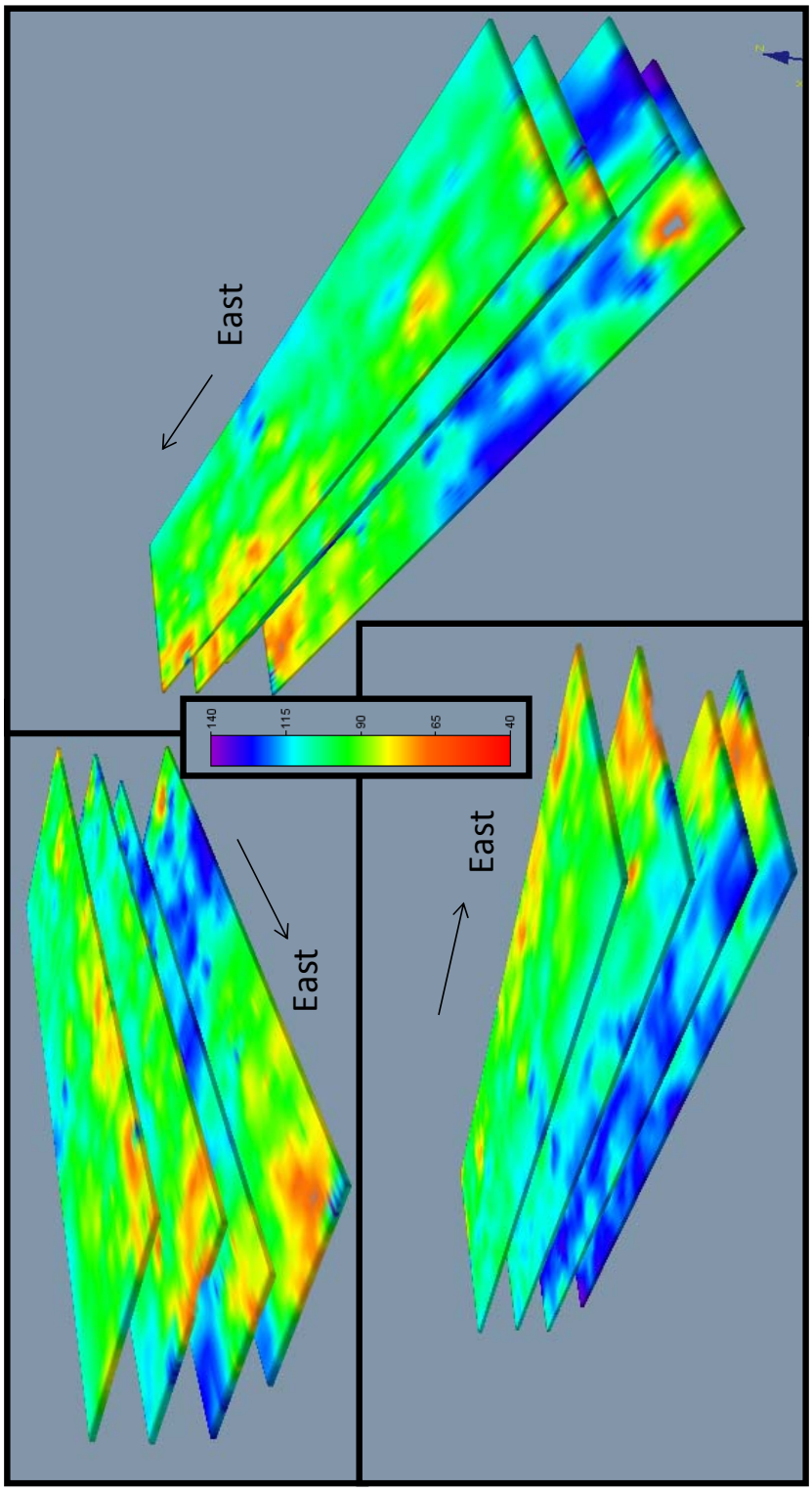

Figure 30. Three-dimensional spatial visualization of MDP_{40} measurements on lifts 2 to 5 – TB3 (note: vertical elevation between each lift exaggerated for clarity)

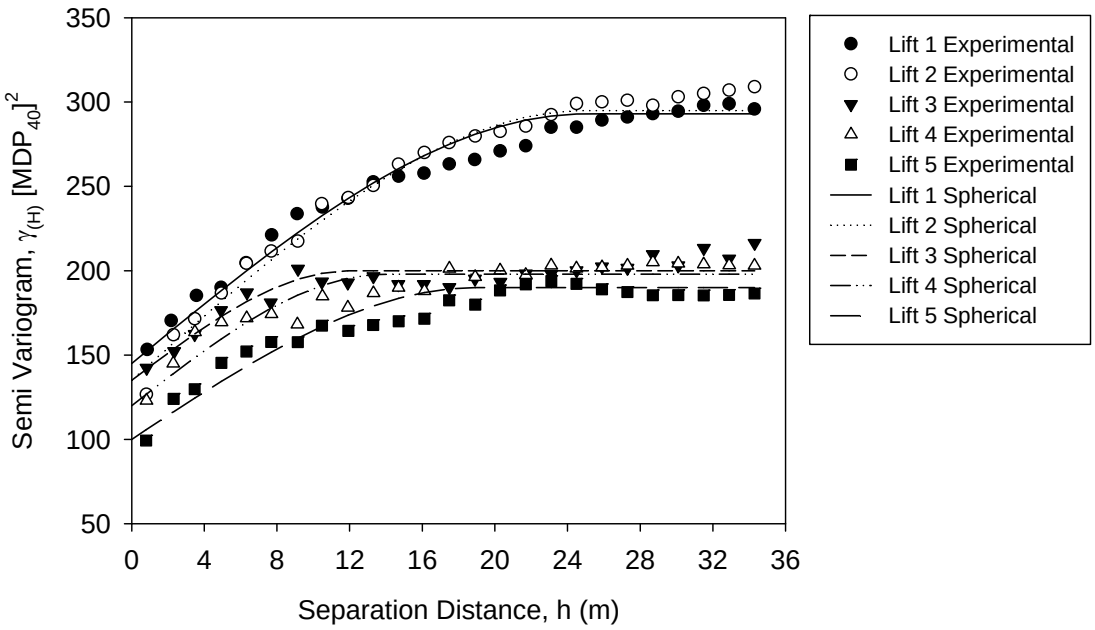

Figure 31. Semivariograms of MDP_{40} measurements on lifts 1 to 5 – TB3

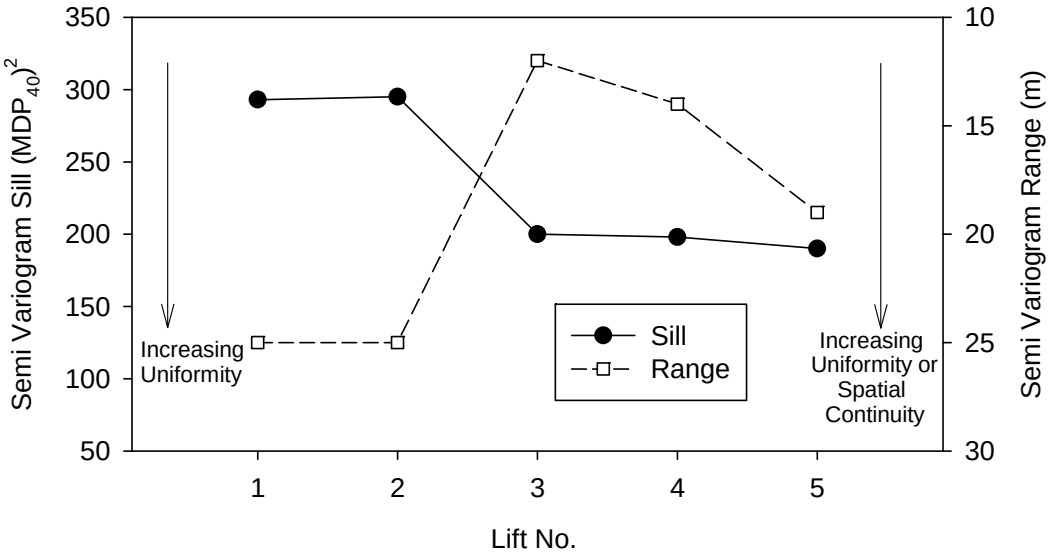

Figure 32. Semi variogram sill and range values on lifts 1 to 5 – TB3

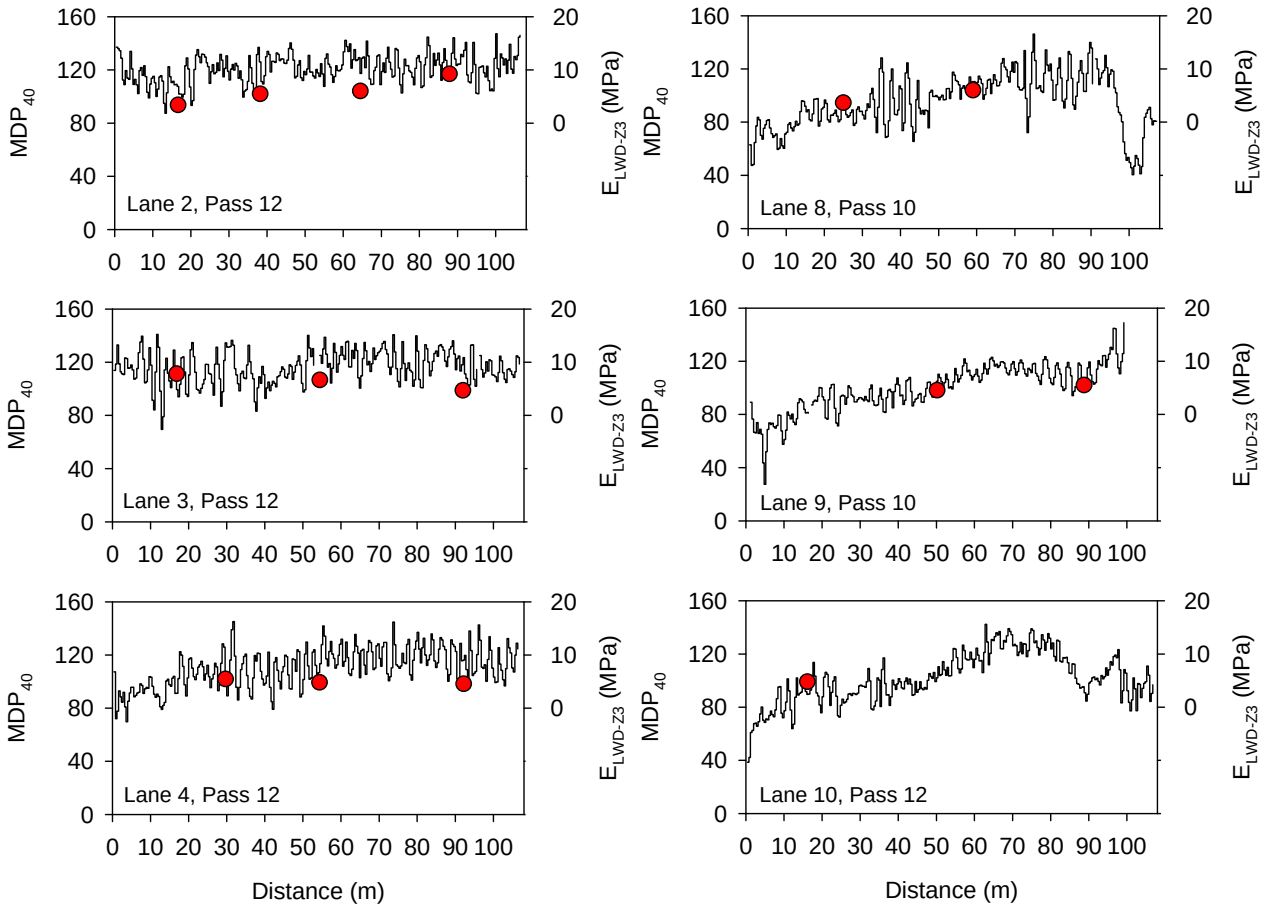

Figure 33. MDP_{40} and in-situ $E_{LWD\text{-}Z3}$ measurements on lift 2 after final pass – TB3

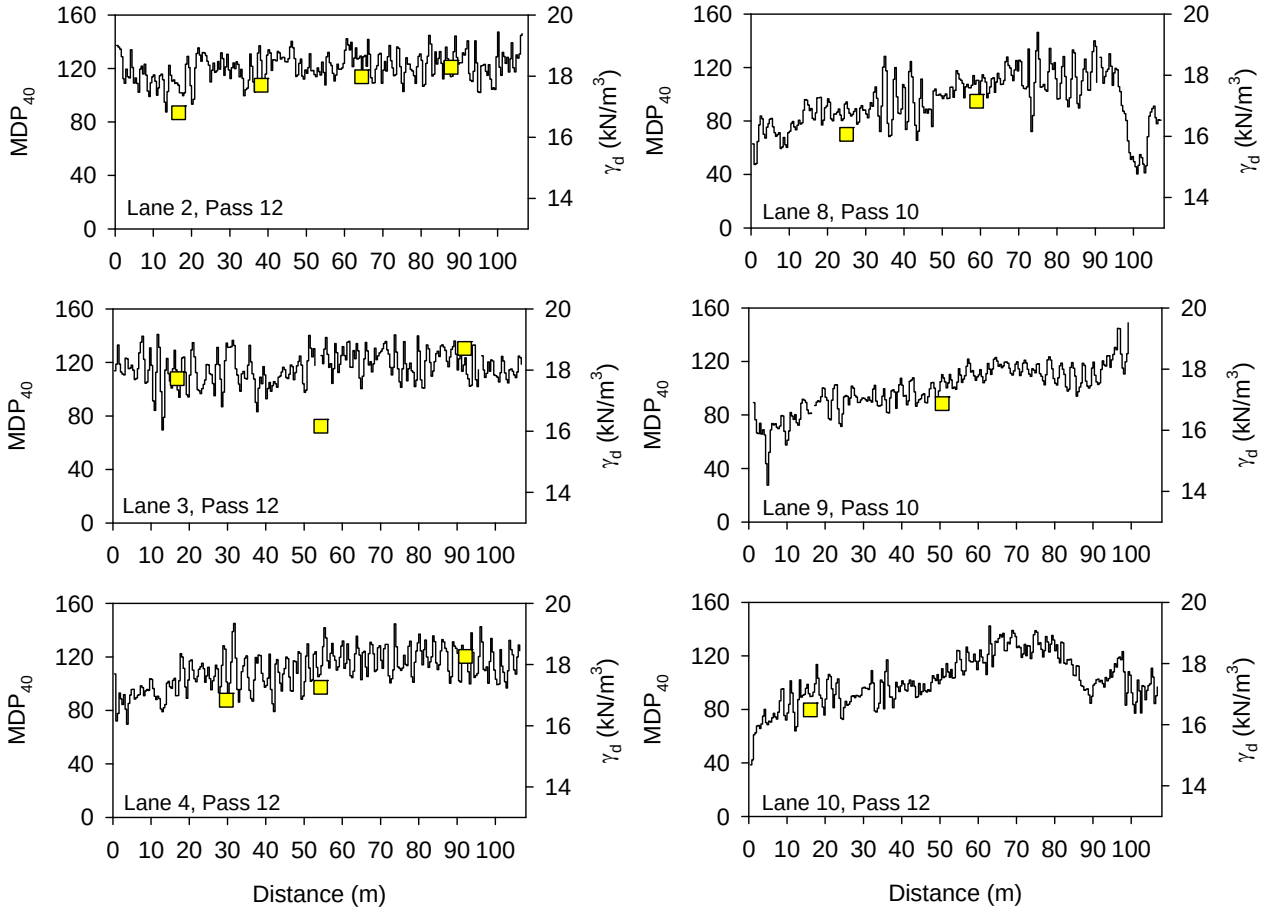

Figure 34. MDP_{40} and in-situ dry density measurements on lift 2 after final pass – TB3

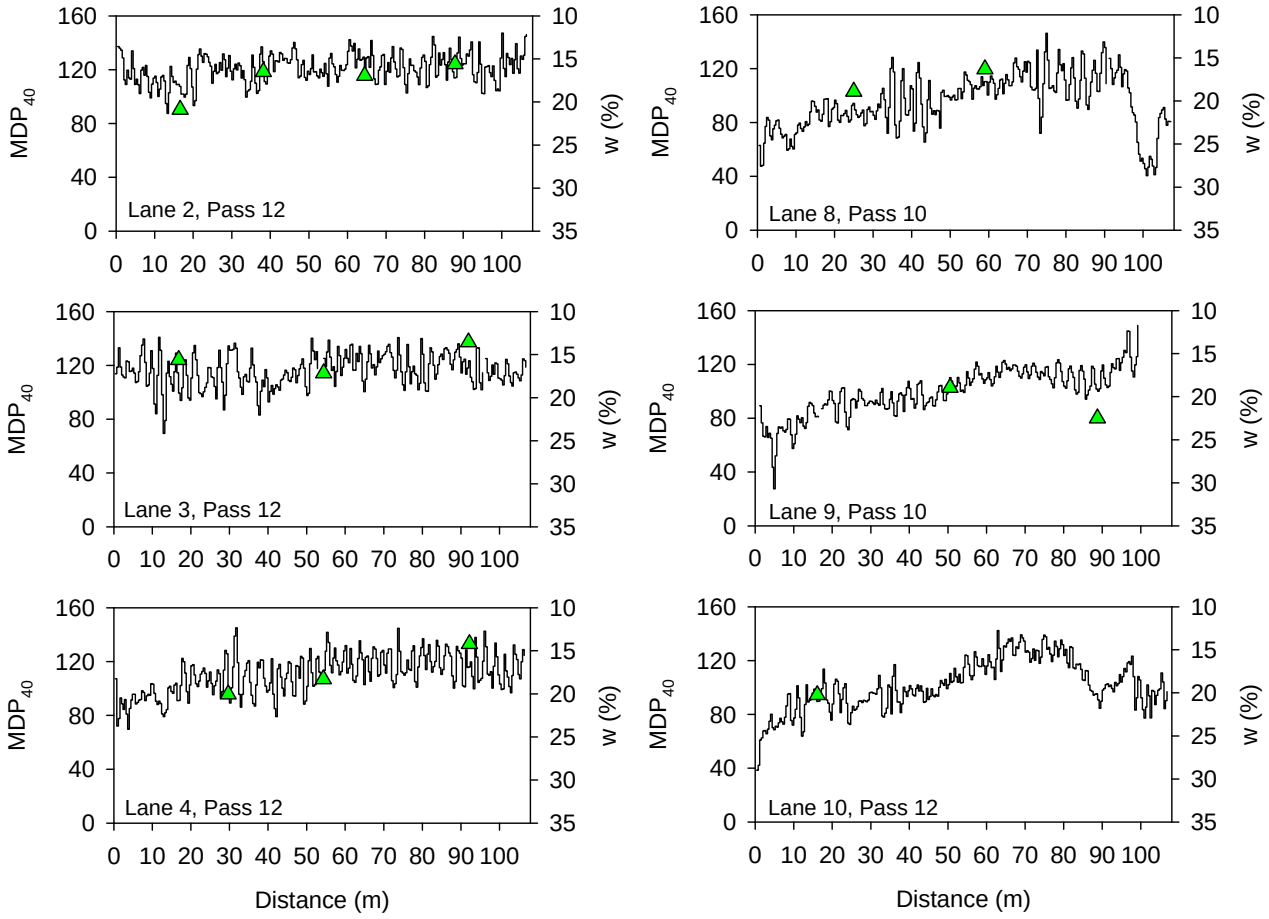

Figure 35. MDP_{40} and in-situ moisture measurements on lift 2 after final pass – TB3

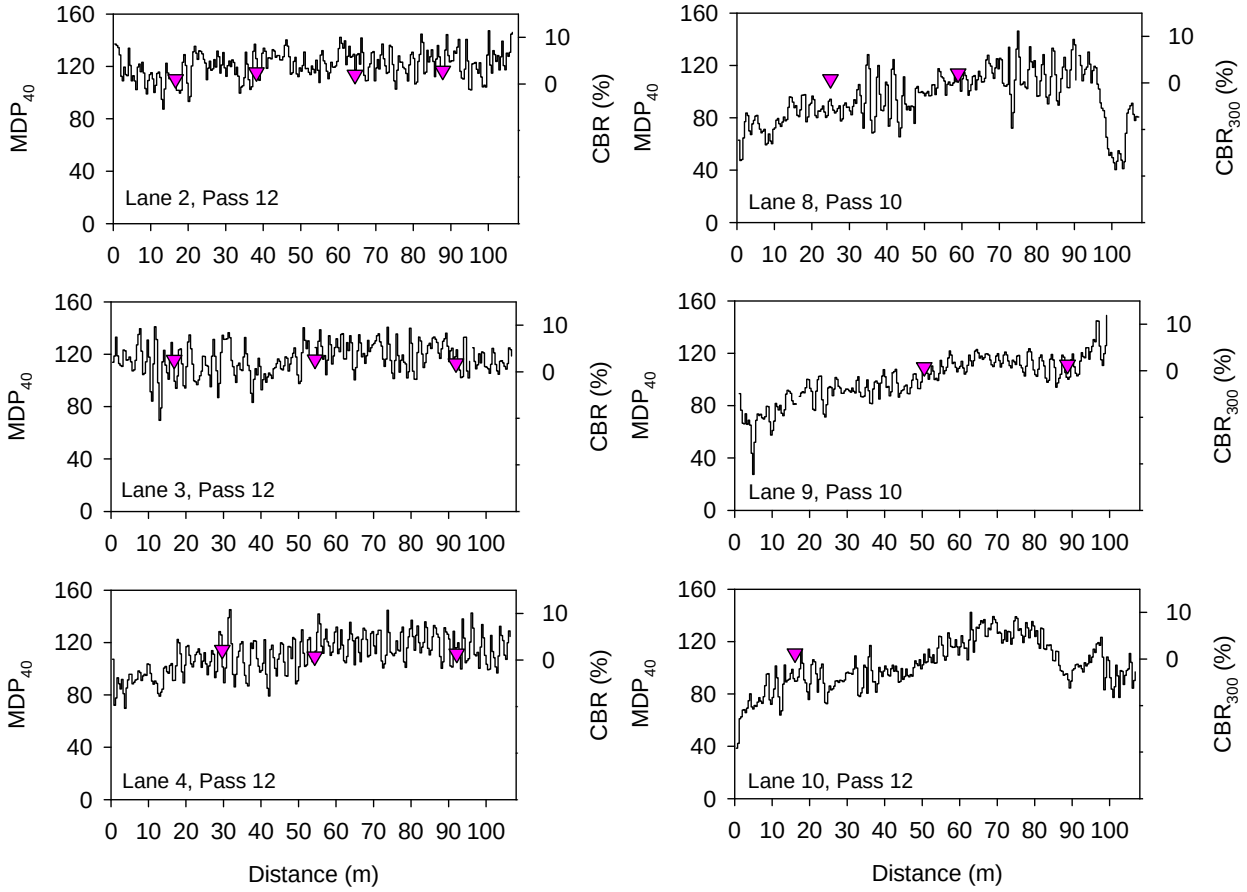

Figure 36. MDP_{40} and in-situ CBR_{300} measurements on lift 2 after final pass – TB3

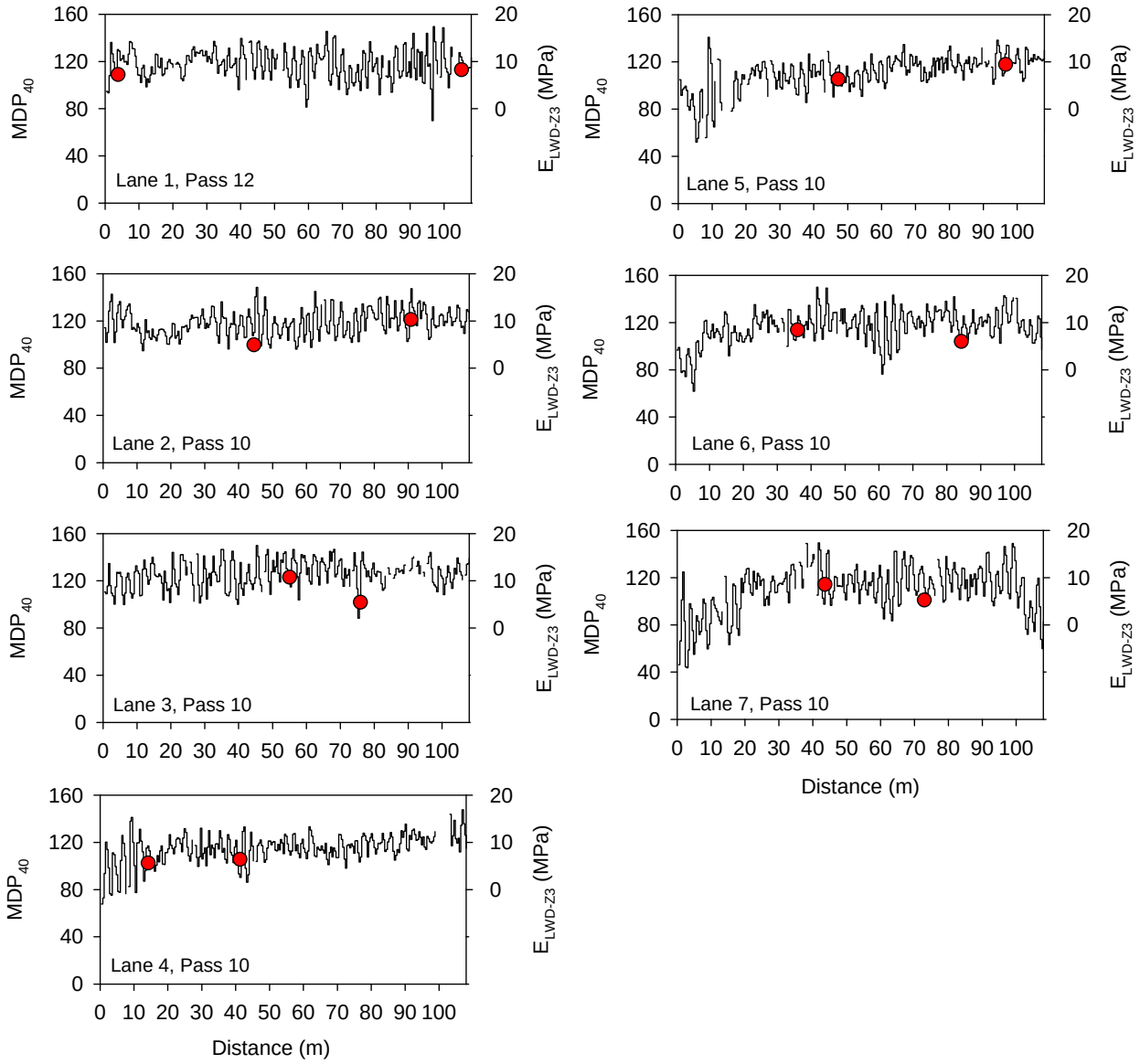

Figure 37. MDP_{40} and in-situ $E_{LWD\text{-}Z3}$ measurements on lift 3 after final pass – TB3

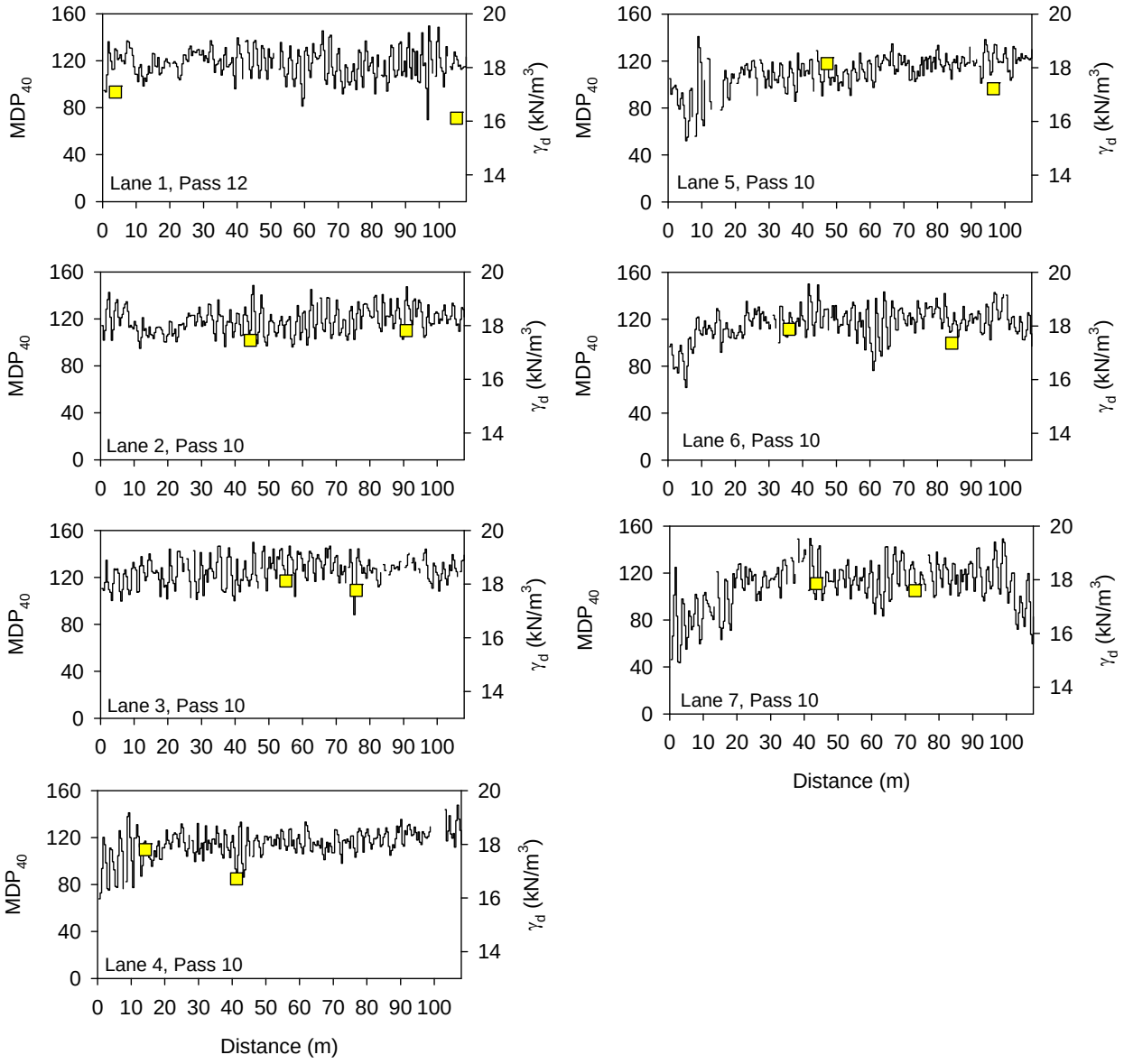

Figure 38. MDP_{40} and in-situ dry density measurements on lift 3 after final pass – TB3

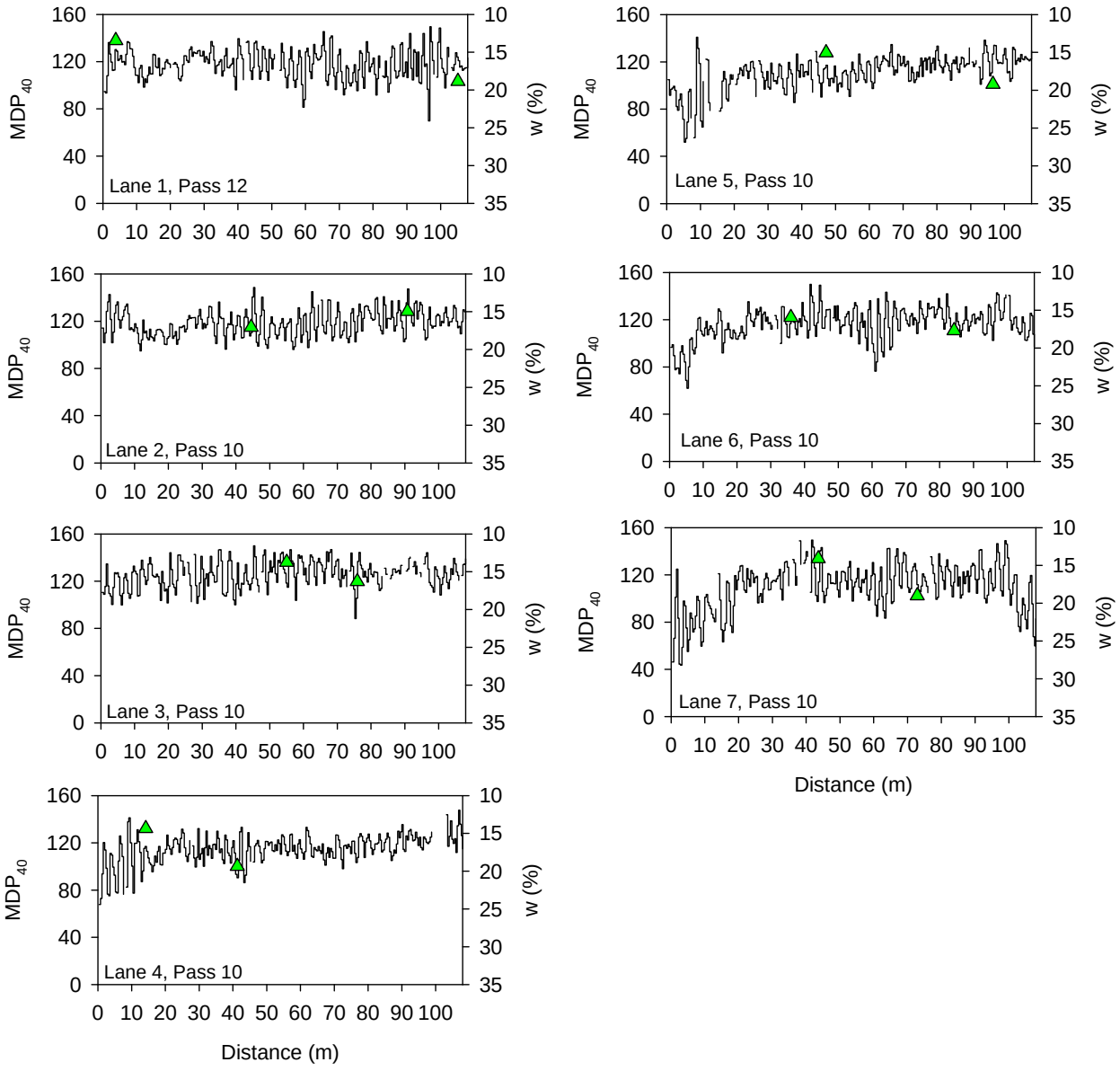

Figure 39. MDP_{40} and in-situ moisture content measurements on lift 3 after final pass – TB3

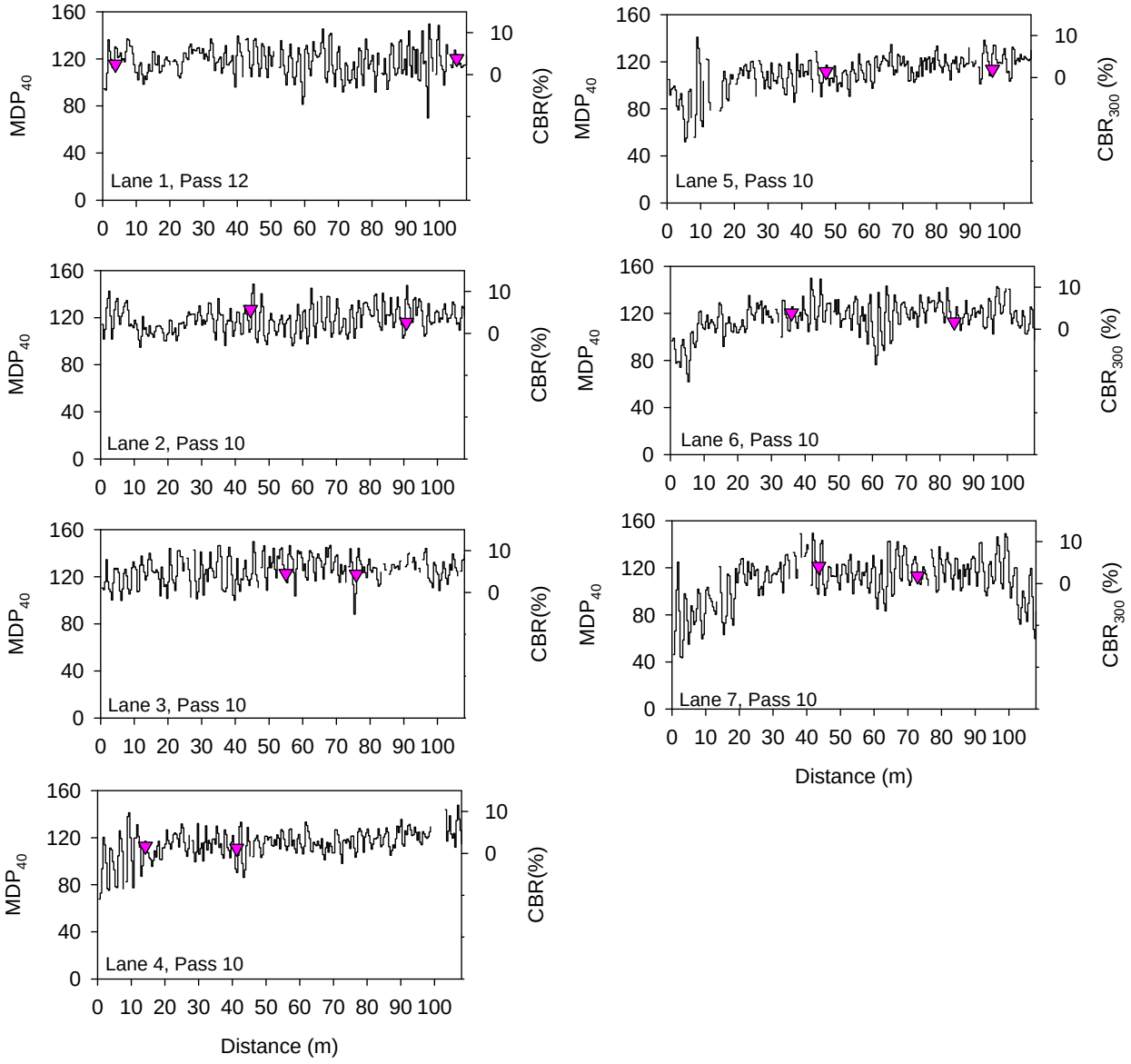

Figure 40. MDP_{40} and in-situ CBR_{300} measurements on lift 3 after final pass – TB3

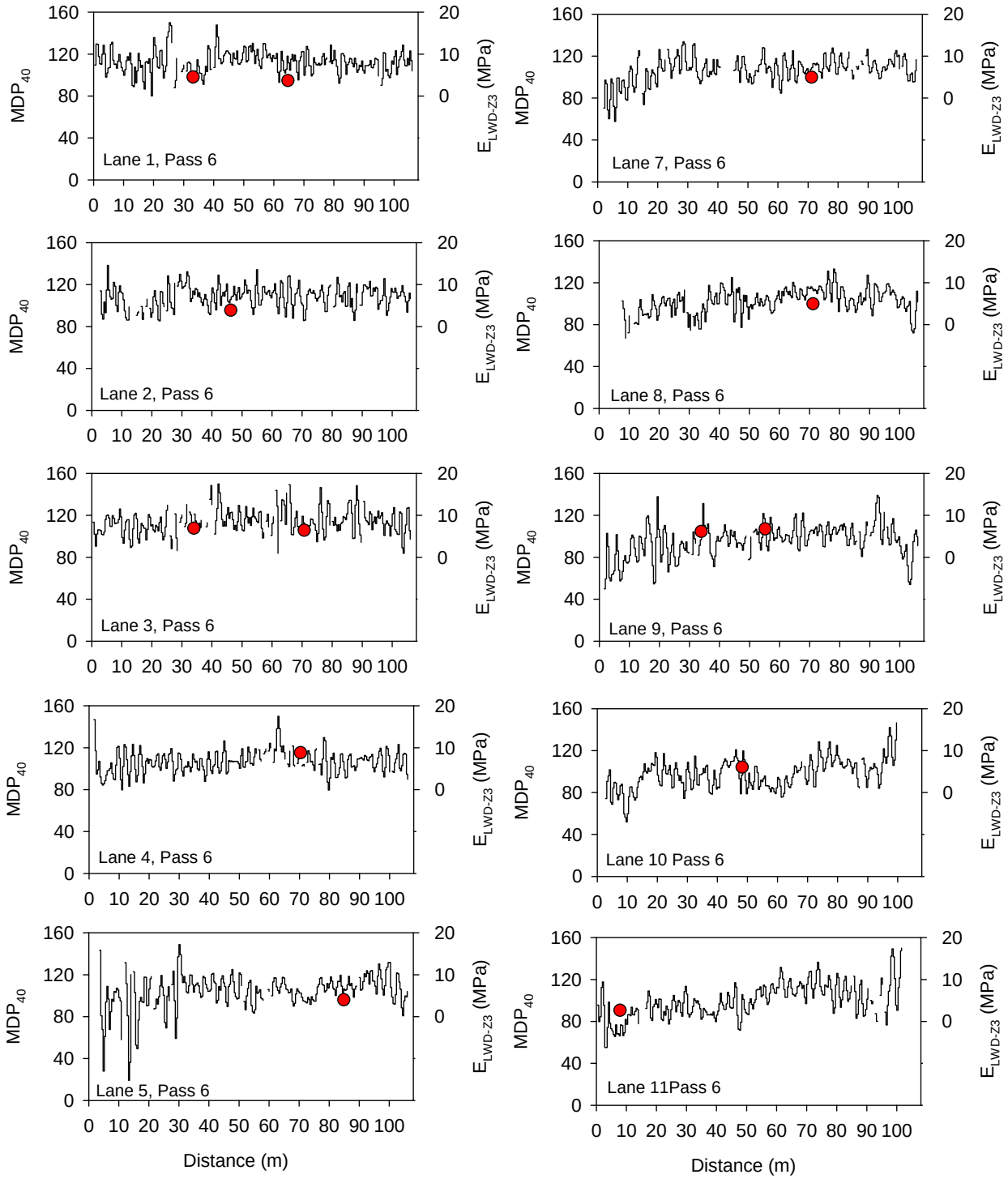

Figure 41. MDP_{40} and in-situ $E_{LWD\text{-}Z3}$ measurements on lift 4 after final pass – TB3

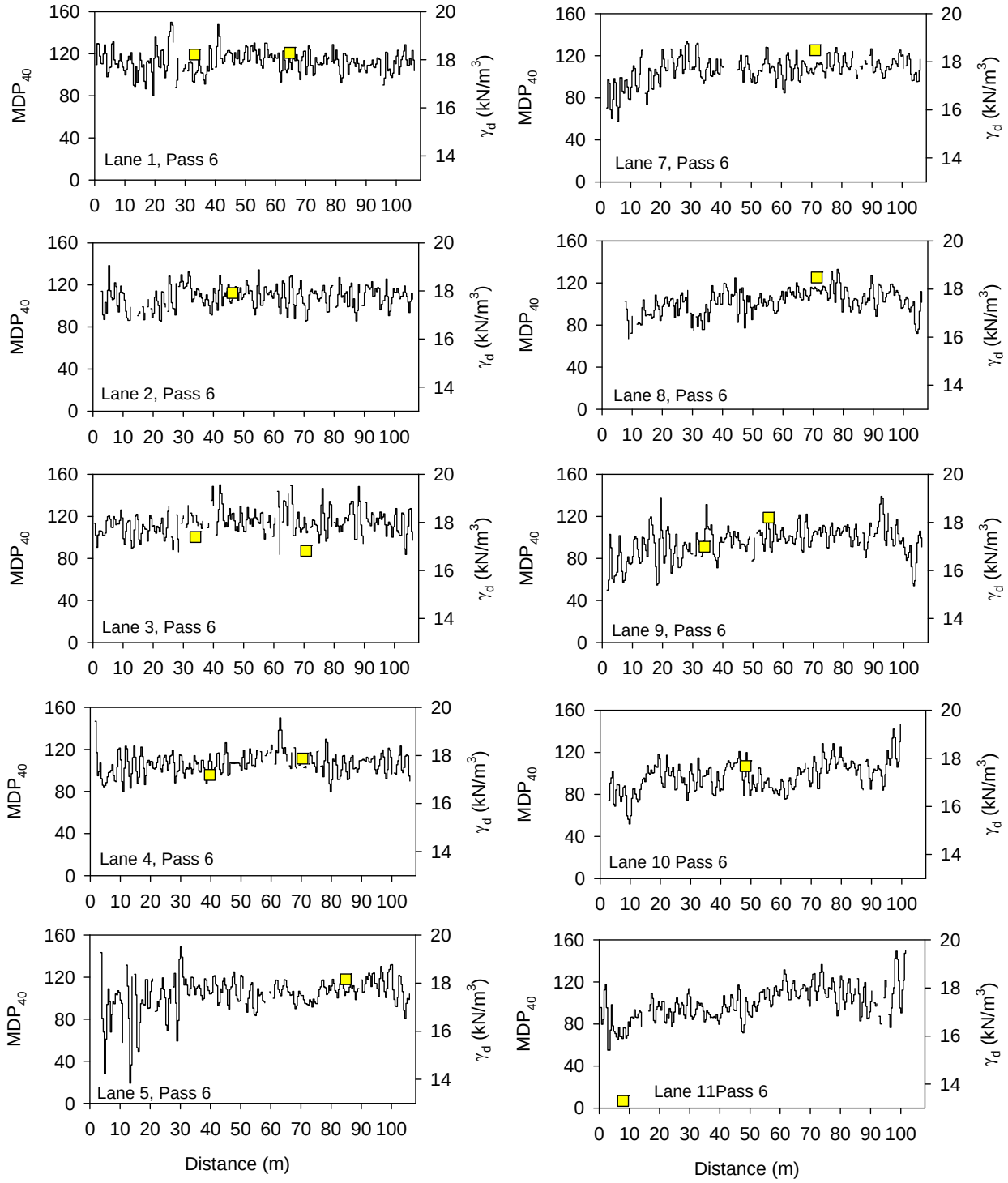

Figure 42. MDP_{40} and in-situ dry density measurements on lift 4 after final pass – TB3

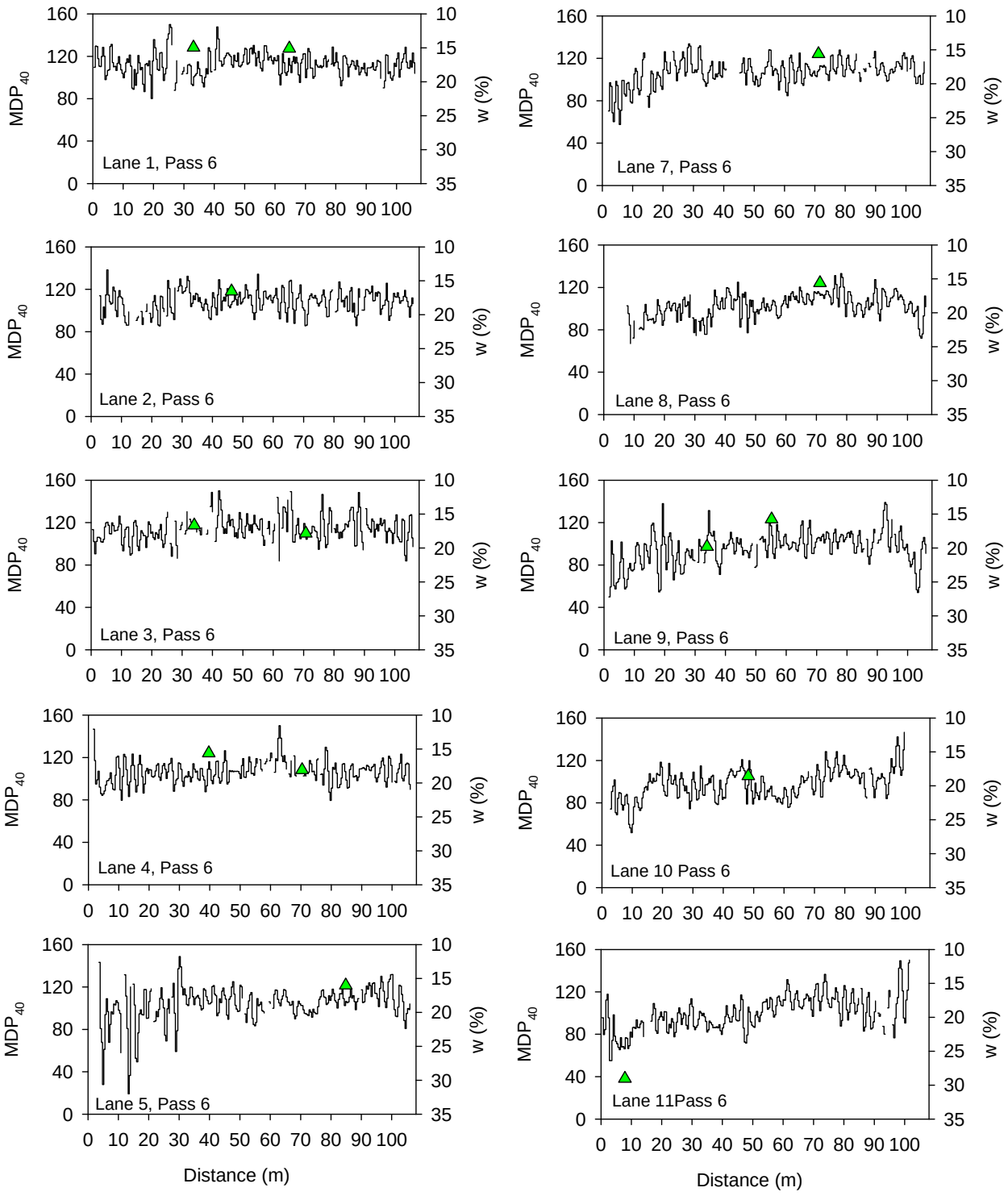

Figure 43. MDP_{40} and in-situ moisture content measurements on lift 4 after final pass – TB3

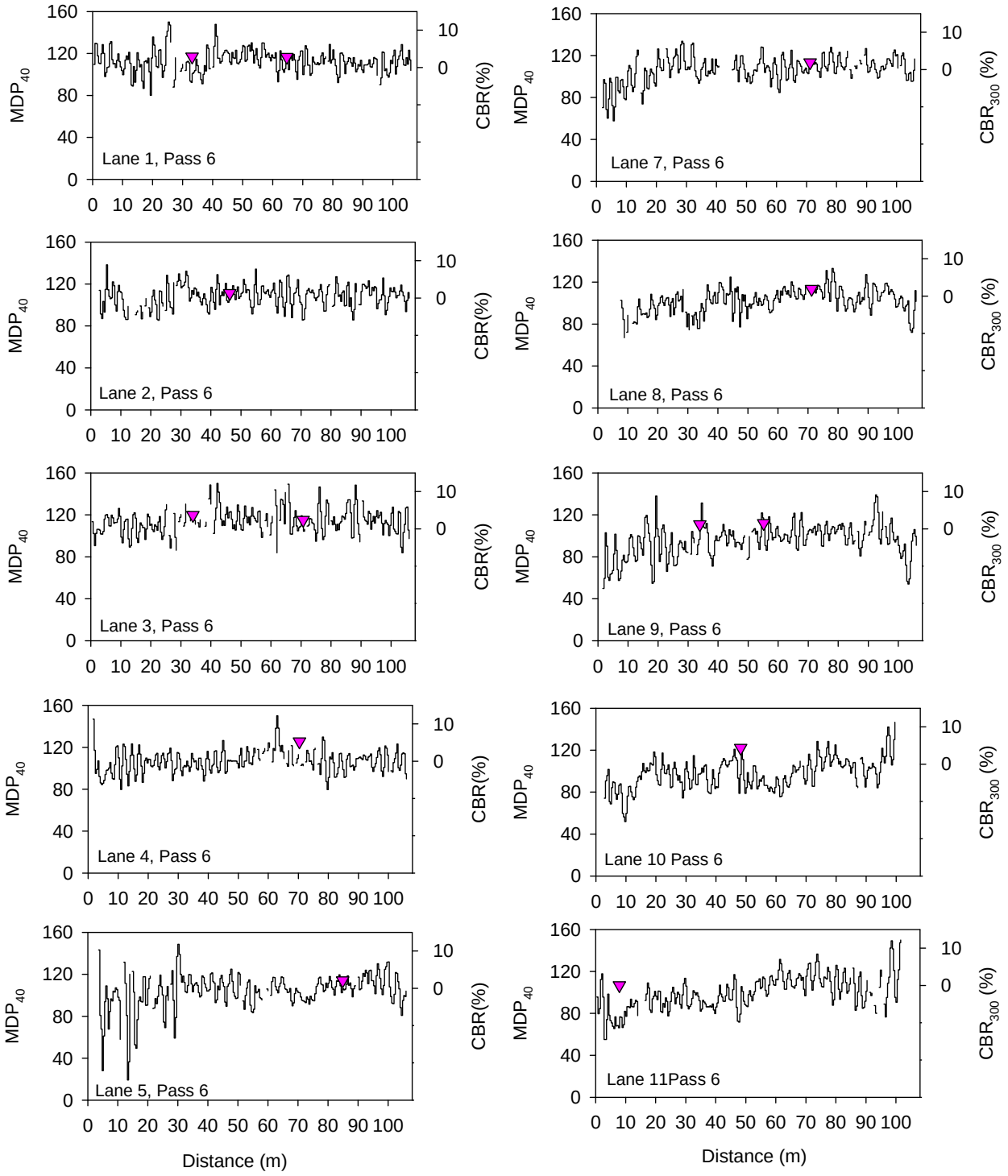

Figure 44. MDP_{40} and in-situ CBR_{300} measurements on lift 4 after final pass – TB3

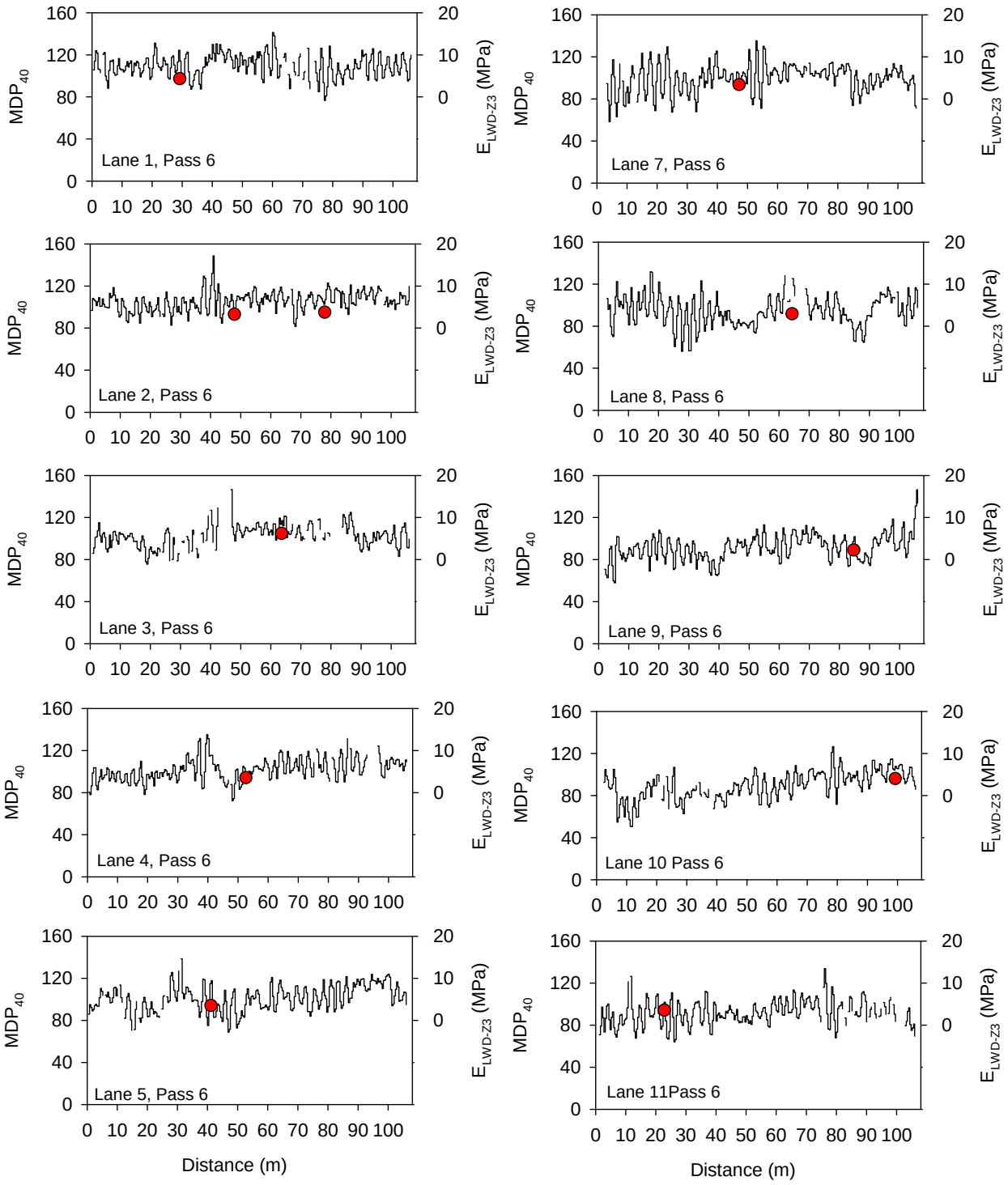

Figure 45. MDP_{40} and in-situ $E_{LWD\text{-}Z3}$ measurements on lift 5 after final pass – TB3

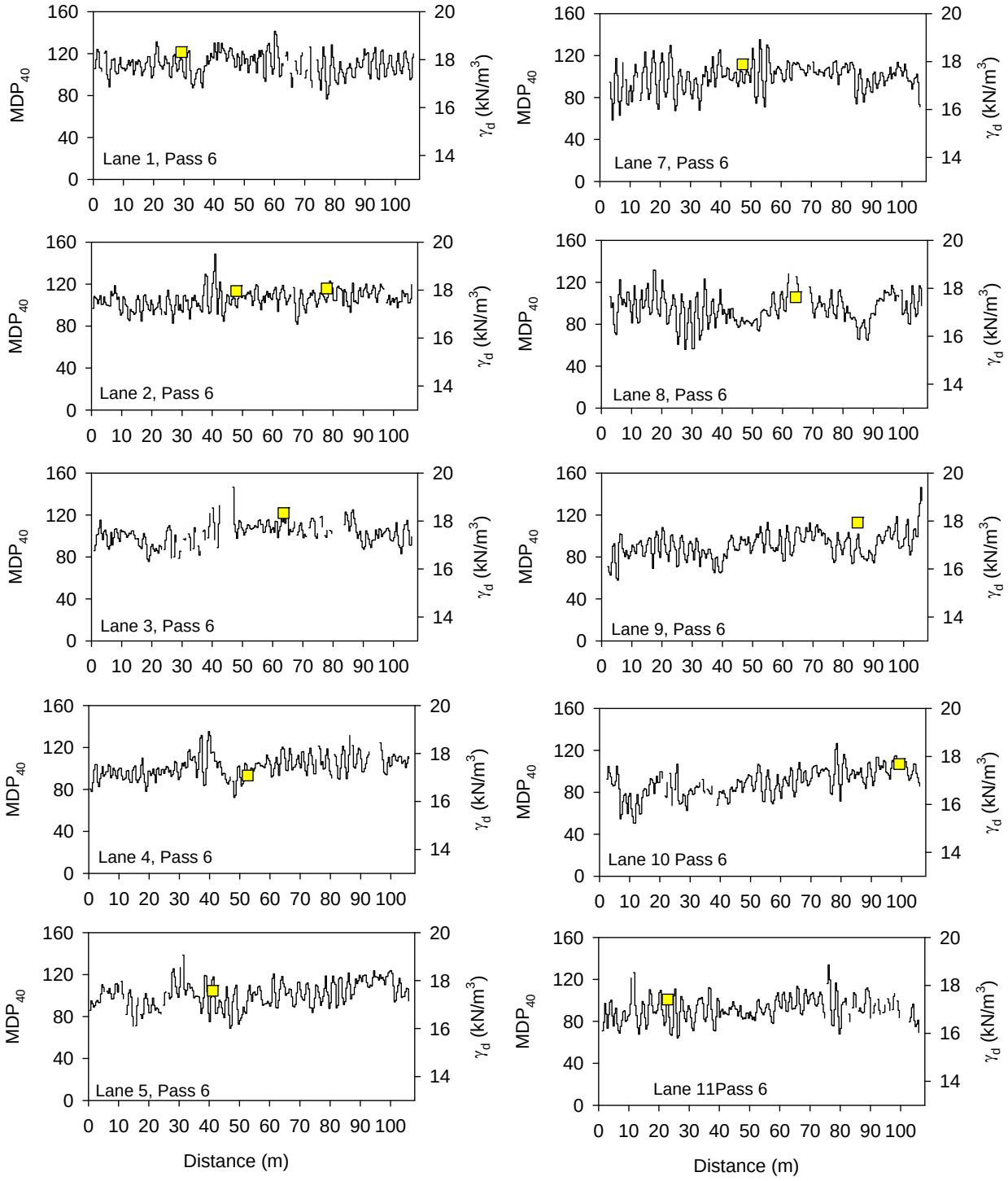

Figure 46. MDP_{40} and in-situ dry density measurements on lift 5 after final pass – TB3

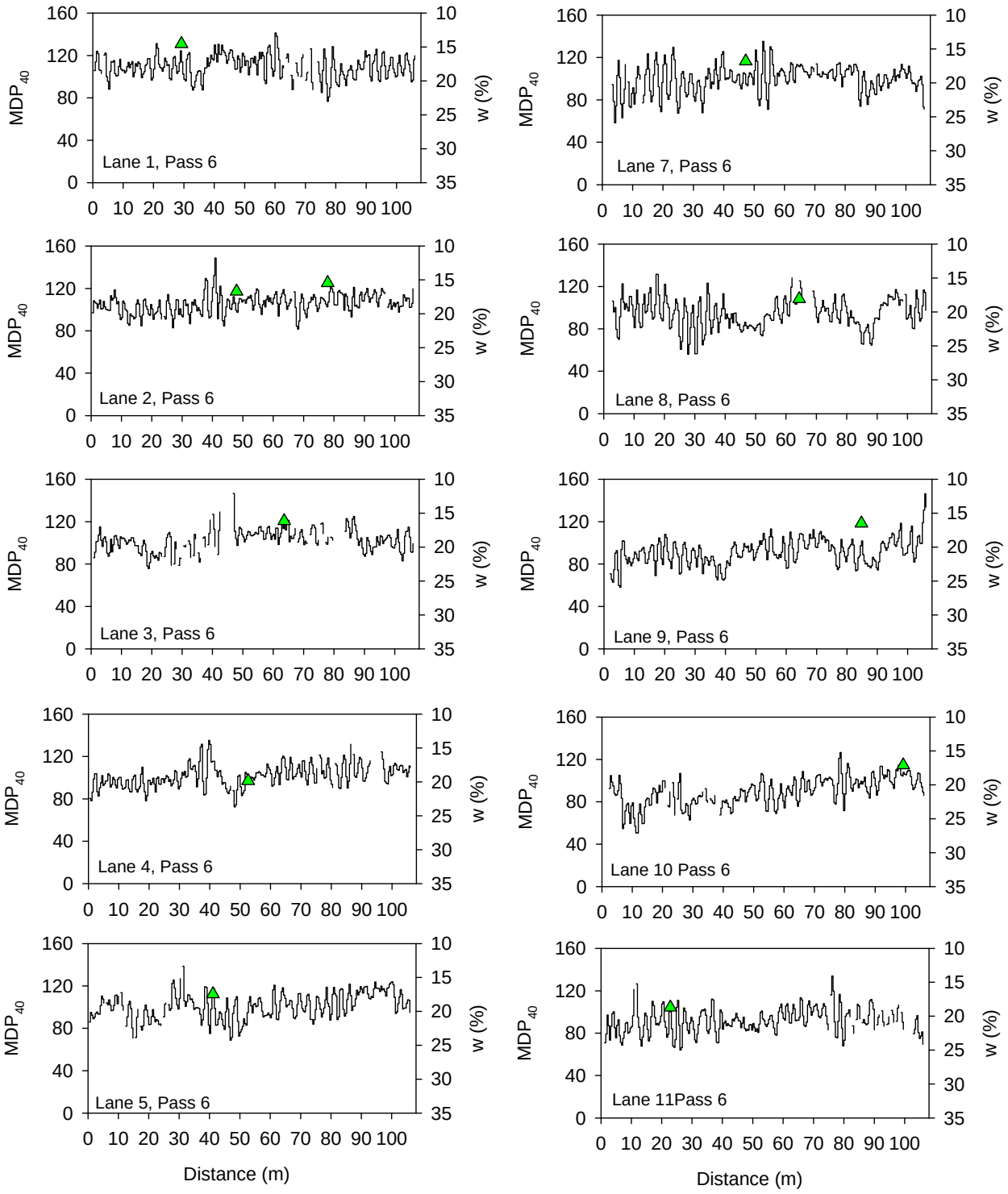

Figure 47. MDP_{40} and in-situ moisture content measurements on lift 5 after final pass – TB3

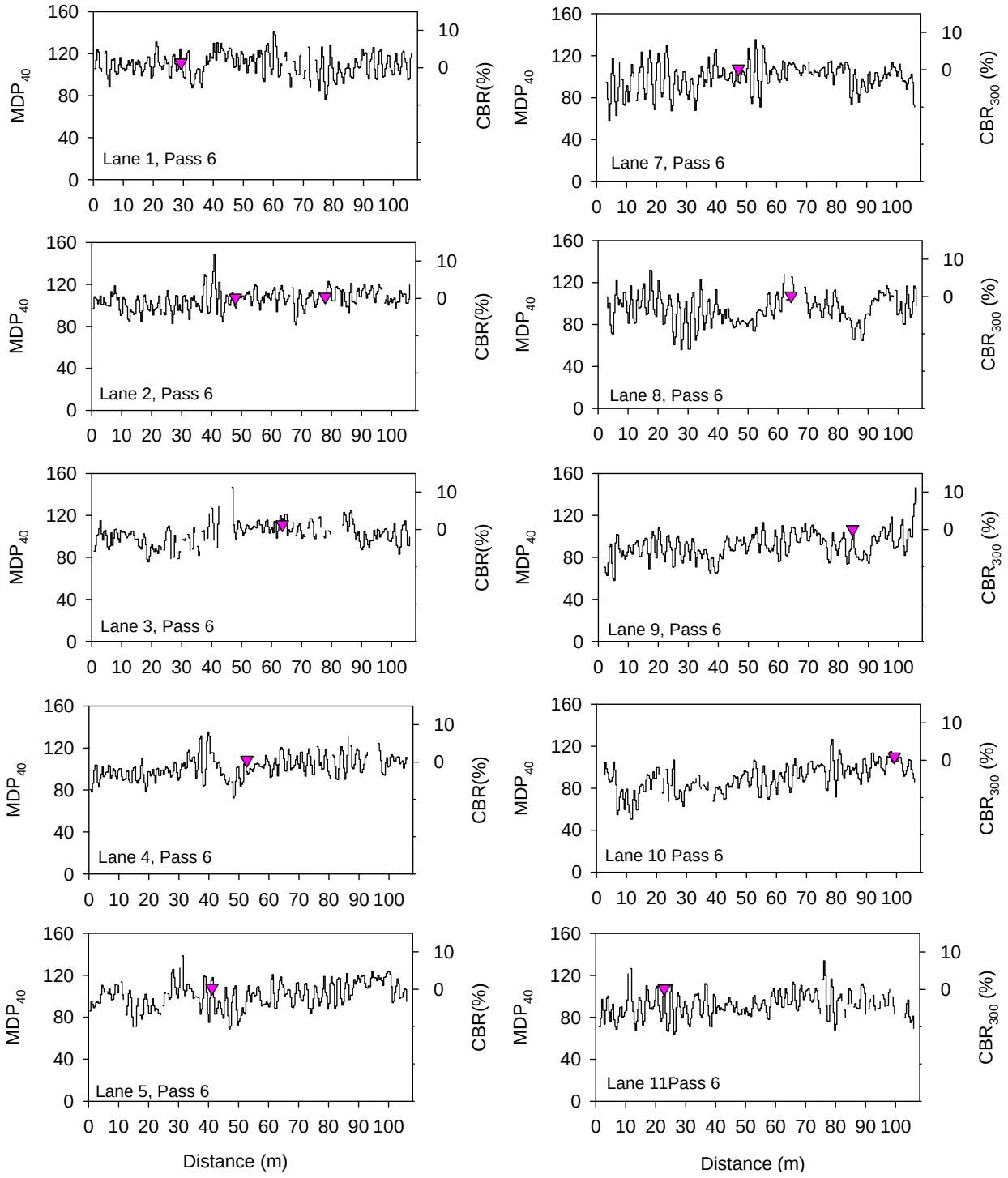

Figure 48. MDP_{40} and in-situ CBR_{300} measurements on lift 5 after final pass – TB3

Table 7. Summary statistics (univariate and spatial) of in-situ test results – TB3 (lifts 1 to 5)

Lift	Measurement Value	n	μ	σ	COV
1	MDP_{40} (full test area)	3128	97.4	17.1	18
	MDP_{40} (at in-situ test points)		Could not be obtained		
	Dry unit weight, γ_d (kN/m^3)	3	15.77	0.21	1
	Dry unit weight, γ_d (pcf)	3	100.4	1.3	1
	Relative compaction RC (%)	3	85.3	1.1	3
	Moisture content, *w* (%)	3	18.0	0.8	4
	Modulus, $E_{LWD\text{-}Z3}$ (MPa)	3	3.4	0.1	2
	CBR_{300} (%)	3	0.5	0.2	40
2	MDP_{40} (full test area)	2943	106.9	19.1	18
	MDP_{40} (at in-situ test points)	19	104.7	8.1	8
	Dry unit weight, γ_d (kN/m^3)	19	17.00	1.06	6
	Dry unit weight, γ_d (pcf)	19	108.2	6.7	6
	Relative compaction RC (%)	19	92.0	5.7	6
	Moisture content, *w* (%)	19	17.9	2.9	16
	Modulus, $E_{LWD\text{-}Z3}$ (MPa)	19	5.3	1.5	29
	CBR_{300} (%)	19	2.1	2.1	99
3	MDP_{40} (full test area)	2300	116.2	15.1	13
	MDP_{40} (at in-situ test points)	14	111.6	7.1	6
	Dry unit weight, γ_d (kN/m^3)	14	17.49	0.57	3
	Dry unit weight, γ_d (pcf)	14	111.4	3.6	3
	Relative compaction RC (%)	14	94.7	3.0	3
	Moisture content, *w* (%)	14	16.4	2.2	13
	Modulus, $E_{LWD\text{-}Z3}$ (MPa)	14	7.4	1.9	26
	CBR_{300} (%)	14	2.9	1.4	48
4	MDP_{40} (full test area)	3429	104.6	14.9	14
	MDP_{40} (at in-situ test points)	14	105.3	12.5	12
	Dry unit weight, γ_d (kN/m^3)	14	17.53	1.35	8
	Dry unit weight, γ_d (pcf)	14	111.6	8.6	8
	Relative compaction RC (%)	14	94.9	7.3	8
	Moisture content, *w* (%)	14	17.5	3.6	21
	Modulus, $E_{LWD\text{-}Z3}$ (MPa)	13	5.3	1.7	32
	CBR (%)	13	2.4	1.4	57
5	MDP_{40} (full test area)	3536	99.1	13.7	14
	MDP_{40} (at in-situ test points)	10	98.5	6.6	7
	Dry unit weight, γ_d (kN/m^3)	12	17.82	0.37	2
	Dry unit weight, γ_d (pcf)	12	113.5	2.3	2
	Relative compaction RC (%)	12	96.5	2.0	2
	Moisture content, *w* (%)	12	16.9	1.5	9
	Modulus, $E_{LWD\text{-}Z3}$ (MPa)	12	3.6	1.0	26
	CBR_{300} (%)	12	0.5	0.4	83

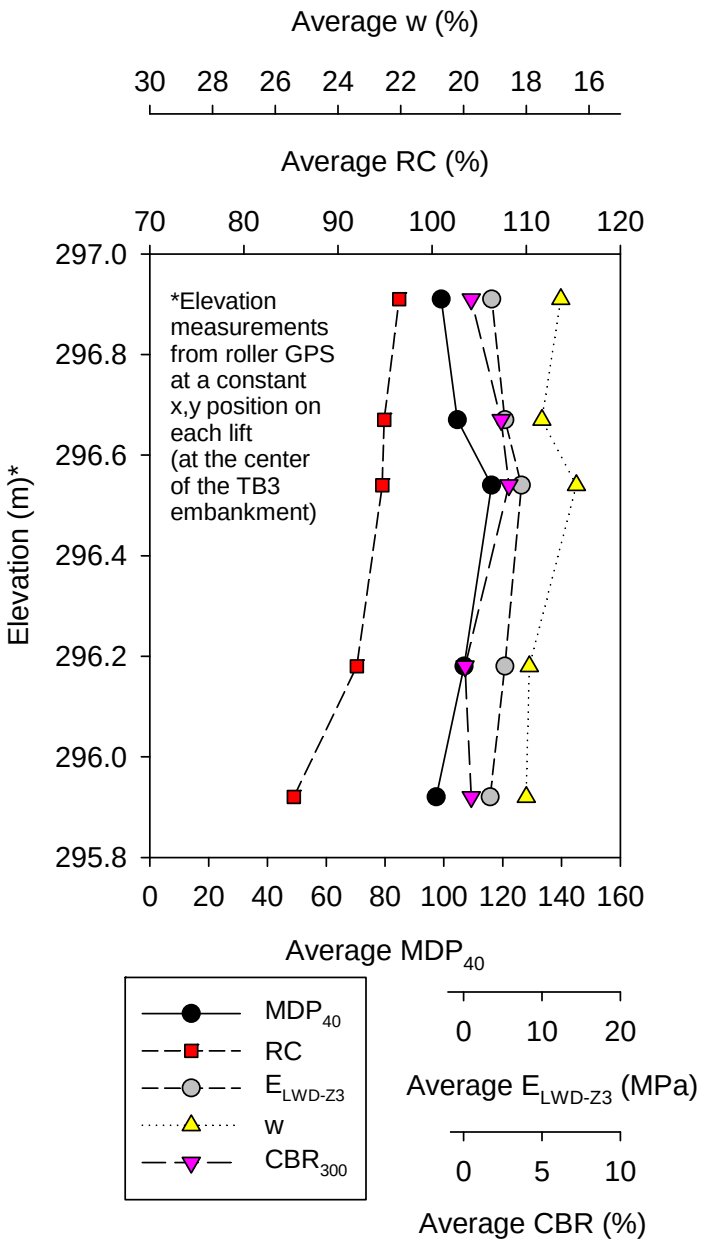

Figure 49. Average MDP_{40} and in-situ point measurements on lifts 1 to 5 – TB3

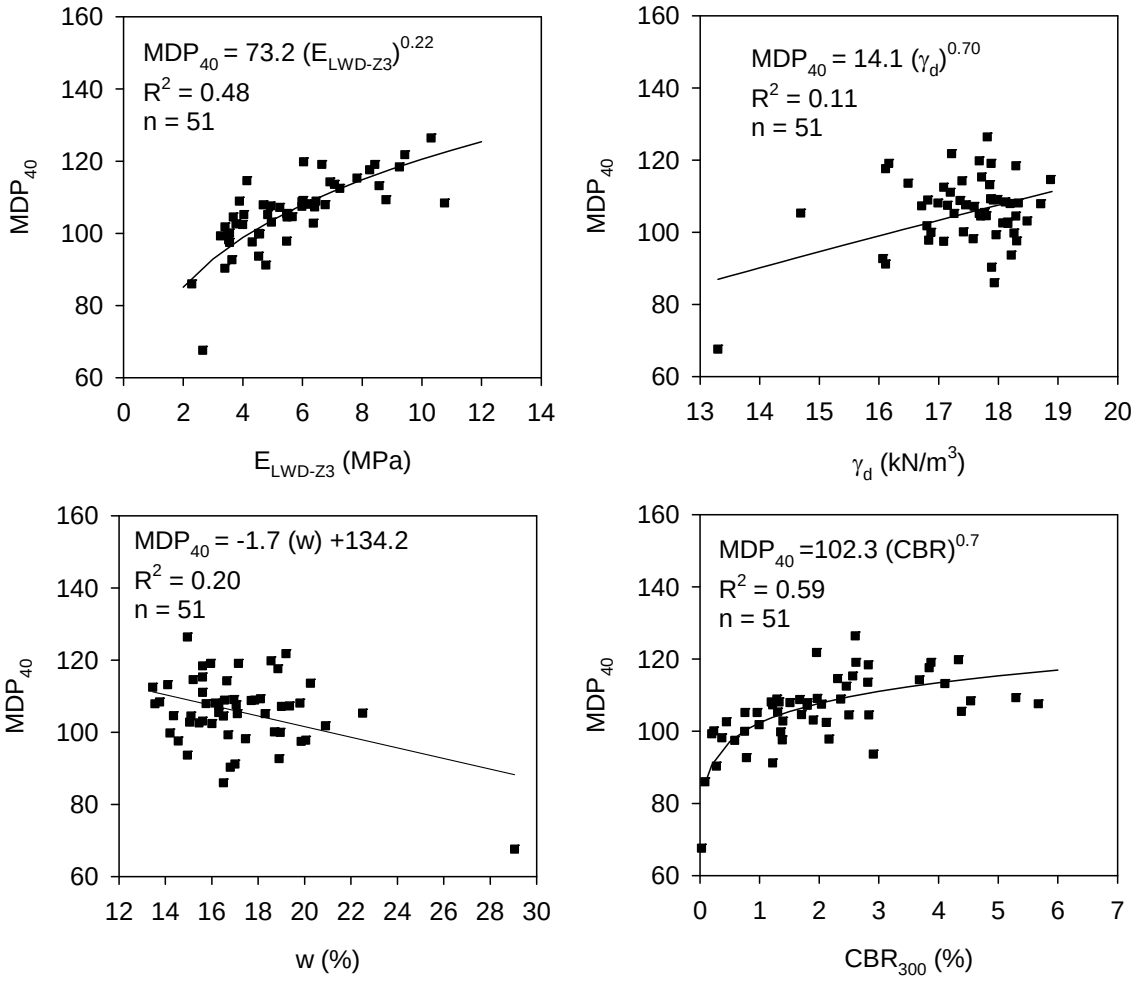

Figure 50. Correlations between MDP_{40} and in-situ point measurements – TB3

Combined Regression Analysis

The data obtained from multiple test beds are combined to develop site wide correlation results as presented in Figure 51. Non-linear power relationships showed the best fit for MDP_{40} relationships with E_{LWD-Z3} and CBR_{300} with $R^2 > 0.5$. Correlation between γ_d and MDP_{40} did not yield a statistically significant relationship. Correlation between MDP_{40} and *w* yielded a linear relationship with $R^2 = 0.20$.

Multivariate non-linear regression analysis was attempted on this dataset by combining the MDP_{40}-E_{LWD-Z3} power relationship and the MDP_{40}-*w* linear relationship to assess the influence of including a moisture content parameter in predicting MDP_{40}. Results from this analysis are presented in Figure 52, which showed $R^2 = 0.71$. This is a slight improvement over the MDP_{40}-E_{LWD-Z3} power model without the moisture content parameter ($R^2 = 0.63$). Similar analysis was performed for MDP_{40}-CBR_{300} dataset which showed that moisture content was a statistically significant parameter but did not show any improvement in the R^2 value (Figure 52). MDP-γ_d dataset combined with moisture content did not show a statistically significant relationship.

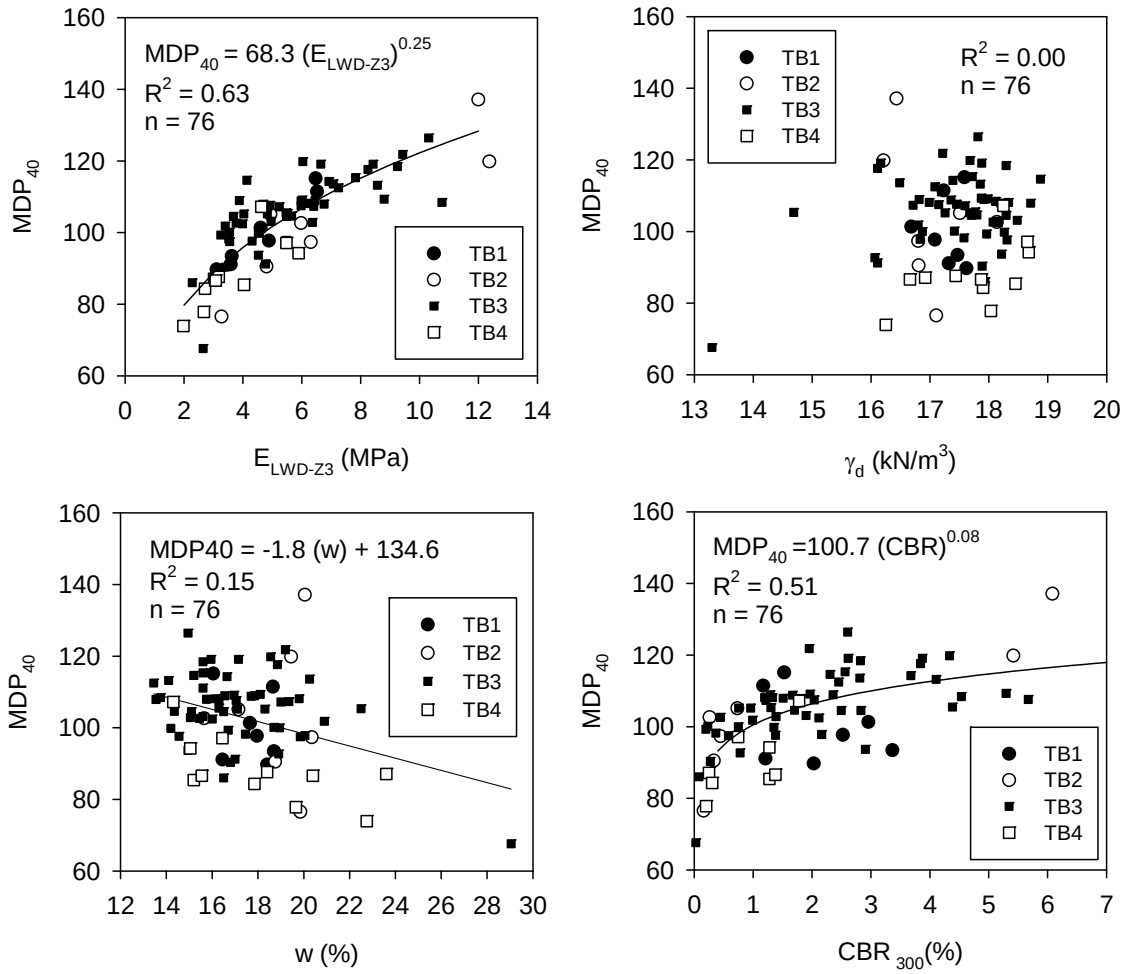

Figure 51. Correlations between MDP_{40} and in-situ point measurements (TBs 1, 2, 3,and 4) – US30 project

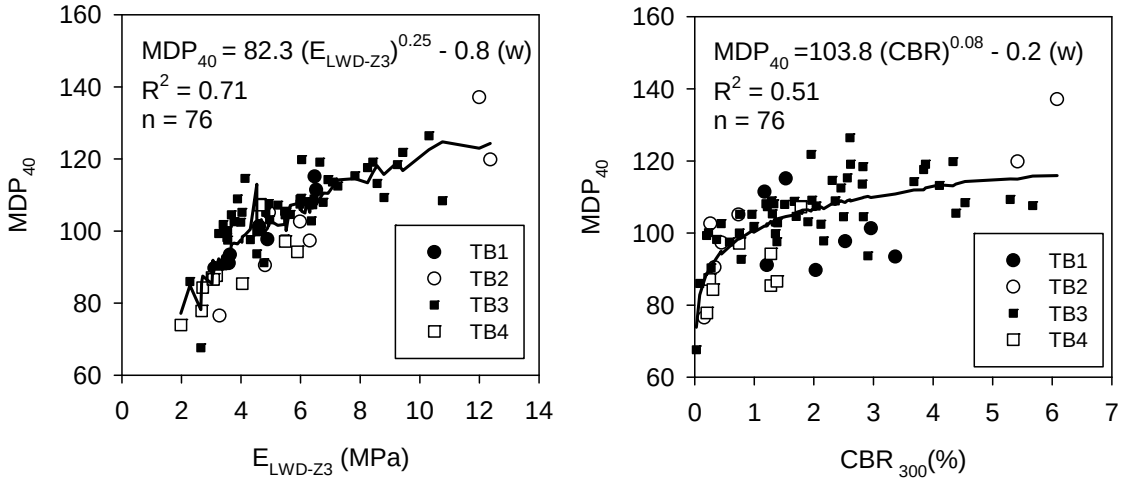

Figure 52. Multivariate non-linear regression analysis results – US30 project

Summary of Key Findings

Experimental test results and field observations from a demonstration project conducted on US30 near Colo, Iowa using Caterpillar IC padfoot roller equipped with MDP_{40} measurement system is presented above. The project involved construction and testing of four test beds wherein IC-MVs and in-situ point-MVs were obtained.

In summary, TB1 consisted of a one-dimensional test strip where multiple roller passes were performed to develop an IC-MV compaction curve and in-situ point-MVs were obtained after the final pass for correlation analysis. TBs 2 and 4 consisted of mapping areas with compacted subgrade material and obtaining point-MVs at locations selected based on IC-MV map on the on-board display. TB3 involved compaction of five lifts of subgrade fill in a production area and continuously monitoring the number of roller passes and IC-MVs. In-situ point-MVs were obtained following the final pass on each lift at locations selected based on the IC-MV map on the on-board display. Data obtained from each test bed was analyzed separately to develop correlations. In the end, data obtained from all the test beds were combined to develop site wide correlations over a wide measurement range. Following are some of the key findings from the analysis presented above.

- The moisture content of the subgrade materials was generally wet of optimum (about 5% wet of w_{opt}) and the relative compaction of the materials varied on average (per test bed) from 90% to 97% of standard Proctor γ_{dmax}. The material was in wet conditions due to frequent rain events at the time of project demonstration.
- MDP_{40} IC-MV compaction curves are affected by roller "off-tracking", i.e., roller operator not maintaining the same track as the previous pass.
- Spatial visualization of MDP_{40} IC-MV maps from multiple lifts in a production area (TB3) indicated that a "soft" zone with relatively low MDP_{40} values (< 70) on lift 1 reflected through the successive lifts 2, 3, 4, and 5 with similarly low MDP_{40} values in that zone. Geostatistical semivariogram analysis on MDP_{40} measurements on lifts 1 to 5 indicated that the variability reduced and the spatial continuity of the measurements improved from lifts 1 to 5 as demonstrated by a decrease in the sill and an increase in the range values.
- Regression analysis results indicated better correlations between MDP_{40} and $E_{LWD\text{-}Z3}$ and CBR_{300} point-MVs compared to γ_d measurements. Combining data from all test beds, MDP_{40} vs. $E_{LWD\text{-}Z3}$ and CBR_{300} yielded a non-linear power relationship with $R^2 > 0.50$. MDP vs. γ_d did not yield a statistically significant relationship. MDP_{40} measurements were somewhat sensitive to moisture content (MDP_{40} decreased with increasing w). Correlation between MDP_{40} and w yielded a linear relationship with $R^2 = 0.20$.
- Multivariate non-linear regression analysis was performed to assess the influence of including a moisture content parameter in predicting MDP_{40} from $E_{LWD\text{-}Z3}$ measurements. This analysis showed $R^2 = 0.71$, which is a slight improvement over the simple regression model without the moisture content parameter ($R^2 = 0.63$). Similar analysis was performed to predict MDP_{40} from CBR_{300} measurements, but it did not show any improvement in the R^2 value. MDP-γ_d dataset combined with moisture content did not show a statistically significant relationship.

CHAPTER 6: DEMONSTRATION PROJECT 2 — US218 CORALVILLE, IOWA

Project Description

This demonstration project was located on US218 (Figure 53) from one mile south of Riverside Drive to I-80 in Johnson County, Iowa (Sta. 338+80 mile post 89.05 to Sta. 1162+00 mile post 97; Iowa DOT project number NHSX-218-4(35)--3H-52). The project involved HMA resurfacing over the existing portland cement concrete (PCC) pavement. The DOT QA requirements were to achieve a relative compaction of 95% of the bulk specific gravity (G_{mb}). The ISU research team was present on-site periodically during paving operations for three days (August 31 to September 2, 2009) to observe the paving operations and conduct in-situ testing. During this time, compaction occurred on south bound from I-80 interchange to mile post 92 (which is about 1 mile south of the Melrose Avenue bridge) on the intermediate course layer. HMA 30M mix type was utilized for this layer. Core samples for density and bulk samples for gradation tests were obtained by the DOT personnel from random locations. The HMA intermediate course layer (38 mm (1.5 in) in thickness) was compacted using two Sakai dual drum rollers in the breakdown position. Only one of the two breakdown rollers was equipped with the IC monitoring system. The IC system included monitoring roller pass coverage and IC-MVs (Sakai CCV), and displaying data in real time on the on-board display monitor located in front of the roller operator. A temperature sensor was present on the roller and the readings were linked to GPS measurements to provide a continuous record of the temperature of HMA surface.

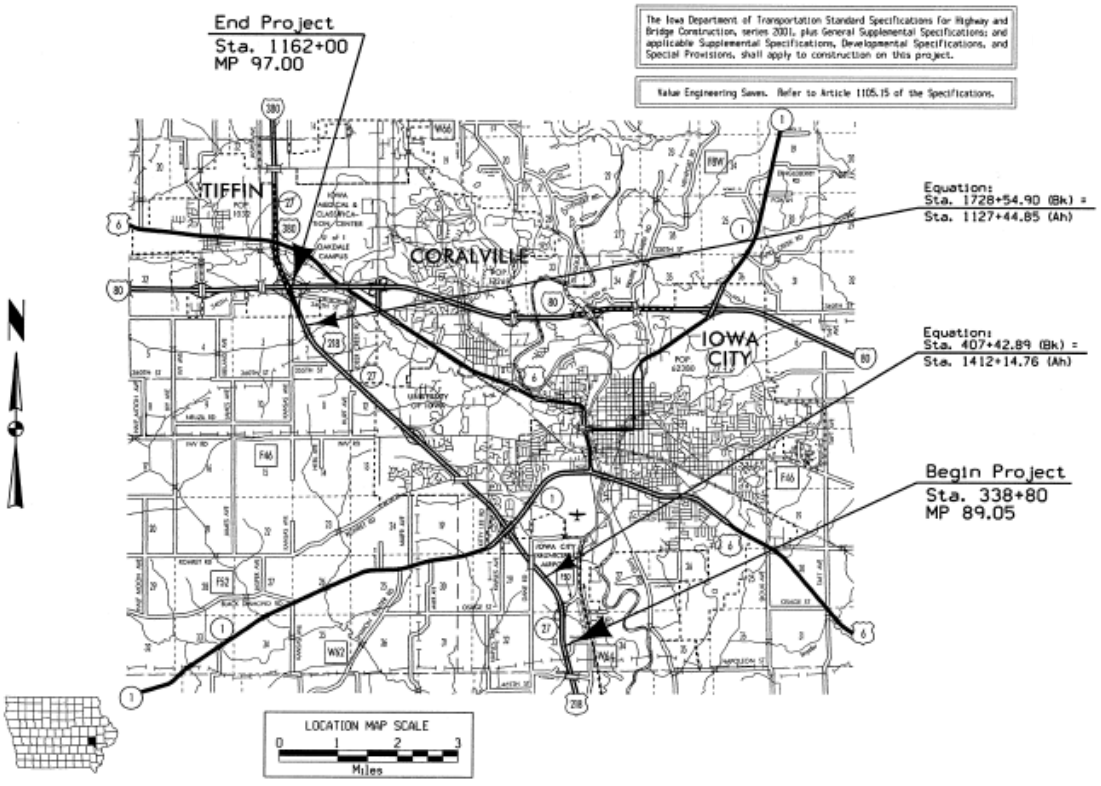

Figure 53. Project location map – US218 demonstration project

Experimental Testing

A summary of the test beds and testing performed on the project is provided in Table 4. On day 1, the compaction monitoring system on the roller was switched on but the on-board display monitor was closed for viewing by the operator. On days 2 and 3, the roller operator was allowed to use the on-board display to aid in "uniform" roller pass coverage. The roller operator was instructed to perform four passes (two forward and two reverse passes). The two Sakai rollers on the project were generally following each other resulting in a total of eight roller passes (again, note that compaction monitoring was available on only one roller). On day 3, in-situ point-MVs (RC and $E_{FWD\text{-}K3}$), and asphalt mat temperature measurements using a FLIR thermal imaging camera (T_{FLIR}) provided by the Iowa DOT and infrared camera mounted on the FWD trailer (T_{FWD}), were obtained. RC values were obtained by using a bulk specific gravity G_{mb} = 2.41 (23.63 kN/m^3, 150.4 pcf) value provided by the Iowa DOT. Point-MVs were obtained on mainline and over the shoulder lane. Photographs of construction operations and in-situ testing are provided in Figure 54.

Table 8. Summary of test beds and in-situ testing

TB	Date	Theoretical Amplitude (mm), Frequency (vpm), Speed (km/h)*	In-situ Test Measurements	Comments
1	08/31 to 09/01	0.30, 4000, 4	—	Display unit was covered – Blind study
2	09/01 to 09/02	0.30, 4000, 4	—	Display unit was open to the roller operator
3	09/02 to 09/03	0.30, 4000, 4	$E_{FWD\text{-}K3}$, RC, T_{FWD}, T_{FLIR}	Display unit was open to the roller operator. In-situ tests performed on mainline and shoulder shortly after compaction.

Notes: TB – test bed, * nominal, γ_d – dry unit weight using the Humboldt nuclear gauge, $E_{FWD\text{-}K3}$ – elastic modulus determined using 300 mm diameter plate KUAB falling weight deflectometer (FWD), T_{FWD} – temperature determined from thermal camera mounted on the FWD, T_{FLIR} – temperature measured using the FLIR thermal camera.

Figure 54. Photographs of paving operations and compaction, and in-situ testing

In-Situ Test Results and Analysis

Pass coverage and CCV maps from days 1, 2, and 3 generated from the Sakai Aithon MT software are presented in Figure 55 to Figure 60. FLIR thermal images showing spatial variation in the asphalt surface temperatures are presented in Figure 61. Histogram plots of roller pass coverage data, temperature, and CCV data obtained from days 1, 2, and 3 are presented in Figure 62. The histogram plots did not reveal any significant differences in the number of roller passes, temperature, and CCV from the three days. To further analyze any differences in the "uniformity" of pass coverage between days 1 to 3, geostatistical semivariograms of number of roller passes are developed as shown in Figure 63. The semivariograms indicate improved uniformity in pass coverage on day 3 compared to day 1. This is a significant finding which provides quantitative evidence of improvement in compaction operations by viewing the data in real time.

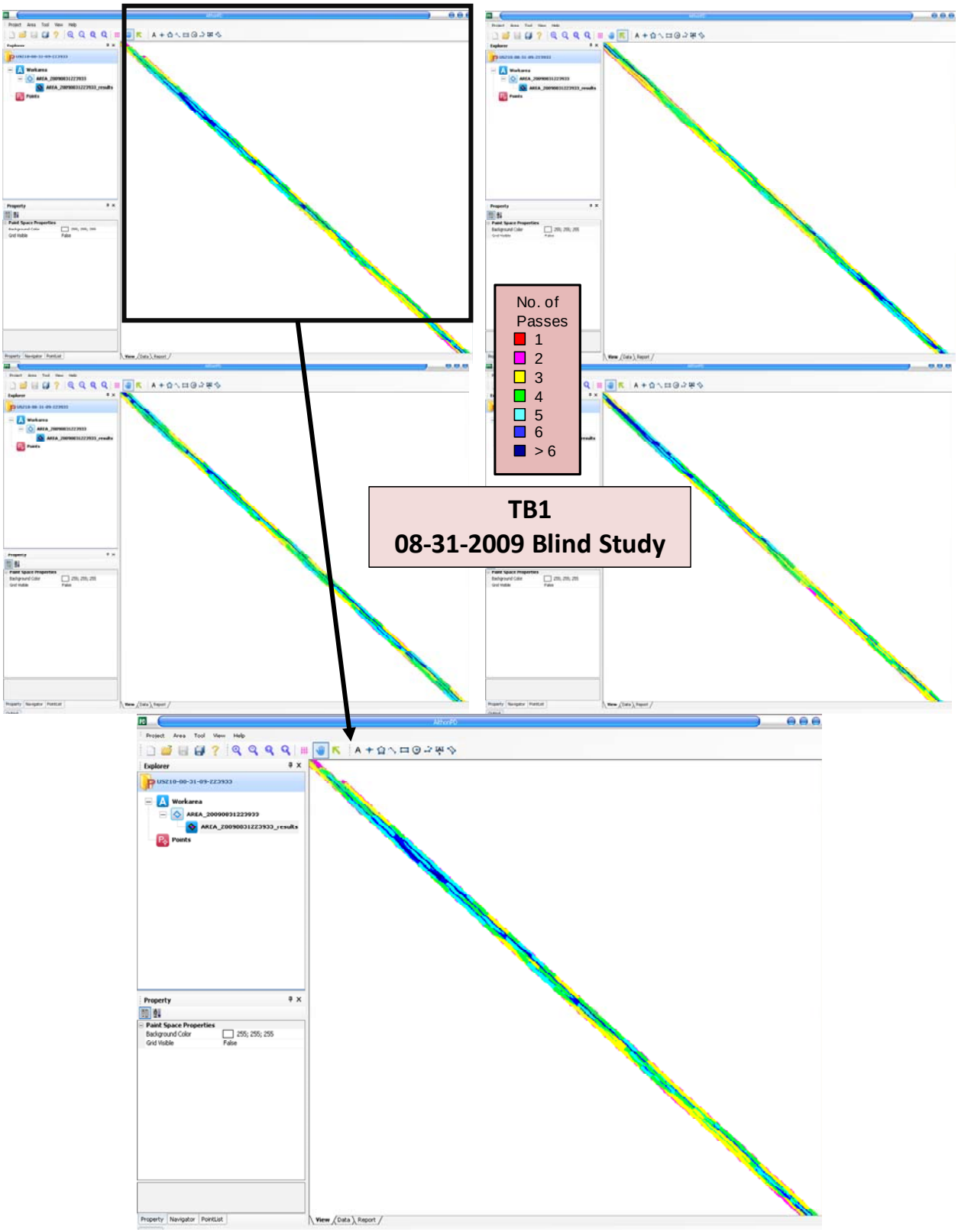

Figure 55. Example pass coverage maps from day 1 blind study – TB1 (approximate mile posts 95 to 97)

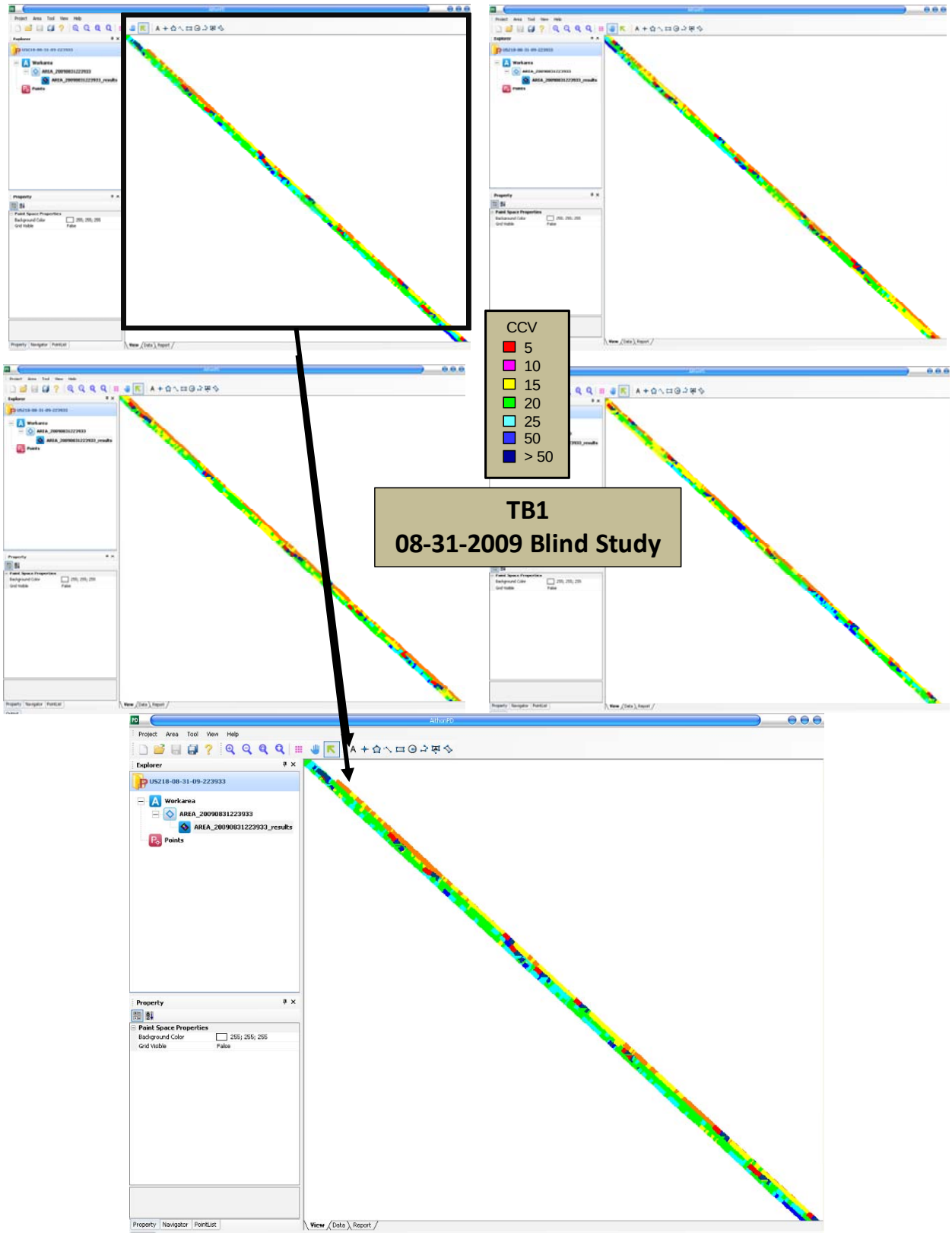

Figure 56. Example CCV maps from day 1 blind study – TB1 (approximate mile posts 95 to 97)

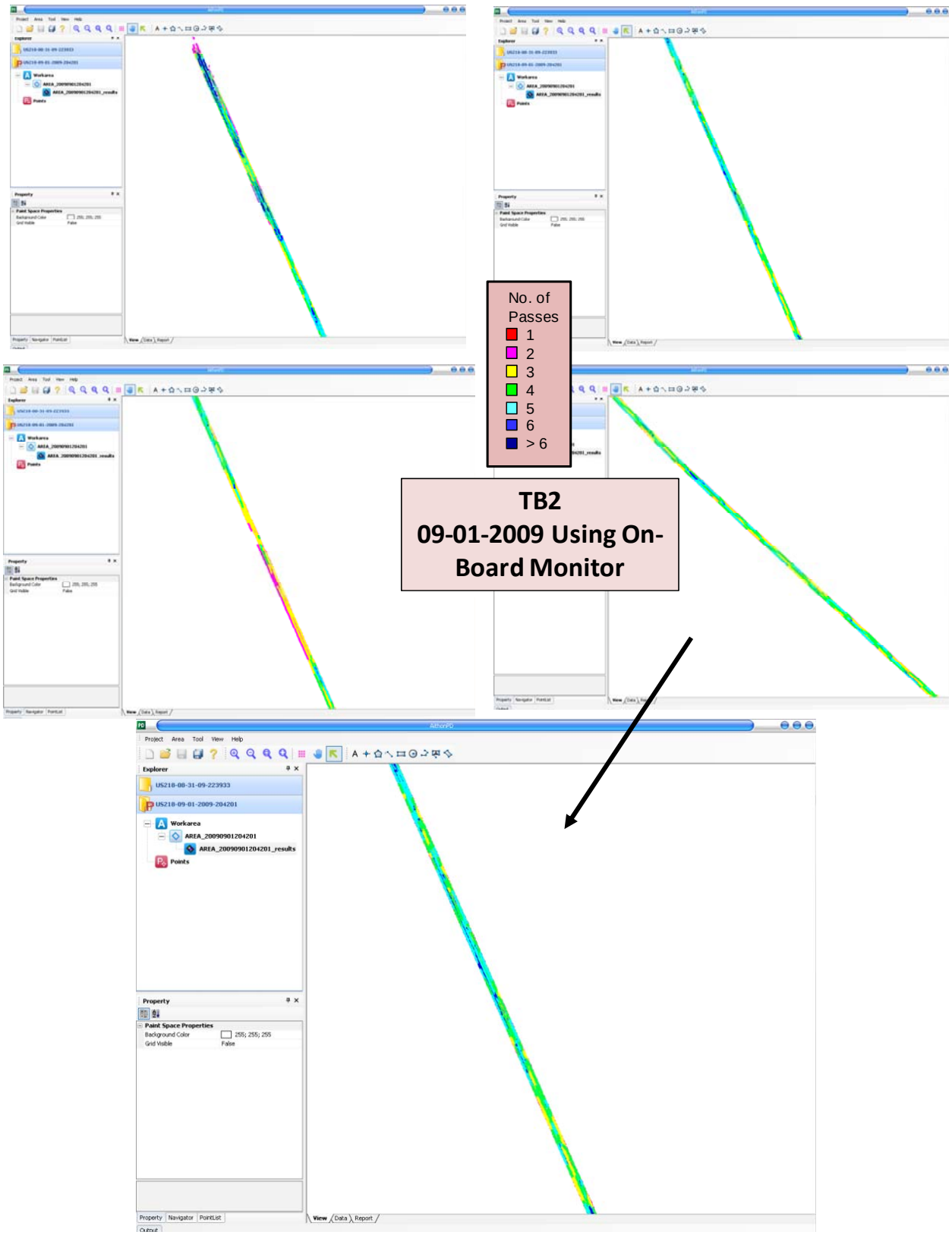

Figure 57. Example pass coverage maps from day 2 with operator using on-board monitor – TB2 (approximate mile posts 95 to 92)

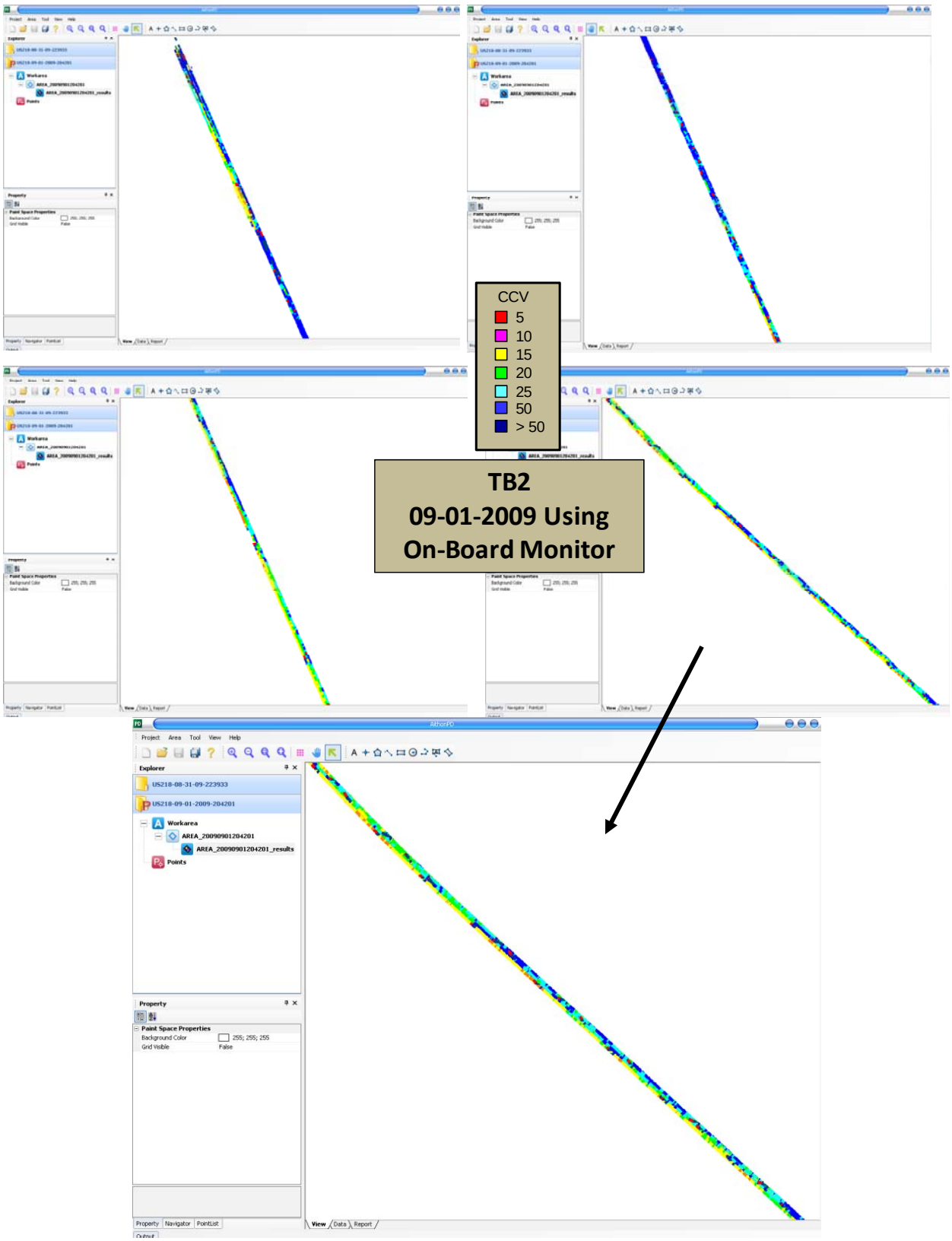

Figure 58. Example CCV maps from day 2 with operator using on-board monitor – TB2 (approximate mile posts 95 to 92)

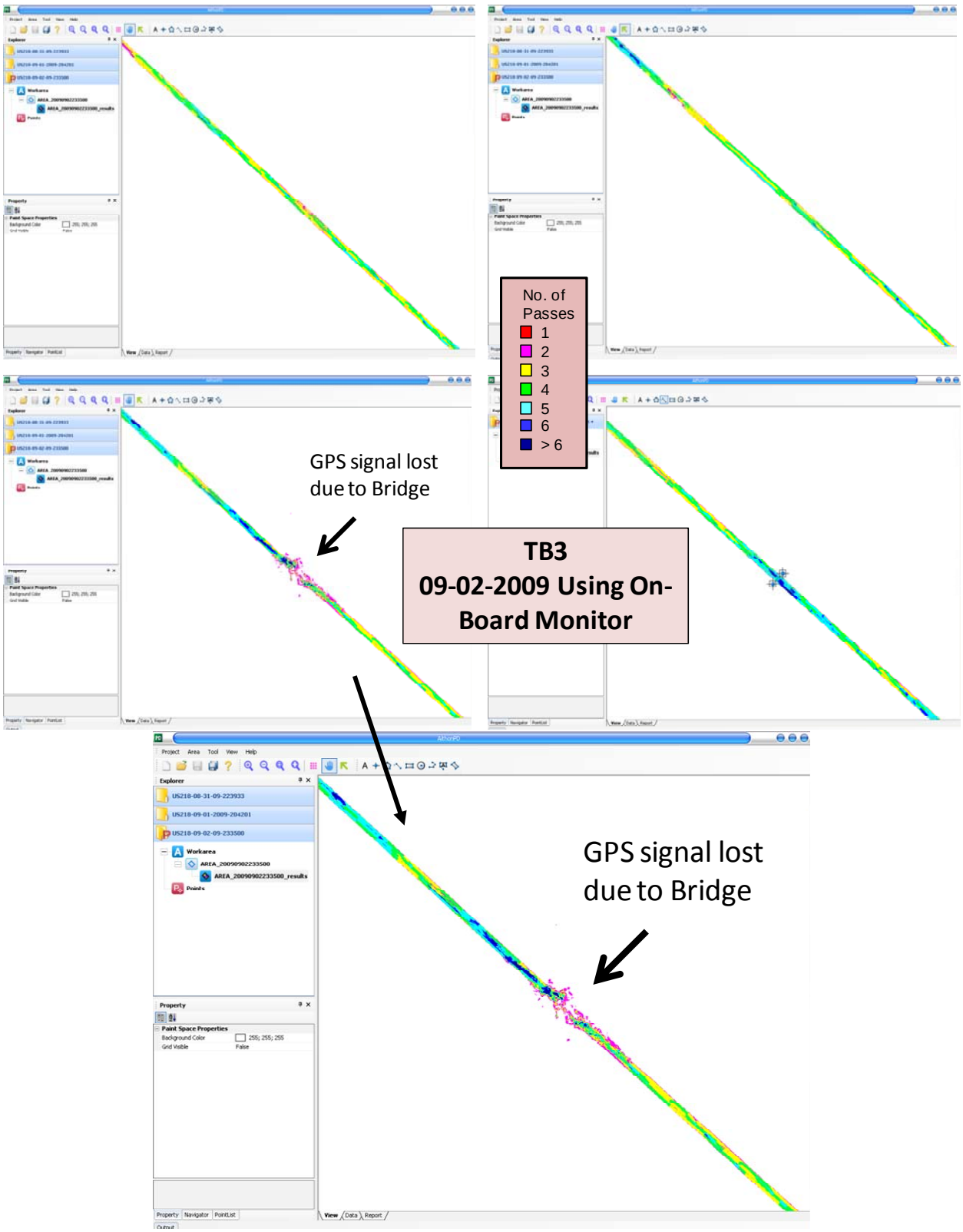

Figure 59. Example ass coverage maps from day 3 with operator using on-board monitor – TB3 (note: the bridge is at the Melrose Avenue interchange)

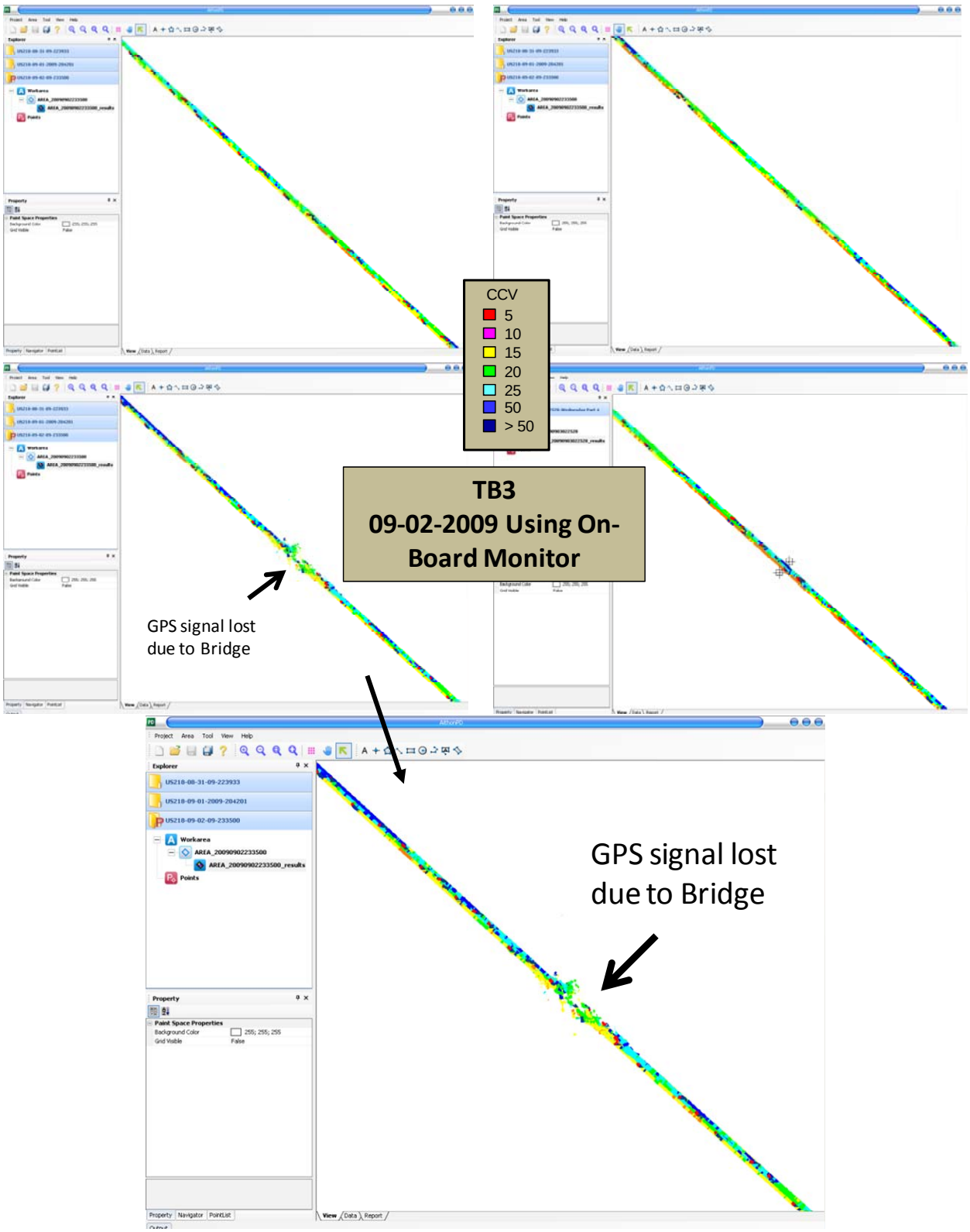

Figure 60. Example CCV maps from day 3 with operator using on-board monitor – TB3 (note: the bridge is at the Melrose Avenue interchange)

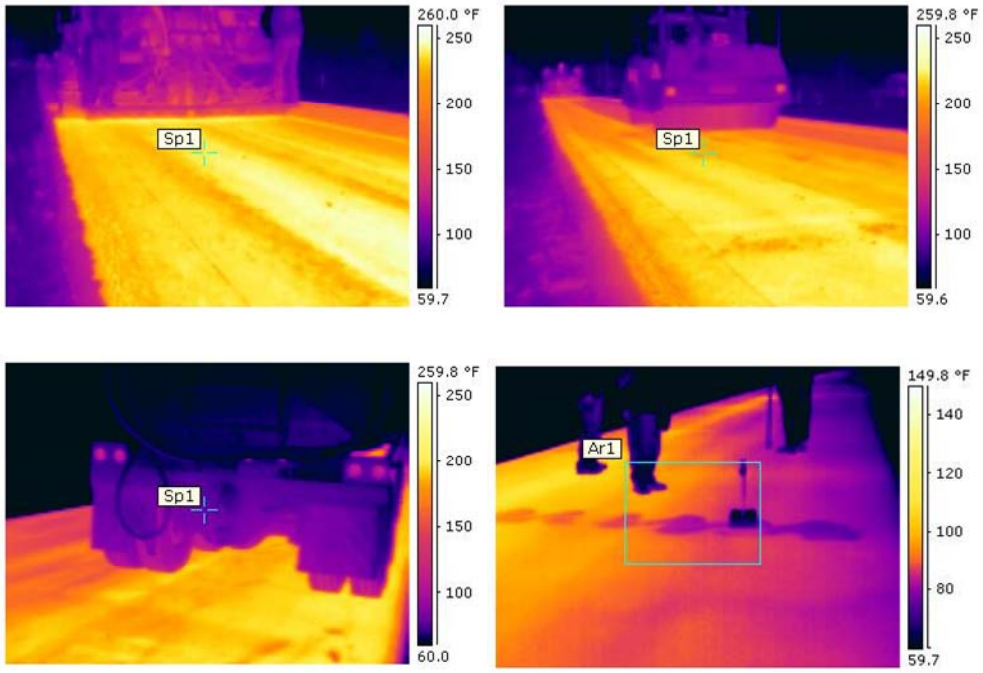

Figure 61. FLIR thermal images: in front of paver (top left), in front of break down roller (top right), behind water truck during finish rolling (bottom left), and nuclear gauge testing on the final compacted surface (bottom right)

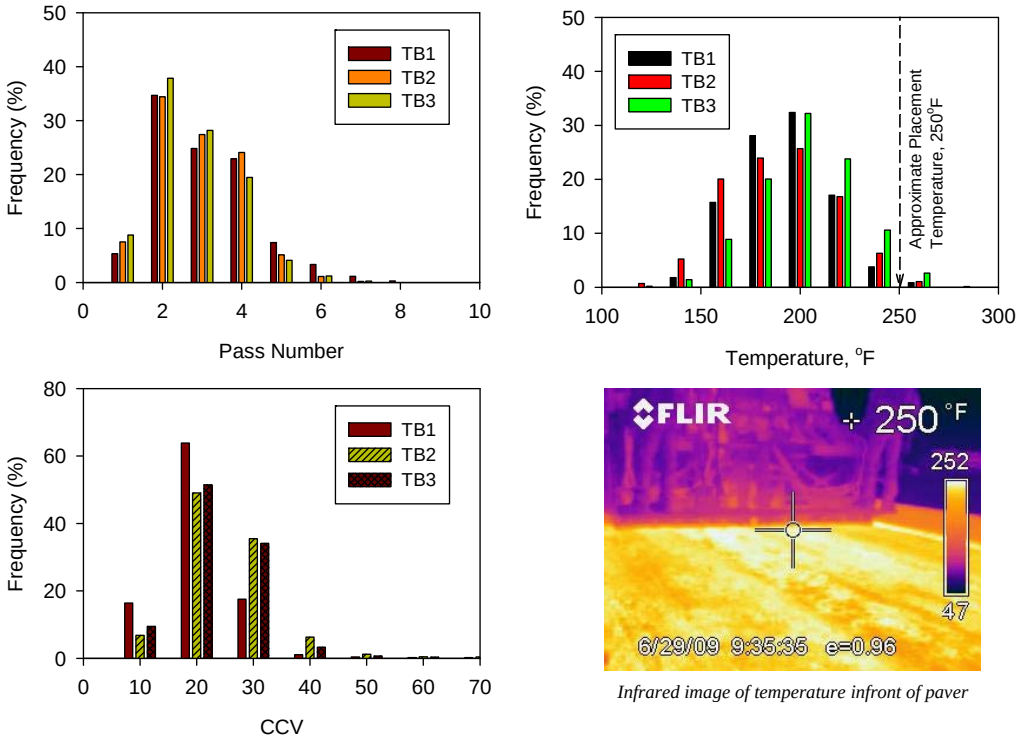

Infrared image of temperature infront of paver

Figure 62. Histogram plots of number of passes, measured temperature, and CCV measurements from the IC rollers from TBs 1, 2, and 3

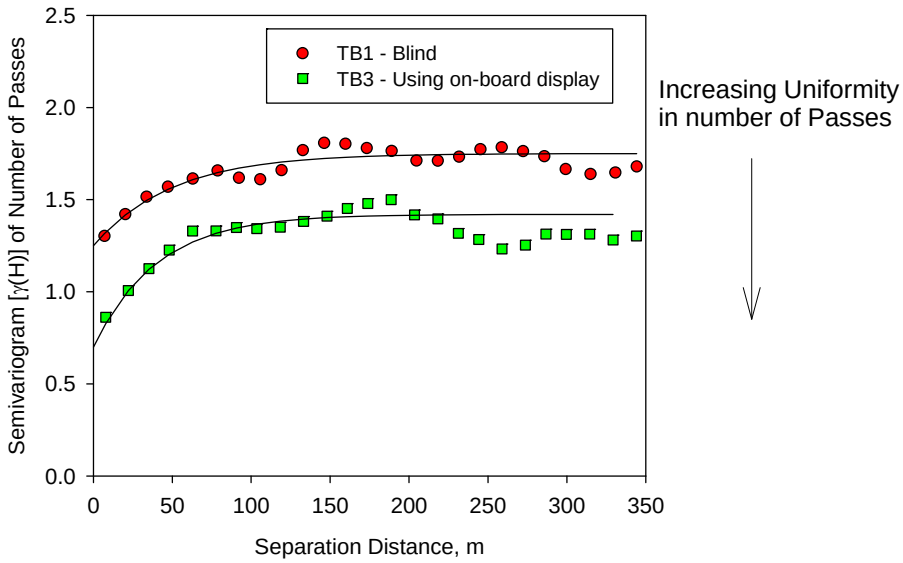

Figure 63. Comparison of semivariogram of number of roller passes from day 1 (TB1 – blind study) and day 3 (with aid of on-board monitor) assessing uniformity in pass coverage

T_{FLIR} and RC measurements were obtained at two locations with several measurements across the pavement width (including mainline and shoulder) at each location. These results are presented in Figure 64 along with the CCV map at one test location (location 2). Results indicated that the HMA temperature on the shoulder was on average about 29°F warmer than on the mainline. The RC of the HMA layer on the shoulder was on average about 6% lower than on the mainline. These differences in temperature and RC measurements are because of greater HMA layer thickness on the shoulder lane compared to the mainline.

RC, E_{FWD-K3}, and T_{FLIR} in-situ point-MVs obtained at 50 test locations along a stretch of about 1.3 km on mainline and shoulder lane are compared with roller CCV measurements in Figure 65. Similar to observations described above, the HMA temperature on the shoulder was on average about 17°F warmer than on the mainline. The RC of the HMA layer on the shoulder was on average about 6% lower than on the mainline. On average, E_{FWD-K3} on the mainline was about 5 times greater than on the shoulder lane. Similarly, the average CCV on the mainline was about 2 times greater than on the shoulder lane. This is likely because of potentially weaker support conditions under the shoulder lane compared to the mainline.

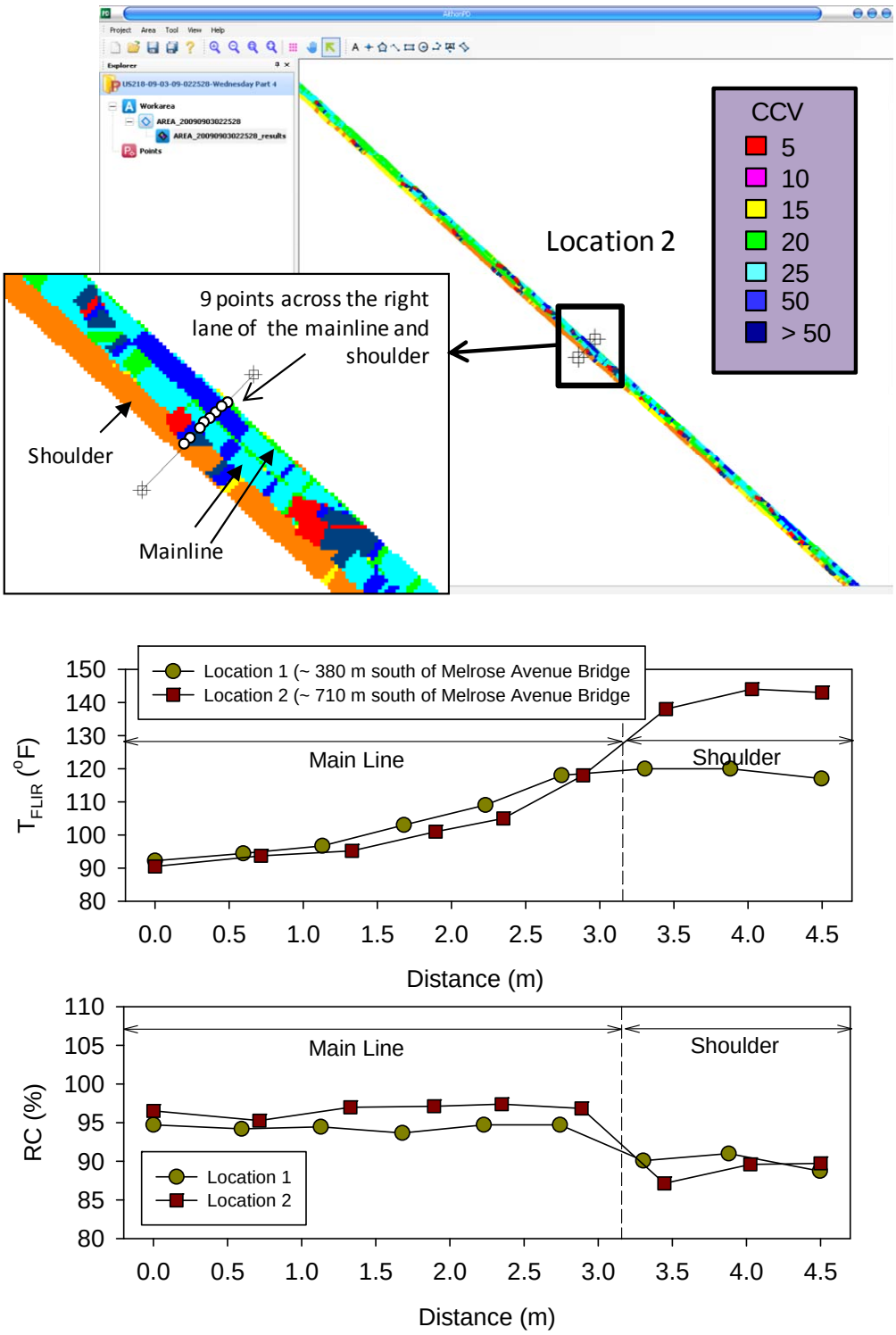

Figure 64. CCV spatial map, and comparison in-situ dry density and temperature measurements across the mainline and shoulder at two select locations (only location 2 is shown in the CCV map; CCV at location 1 is not available)

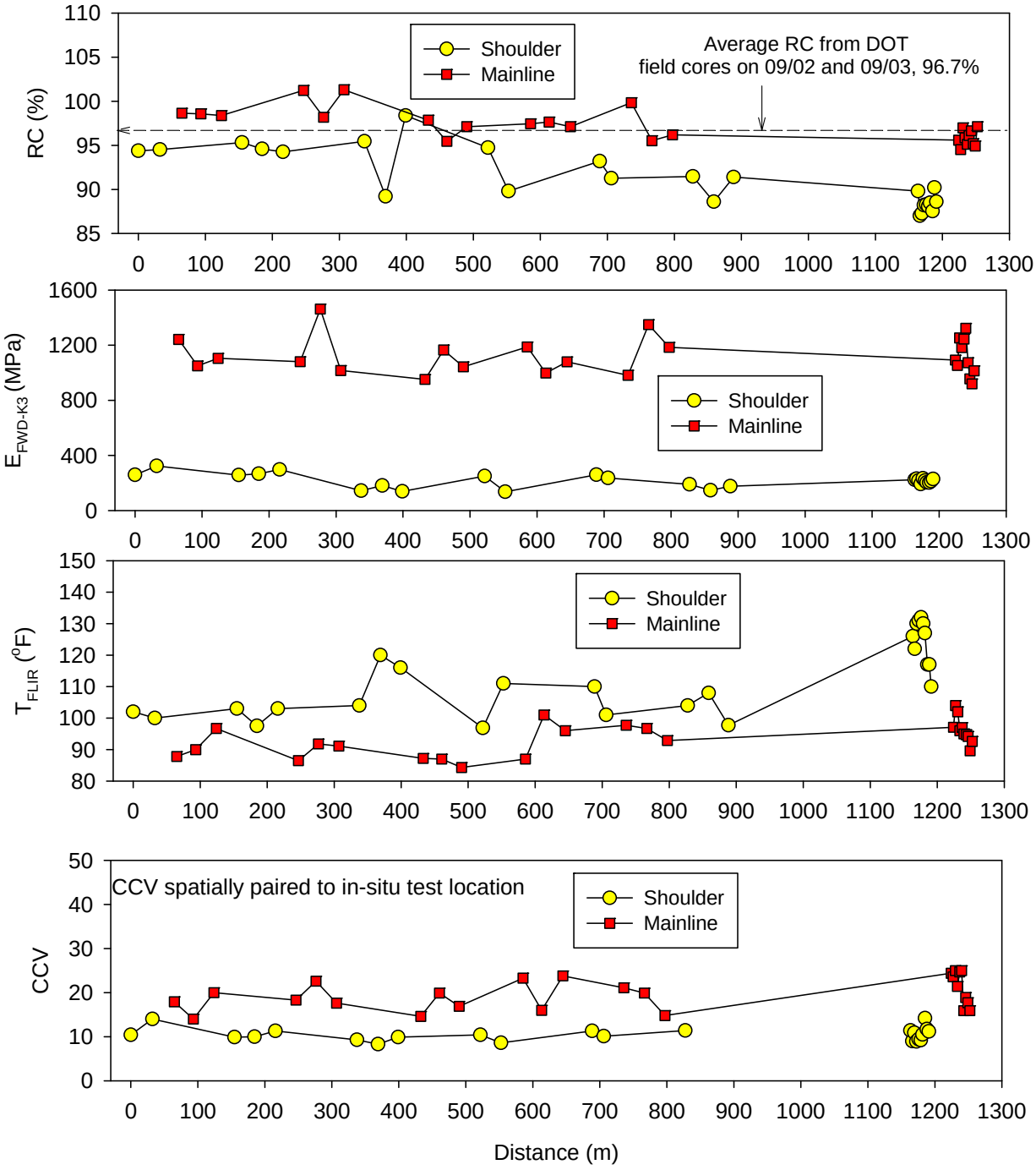

Figure 65. Comparison of CCV, percent compaction, E_{FWD-K3}, and T_{FLIR} along shoulder and mainline – US218 project

Correlations between CCV and RC and E_{FWD-K3} point-MVs are presented in Figure 66. Correlation between CCV and E_{FWD-K3} produced a relatively strong linear regression relationship with $R^2 = 0.8$ compared to correlation between CCV and RC with $R^2 = 0.4$. This should be expected as CCV is a result of drum response under vibratory loading which is a measure of the stiffness and not necessarily related to the density of the material. In addition, various other factors influence both roller and in-point-MVs include: (a) differences in underlying support conditions; (b) differences in measurement influence depths of each device; (c) temperature at the time of the measurement; and (c) direction of roller travel.

The influence of differences in underlying support conditions is clearly reflected with data groupings in the correlations (Figure 66). Results presented in Figure 67 indicate that CCV, RC, and E_{FWD-K3} measurements are influenced by temperature (note that these temperature measurements are obtained at the time the in-situ test measurements were obtained). Roller direction of travel did not show a statistically significant influence on CCV measurements (Figure 66).

Temperatures were measured using a thermal imaging camera and a infrared camera on the FWD trailer. Relationship between T_{FLIR} and T_{FWD} are provided in Figure 68 which showed strong correlation ($R^2 = 0.93$) between the two measurements. T_{FWD} measurements are about 1.03 times greater than T_{FLIR} measurements.

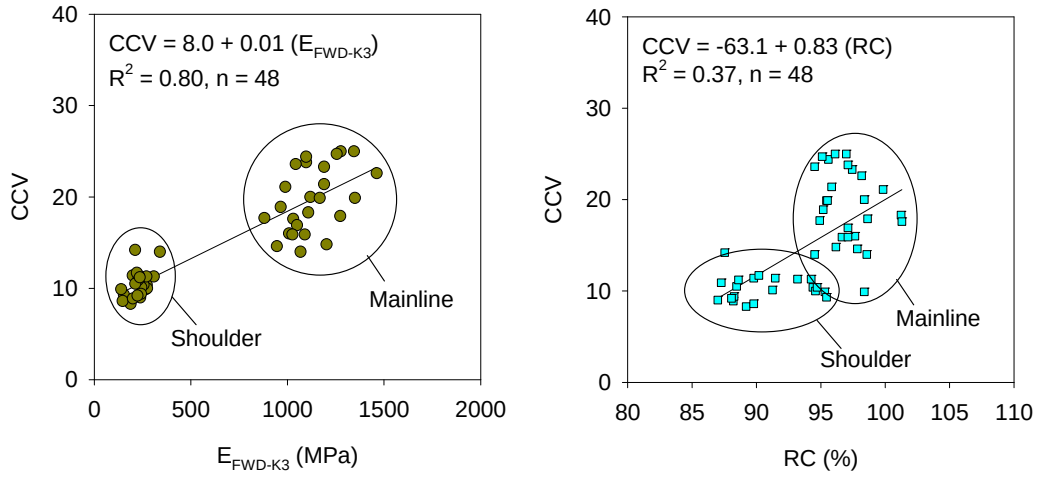

Figure 66. Correlations between CCV, E_{FWD-K3}, and percent compaction – US218 project

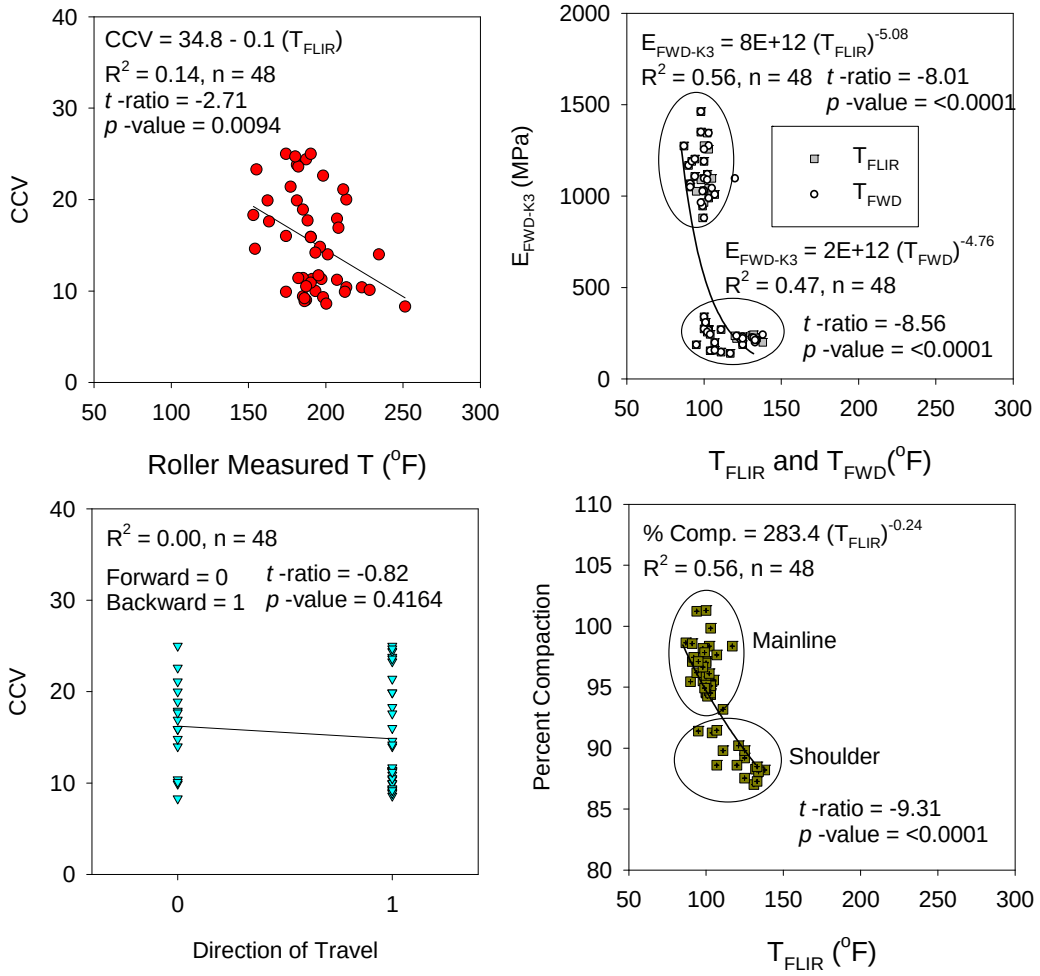

Figure 67. Figure showing influence of temperature on CCV, E_{FWD-K3}, and percent compaction values and influence of direction of travel on CCV – US218 project

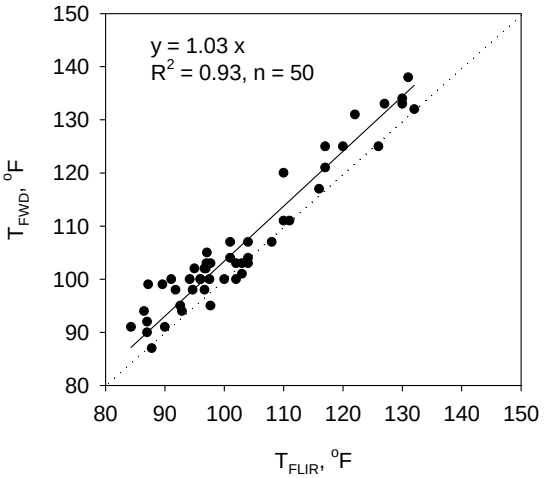

Figure 68. Correlation between FLIR thermal camera and FWD infrared camera temperature measurements

Summary of Key Findings

Experimental test results and field observations from a IC-HMA demonstration project on Highway 218 south of I-80 near Coralville, Iowa using a Sakai dual drum IC roller are presented above. The project involved compaction of HMA overlay over the existing PCC layer. The Sakai IC roller was used for HMA break down rolling along with another Sakai conventional break down roller. Roller pass coverage information, IC-MVs (Sakai CCV) and temperature measurements were continuously recorded and displayed in real-time to the roller operator. Main objectives of testing and data analysis on this project were to: (1) evaluate the impact of using real-time pass coverage information to the roller operator on the uniformity of the pass coverage achieved during compaction; (2) develop correlations between CCV IC-MVs and asphalt density (RC) and modulus (E_{FWD-K3}) point-MVs; and (3) evaluate the influence of temperature measurements on the correlations. Objective (1) was achieved by conducting a blind study on day 1 where the IC monitoring system was switched on but the on-board monitor was closed for viewing by the operator, and by allowing the operator to use the on-board monitor on days 2 and 3 to aid in uniform pass coverage. Objective (2) was achieved by obtaining spatially referenced (with GPS measurements) RC and E_{FWD-K3} point-MVs at 50 test locations and pairing them with spatially nearest CCV IC-MVs to develop correlations. Objective (3) was achieved by obtaining temperature measurements at each in-situ point-MV location and conducting statistical analysis. Following are the key findings from the results and data analysis from this project:

- Univariate statistics (mean and standard deviation) of pass count information on each day did not reveal any differences between day 1 (blind study) and days 2 and 3. Geostatistical semivariogram analysis of pass count information revealed quantitative evidence of improved uniformity in pass coverage on day 3 compared to on day 1.
- The temperature of HMA on the shoulder lane was on average about 19^{o}F warmer than the temperature of the HMA on the mainline. The RC of the HMA layer was on average about 6% lower on the shoulder compared to the mainline. These differences in temperature and RC measurements are attributed to greater HMA layer thickness on the shoulder lane than on the mainline.
- E_{FWD-K3} point-MVs and CCV IC-MVs obtained over a stretch of about 1.3 km showed that the measurements on the shoulder lane were lower than on the mainline. This is likely because of potentially weaker support conditions under the shoulder lane compared to the mainline.
- Correlation between CCV and E_{FWD-K3} showed a relatively strong linear regression relationship with $R^2 = 0.8$ compared to correlation between CCV and RC with $R^2 = 0.4$. This should be expected as CCV is a result of drum response under loading which is a measure of material stiffness and not necessarily related to the density of the material. The regression relationships are influenced by differences in underlying support conditions as it was clearly reflected with data groupings (with separate groups for shoulder lane and mainline measurements) in the correlations. Data analysis indicated that the CCV, RC, and E_{FWD-K3} measurements are influenced by temperature.

CHAPTER 7: DEMONSTRATION PROJECT 3 — I-29 MONONA COUNTY, IOWA

Project Description

This demonstration project was location on I-29 in Monona County, Iowa. The project involved reconstruction of pavement foundation layers (base, subbase, and subgrade) of the existing interstate highway on I-29 north and south bound lanes in Harrison and Monona Counties between just south of county road F-20 to just north of I-75 (Sta. 2097 to 781+70 on north bound (about 11.7 miles) and Sta. 2097+59 to 2675+93 on south bound (about 4.7 miles); Iowa DOT project number ESIMX-029-5(100)95--1S-43). The project location map is shown in Figure 69. The existing subgrade layer was undercut to about 0.30 to 0.60 m below the existing grade. The exposed subgrade in the excavation was scarified and recompacted. The excavation was then replaced with 0.30 to 0.45 m thick recycled HMA ("special backfill subgrade treatment") subbase layer and 0.15 m thick recycled PCC (RPCC) base layer. Crushed limestone material was also used for the subbase layer in some areas.

A Volvo/Trimble vibratory smooth drum IC roller equipped with CMV measurement system was used on this project for demonstration. The Iowa State University research team was present on the project site from August 31 to September 3, 2009 and on September 10, 2010. During this period eleven test beds were constructed and tested. Compaction on the test beds were achieved using the Volvo IC roller. The contractor provided assistance in preparation of the test beds. In-situ LWD, DCP, and NG tests were conducted on the test beds to develop correlations with CMV IC-MVs.

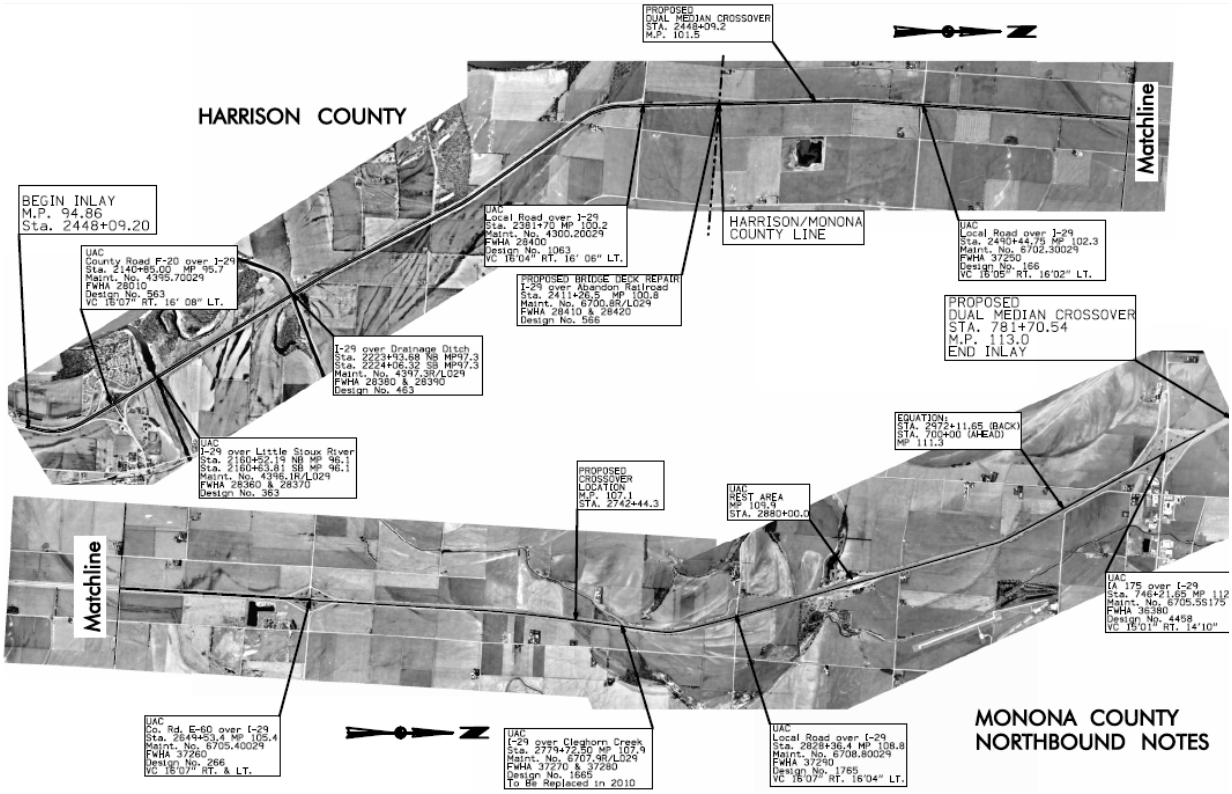

Figure 69. Project location map – I-29 demonstration project

Experimental Testing

A summary of the in-situ test beds and testing performed on the project is provided in Table 9. Approximate location of these test beds is shown in Figure 70. Three test beds included subgrade materials, four test beds included special backfill subbase materials, three test beds included RPCC base material, and one test bed included crushed limestone subbase material. Photographs of subgrade, subbase, and base layer test beds and construction operations are provided in Figure 71 to Figure 73.

A summary of soil index properties for subgrade, subbase, and base materials is provided in Table 10. Figure 74 presents laboratory standard Proctor test results for the subgrade material along with in-situ w-γ_d measurements. The average in-situ w of the subgrade material was about 20.3% (i.e., 0.6% of standard Proctor w_{opt}), and the average RC of the material was about 94% standard Proctor γ_{dmax}. Minimum and maximum dry unit weight of the subbase and base materials were determined following relative density test procedures using oven-dry material and the results are summarized in Table 10.

One-dimensional calibration test strips were constructed on subgrade (TB2), subbase (TB4), and base (TB9) layers where the test strips were scarified down to the compaction layer depth and compacted using the IC roller for multiple roller passes (8 to 12). In-situ point-MVs (γ_d, w, $E_{LWD\text{-}Z3}$, and CBR) were obtained at intermediate roller passes (e.g., after 1, 2, 4, 8, etc.). Spatial maps of IC-MVs were obtained over production subgrade (TBs 1 and 6), subbase (TBs 3, 4, 5, 7, and 11), and base (TBs 8 and 10) layer areas along with in-situ point-MVs at selected locations based on the on-board display IC-MV map. Correlations between CMV IC-MVs and in-situ test point-MVs were developed from calibration and production areas by spatially pairing the two using GPS referenced position measurements.

Figure 70. Approximate location of test beds – I29 project

Table 9. Summary of test beds and in-situ testing – I29 project

TB	Date	Material	Amplitude setting	Point-MV	Comments
1	08/31	Subgrade	Pass 1: low amp Passes 2-3: high amp	w, γ_d, CBR, $E_{LWD\text{-}Z3}$	Spatial maps of subgrade. In-situ test measurements after pass 3.
2		Subgrade	Passes 1-12: low amp	w, γ_d, CBR, $E_{LWD\text{-}Z3}$	One-dimensional subgrade test strip with multiple roller passes. In-situ test measurements after 0, 1, 2, 5, and 12 roller passes
3	08/31 – 09/01	Special backfill (recycled HMA)	Pass 1: low amp Pass 2: high amp	None	Spatial maps of approximately 300 mm thick special backfill placed over subgrade. In-situ test measurements after pass 2.
4	09/01	Special backfill (recycled HMA)	Pass 1: high amp Passes 2-8: low amp	w, γ_d, CBR, $E_{LWD\text{-}Z3}$	One-dimensional special backfill test strip with 300 mm thick layer placed over subgrade. In-situ test measurements after 0, 1, 2, 4, and 8 roller passes
5 (over TB1)		Special backfill (recycled HMA)	Pass 1: low amp Pass 2: high amp	w, γ_d, CBR, $E_{LWD\text{-}Z3}$	Spatial maps of approximately 300 mm thick special backfill placed over TB1 subgrade. In-situ test measurements after pass 2.
6		Subgrade	Passes 1-2: high amp Pass 3: low amp	None	Spatial maps of subgrade.
7 (over TB6)		Special backfill (recycled HMA)	Pass 1: low amp Pass 2: high amp	w, γ_d, CBR, $E_{LWD\text{-}Z3}$	Spatial maps of approximately 300 mm thick special backfill placed over TB6 subgrade. In-situ test measurements after pass 2.
8 (over TB3)	09/02	Recycled PCC Base	Pass 1: low amp Pass 2: high amp	w, γ_d, CBR, $E_{LWD\text{-}Z3}$	Spatial maps of approximately 150 mm thick base layer placed over TB3 subbase. In-situ test measurements after pass 2.
9	09/10	Recycled PCC Base	Passes 1 to 10: low amp	w, γ_d, CBR, $E_{LWD\text{-}Z3}$	One-dimensional base layer test strip with multiple roller passes. In-situ test measurements after 0, 1, 2, 4, and 10 roller passes.
10			Pass 1: low amp Pass 2: high amp	None	Spatial maps of a production area base layer.
11		Special backfill (virgin limestone)	Pass 1: low amp Pass 2: high amp	w, γ_d, CBR, $E_{LWD\text{-}Z3}$	Spatial maps of a production area base layer (underlain by box culvert at an isolated location). In-situ tests after pass 2.

Note: w – moisture content, γ_d – dry unit weight, CBR – California bearing ratio determined from dynamic cone penetrometer (DCP) test, $E_{LWD\text{-}Z3}$ – elastic modulus determined using Zorn model light weight deflectometer (LWD) with a 300 millimeter plate, $E_{FWD\text{-}K3}$ – elastic modulus determined using KUAB falling weight deflectometer (FWD), CMV – compaction meter value measured using Volvo vibratory smooth drum roller.

Figure 71. Photographs of subgrade test beds construction

Figure 72. Photographs of special backfill subbase layer test beds construction

Figure 73. Photographs of aggregate base layer test beds construction

Table 10. Summary of soil index properties – I-29 project

Parameter	Subgrade	Special Backfill Subbase (Recycled asphalt)	Special Backfill Subbase (Crushed limestone)	Aggregate Base (Recycled concrete)
Standard Proctor γ_{dmax} (kN/m^3)	16.47			
Standard Proctor γ_{dmax} (pcf)	104.8			
Standard Proctor w_{opt} (%)	19.7		—	
Modified Proctor γ_{dmax} (kN/m^3)	18.01			
Modified Proctor γ_{dmax} (pcf)	114.7			
Modified Proctor w_{opt} (%)	14.1			
Relative Density Test* γ_{dmin} (kN/m^3)	—	14.82	16.39	14.76
Relative Density Test* γ_{dmin} (pcf)	—	94.3	104.3	94.0
Relative Density Test* γ_{dmax} (kN/m^3)	—	18.87	20.67	19.31
Relative Density Test* γ_{dmax} (pcf)	—	120.1	131.6	122.9
Gravel Content (%) (> 4.75mm)	3	55	37	59
Sand Content (%) (4.75mm – 75μm)	5	45	63	41
Silt Content (%) (75μm – 2μm)	65	0	0	0
Clay Content (%) (< 2μm)	27	0	0	0
Liquid Limit, LL (%)	41			
Plastic Limit, PL (%)	21		Non-Plastic	
Plasticity Index, PI (%)	20			
AASHTO Classification	A-7-6 (19)	A-1-a	A-1-a	A-1-a
USCS Classification	CL	GW	SP	GW
Specific Gravity, G_s (Assumed)	2.65	2.70	2.70	2.70

— Not measured
* at oven-dry moisture content

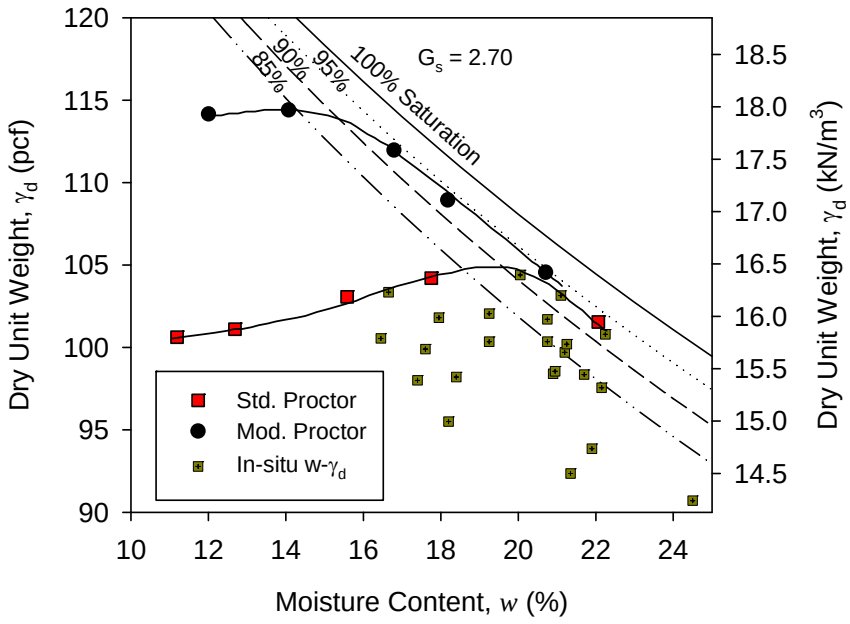

Figure 74. Laboratory standard Proctor test data – I29 subgrade material

In-Situ Test Results and Analysis

Calibration Test Beds

CMV IC-MVs and in-situ point-MVs obtained from multiple roller passes on subgrade (TB2), recycled HMA special backfill subbase (TB4), and RPCC base layer (TB9) calibration test strips are presented in Figure 75, Figure 76, and Figure 77, respectively. Results indicate that the CMV, $E_{LWD\text{-}Z3}$, CBR, and γ_d measurements on the subbase layer are higher than on the subgrade layer. The CMV and $E_{LWD\text{-}Z3}$ values on the base layer are higher than on the subbase layer. The γ_d measurements were slightly lower on the base layer than on the subbase layer. Following are the range of values observed on the three layers after the final pass:

- CMV IC-MVs were: (a) less than about 5 on the subgrade layer, (b) ranged from 5 to 10 on the subbase layer, and (c) ranged from 15 to 26 on the RPCC base layer.
- $E_{LWD\text{-}Z3}$ point-MVs were: (a) less than 10 MPa on the subgrade layer, (b) ranged from 24 to 27 on the subbase layer, and (c) ranged from 36 to 53 on the RPCC base layer.
- CBR point-MVs were: (a) less than 2 on the subgrade layer, and (b) ranged from 8 to 13 on the subbase layer.
- γ_d point-MVs were: (a) 15.48 kN/m^3 (94% RC) to 15.76 kN/m^3 (96% RC) on the subgrade layer; (b) 17.87 kN/m^3 (80% RC) to 18.40 kN/m^3 (91% RC) on the subbase layer; and (c) 15.31 kN/m^3 (15% relative density) to 17.41 kN/m^3 (65% relative density) on the subbase layer.

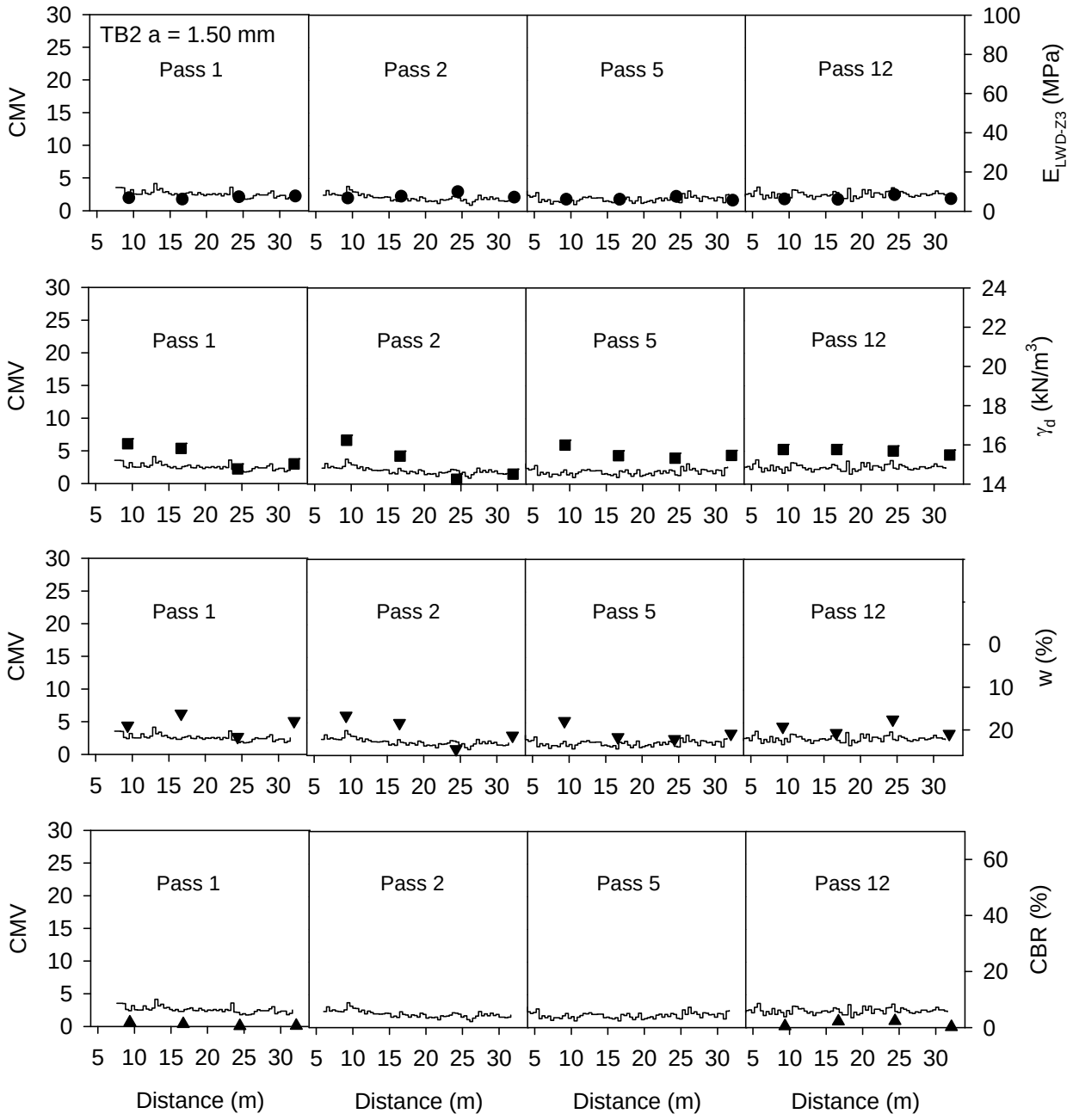

Figure 75. Comparison between CMV and in-situ point measurements after multiple compaction passes – TB2 subgrade

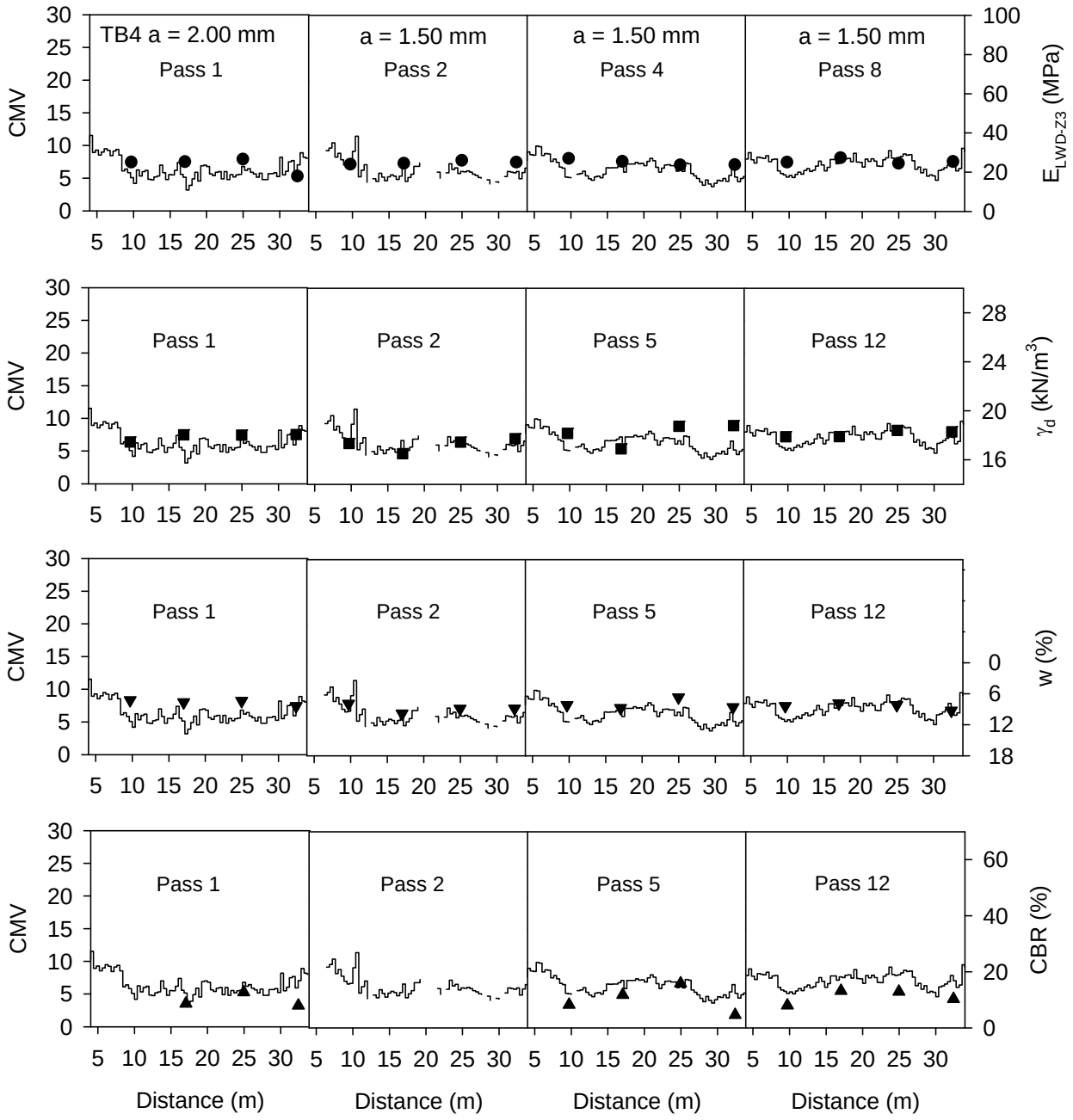

Figure 76. Comparison between CMV and in-situ point measurements after multiple compaction passes – TB4 special backfill subbase

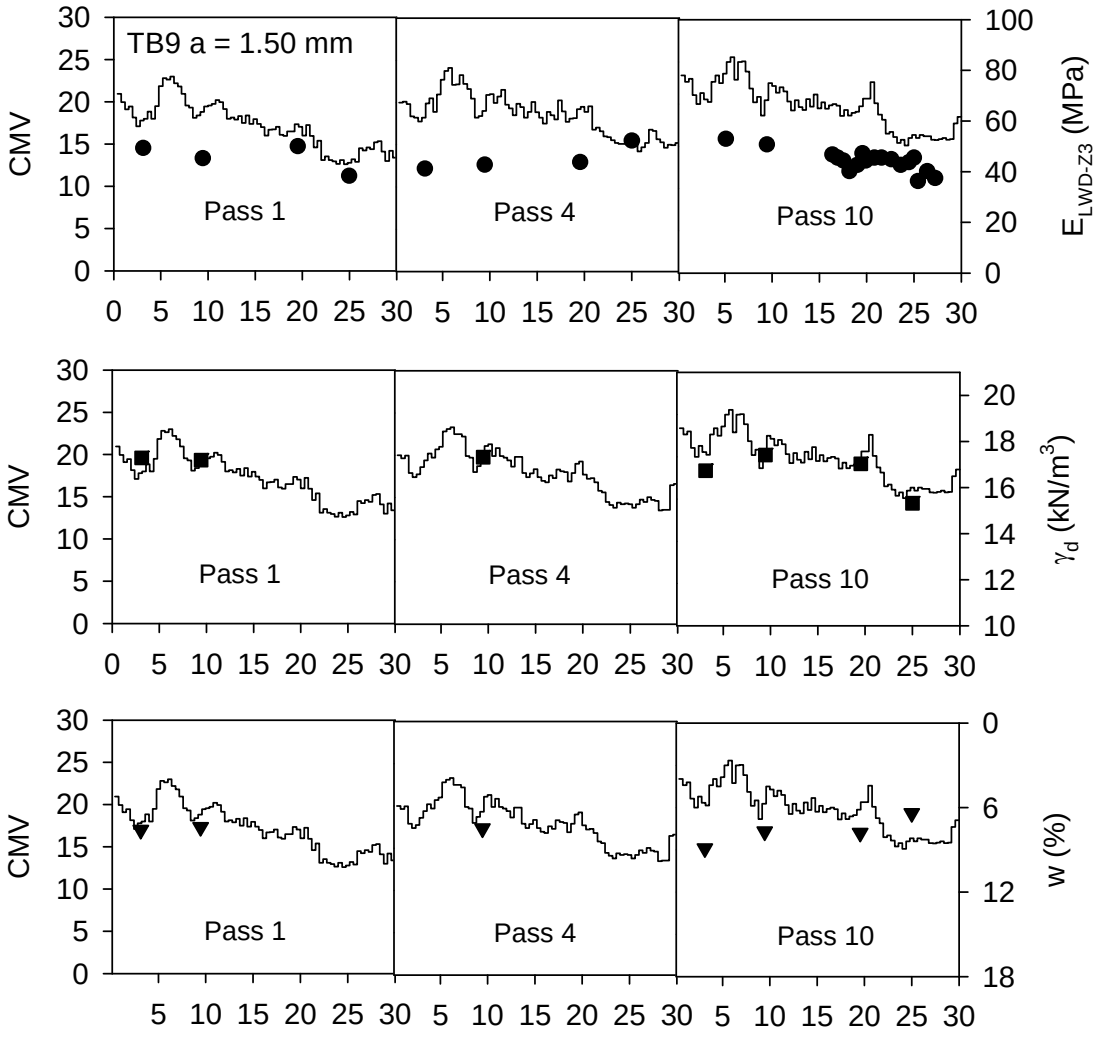

Figure 77. Comparison between CMV and in-situ point measurements after multiple compaction passes – TB9 RPCC base

Change in the average CMV IC-MVs and point-MVs with increasing pass number on the three layers are presented in Figure 78. The average CMV values did not change considerably with increasing pass number on the subgrade (varied from 2 to 3) and subbase layers (varied from 6 to 8), but showed a slight increase (from about 17 to 20) on the base layer. The average E_{LWD-Z3} values on the subgrade and subbase layers increased from pass 0 to 2 and then remained constant up to the final compaction pass. The average E_{LWD-Z3} on the base layer increased from pass 0 to 1, remained constant up to pass 4, and then increased up to pass 10. The average γ_d on all three layers increased from pass 0 to 1 and then generally remained at the same level up to the compaction pass.

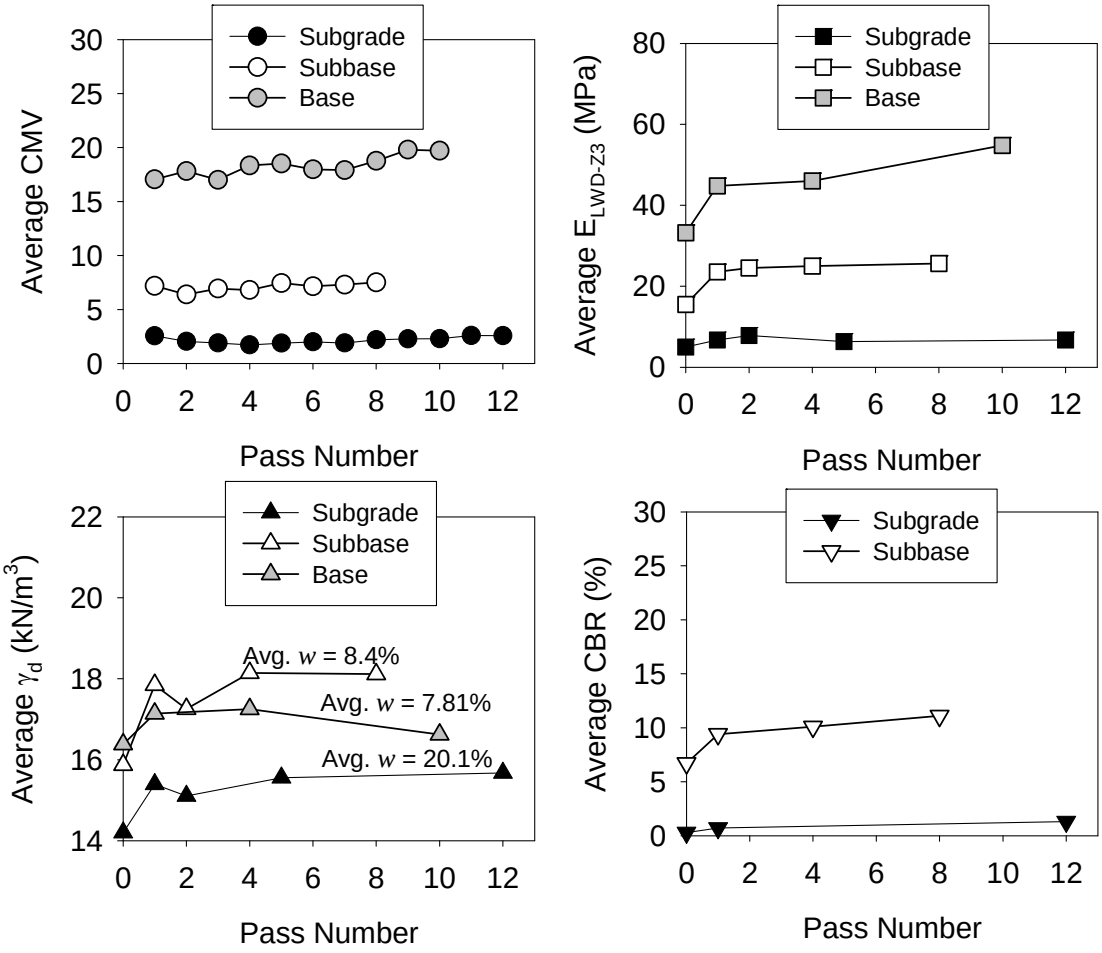

Figure 78. CMV, E_{LWD-Z3}, γ_d, and CBR compaction growth curves for subgrade (TB2), subbase (TB4), and base (TB9) layers

Correlations between CMV IC-MVs and point-MVs for TB2 subgrade, TB4 subbase, and TB9 base layers are presented in Figure 79, Figure 80, Figure 81, respectively. Generally, the correlations yielded weak correlations with $R^2 < 0.4$, with the exception of CMV vs CBR linear regression relationship with $R^2 = 0.5$ and CMV vs. w linear regression relationship with $R^2 = 0.9$. Primary reason for such weak correlations is the narrow range over which the measurements were obtained. Measurements obtained from multiple test beds are combined in the following sections of the report to obtain regression relationships over a wide measurement range.

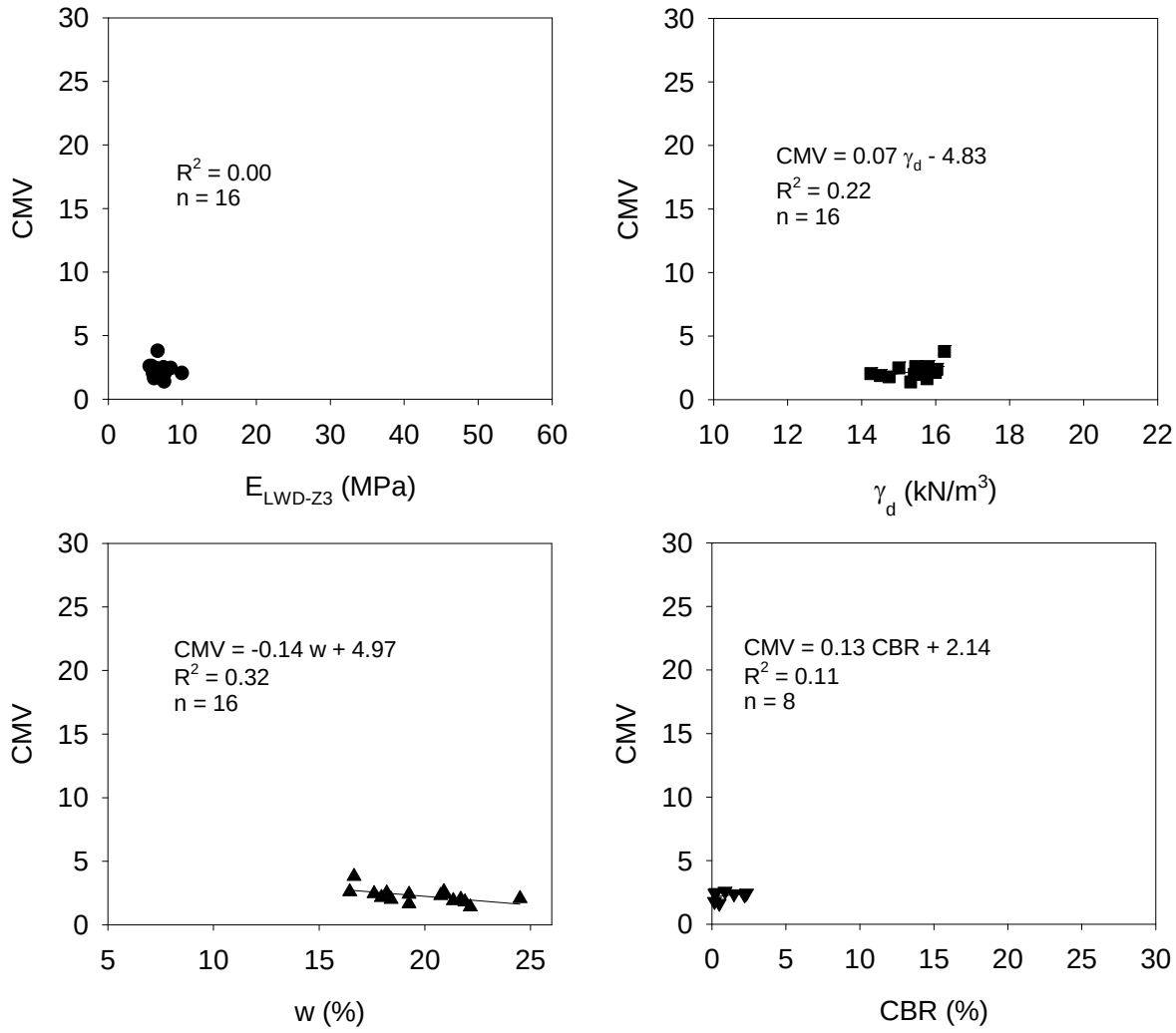

Figure 79. Correlations between CMV and in-situ point measruements – TB2 subgrade (*a* = 1.50 mm)

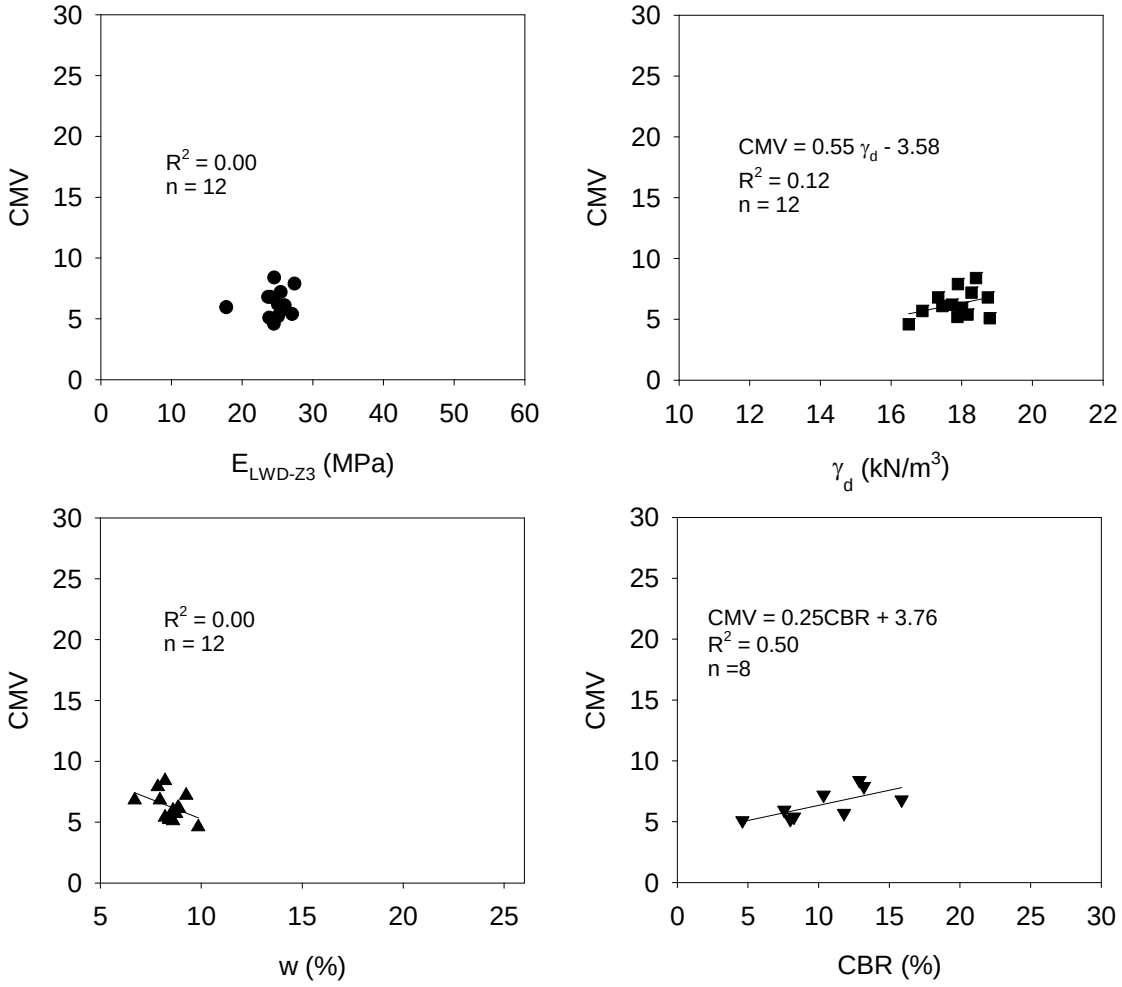

Figure 80. Correlations between CMV and in-situ point measurements – TB4 special backfill subbase (*a* = 1.50 mm)

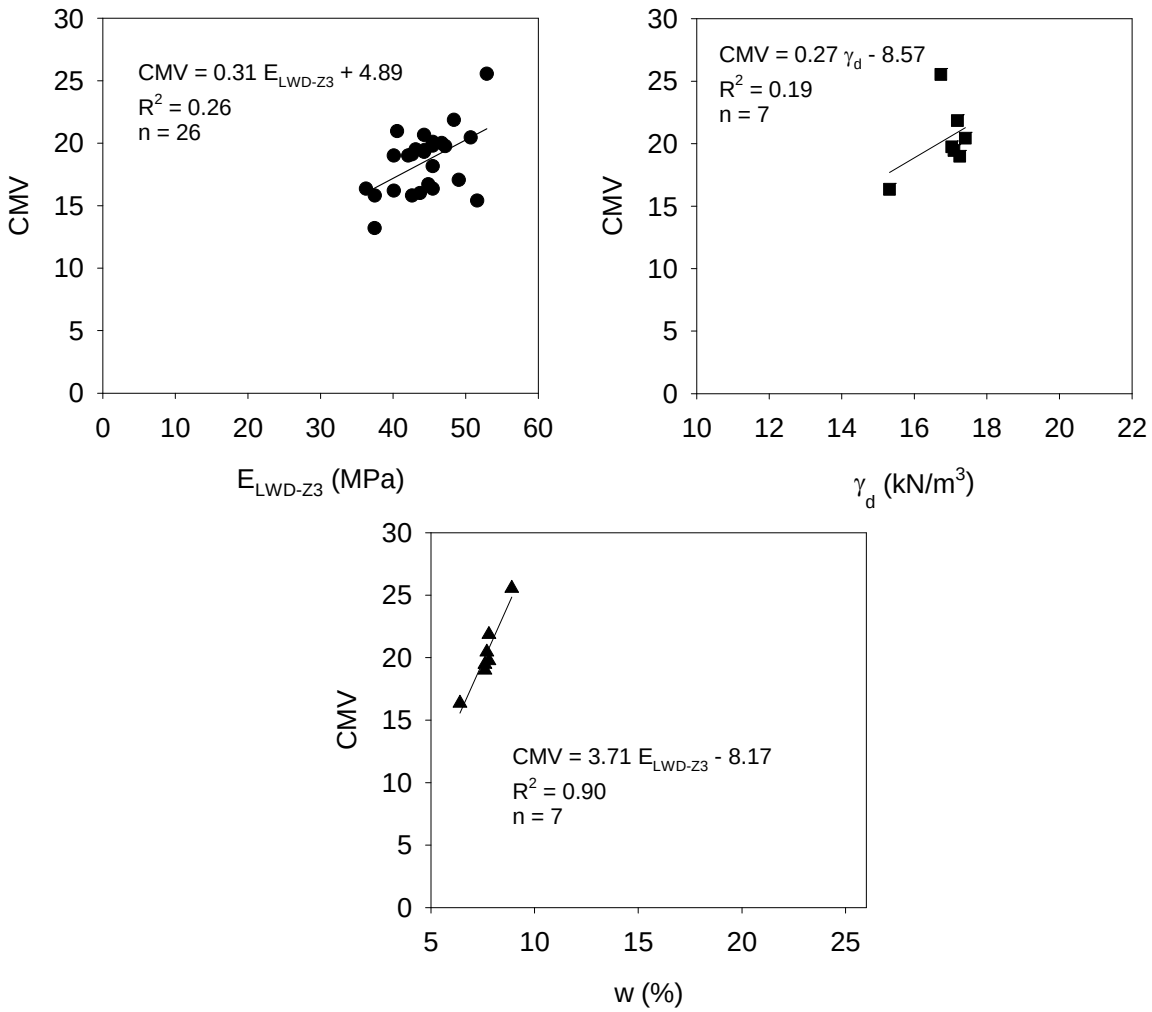

Figure 81. Correlations between CMV and in-situ point measurements – TB9 RPCC base (*a* = 1.50 mm)

Production Area Test Beds

A total of seven production area test beds were constructed and tested as part of this study. Production area maps were obtained by performing two to three roller maps in different amplitude settings (i.e., low and high amplitude) to obtain data to assess the influence of vibration amplitude on the CMV measurements and correlations with point-MVs. The in-situ point-MV locations were selected based on the IC-MV map, i.e., at locations with relatively high, medium, and low CMV.

CMV IC-MV screen shots from the Sitevision office software for TBs 1, 3, 5, 6, 7, and 8 are presented in Figure 82 to Figure 84. Kriged contour maps for CMV were generated for visualization purposes. CMV IC-MV Kriged contour maps of subgrade layers and the overlaid special backfill subbase layers in the same areas are presented in Figure 85 for TBs 1 and 5 and Figure 86 for TBs 6 and 7. In-situ point-MVs and DCP-CBR profiles at the test locations are also presented in these figures. Similarly, Kriged maps of RPCC base and special backfill subbase layers in the same area are presented in Figure 87 for TBs 3 and 8 along with the in-situ point-

MVs. Figure 88 presents CMV Kriged contour maps for two passes on a crushed limestone special backfill subbase layer (TB11).

Comparison of CMV IC-MV maps with in-situ point MVs generally indicate that relatively low, medium, and high CMV locations match with relatively low, medium, and high $E_{LWD\text{-}Z3}$ point-MVs and in some cases (e.g., on TB11) with CBR point-MVs. CMV maps obtained on special backfill subbase and the overlaid RPCC base layers indicate that "hard" and "soft" zones in the subbase layer maps are reflected on the RPCC base layer maps as shown in Figure 87.

TB11 maps on Figure 88 identify the location of a utility concrete culvert (photo shown in Figure 89). The CMV measurements directly over the top of the concrete culvert were higher. In-situ point-MVs ($E_{LWD\text{-}Z3}$, γ_d, w, and CBR) were obtained from directly above the culvert area (points 5 to 8) and along the edge of the culvert (points 1 to 4). $E_{LWD\text{-}Z3}$,CBR, and γ_d measurements obtained directly above the culvert area showed relatively high values compared to measurements along the edge of the culvert (average $E_{LWD\text{-}Z3}$ = 25.2 MPa along the edge and 37.7 MPa above the culvert, CBR = 8.3 along the edge and 16.1 above the culver, γ_d = 21.00 kN/m^3 along the edge and 21.46 kN/m^3 above the culvert). This condition with relatively CMV and point-MVs along the edge of the culvert is a commonly encountered because it is difficult to compact material along the edge of the concrete walls.

CMV maps in different amplitude settings indicate that the CMV measurements are influenced by vibration amplitude. CMV measurements on the subgrade were on average about 1.1 to 1.3 times greater in high amplitude setting (i.e., a = 2.00 mm) than in low amplitude setting (i.e., a = 1.50 mm). Similarly, CMV measurements on the subbase and base layers were on average about 1.2 to 1.5 times greater in high amplitude setting than in low amplitude setting. This is likely due to potential differences in the magnitude of stresses applied on the materials by the roller drum under different amplitude settings (Vennapusa et al. 2010b).

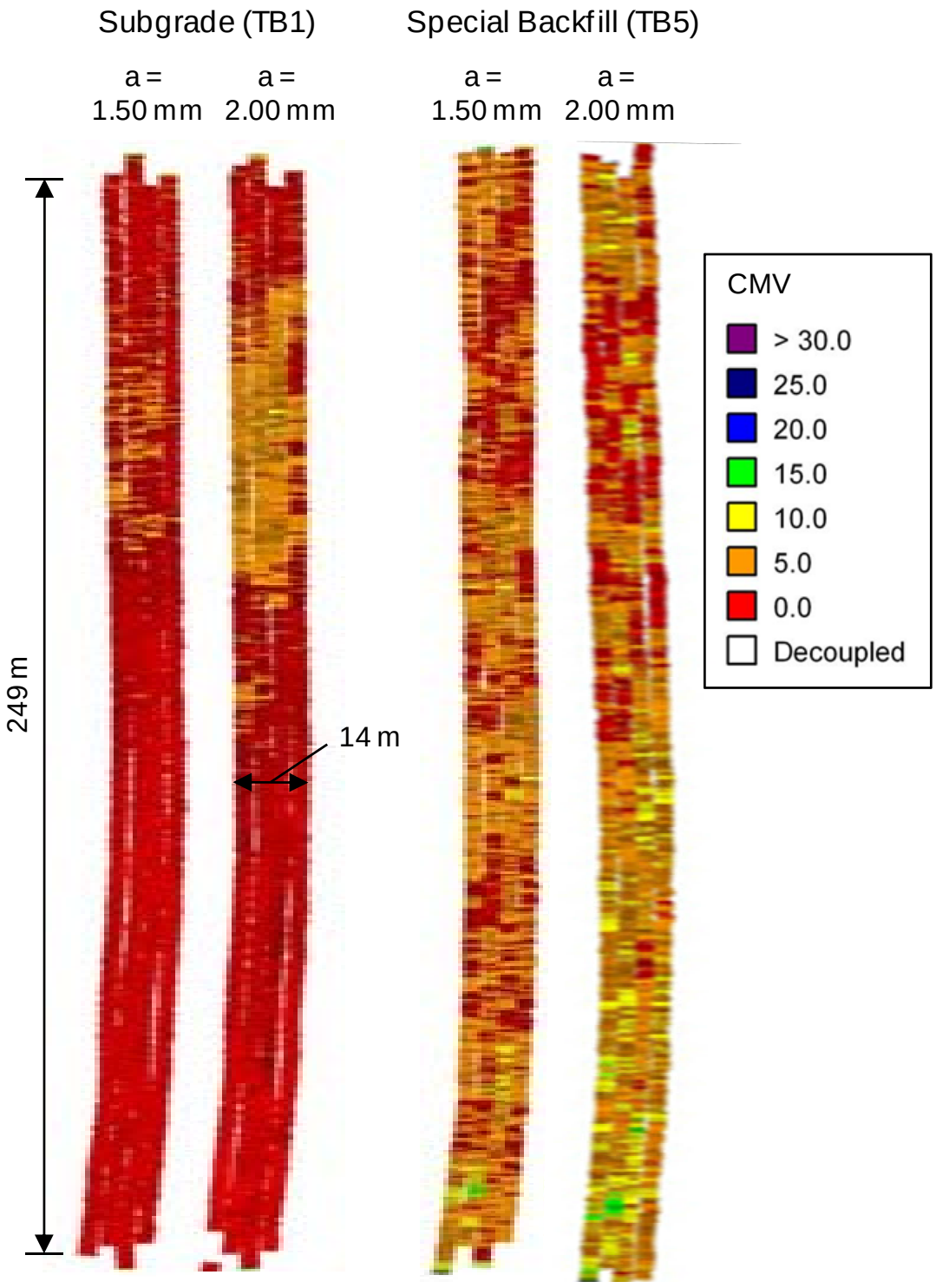

Figure 82. CMV map screenshots from Sitevision software for TB1 subgrade layer and overlying TB5 recycled HMA special backfill subbase layer

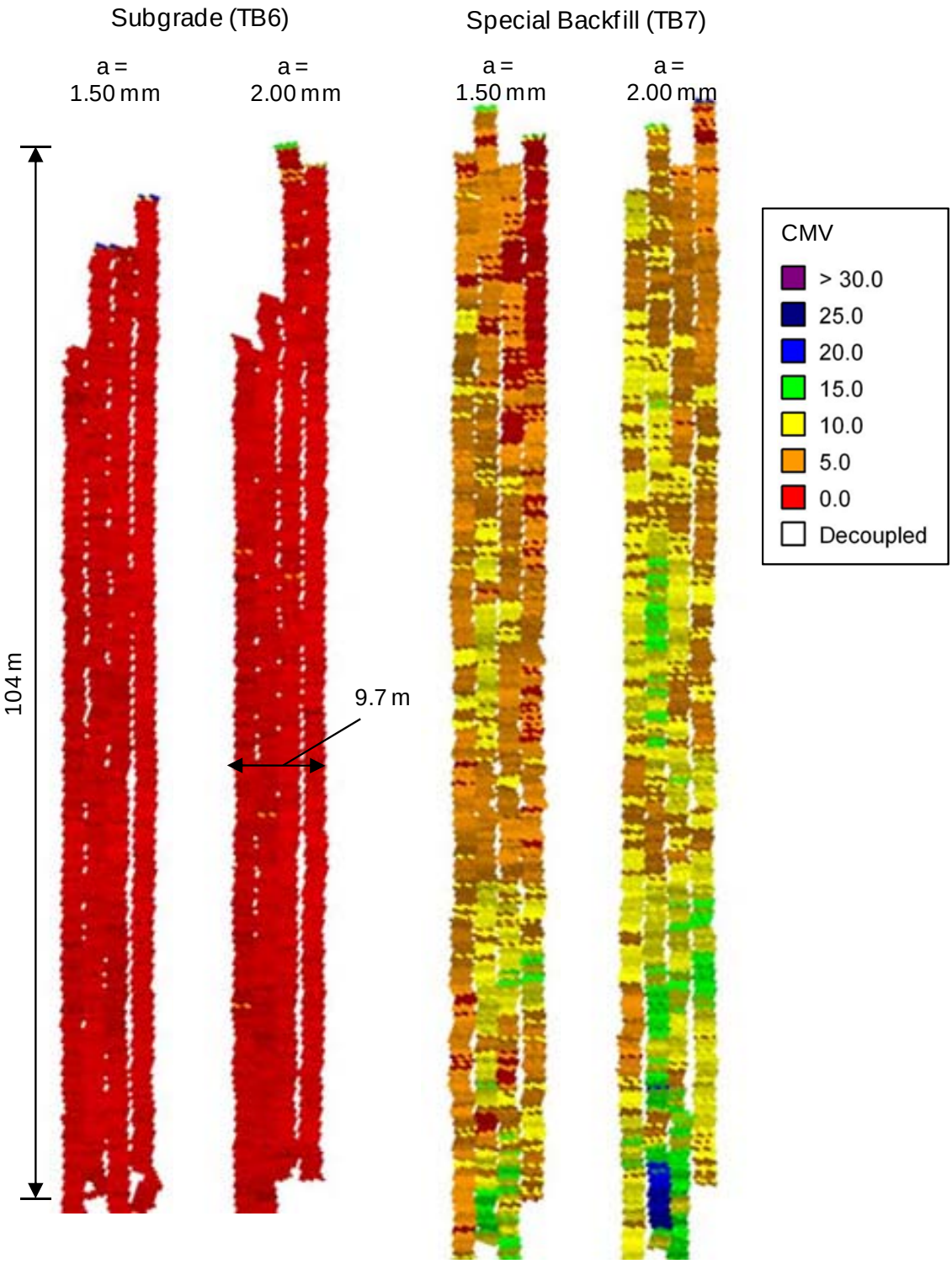

Figure 83. CMV map screenshots from Sitevision software for TB6 subgrade layer and overlying TB7 recycled HMA special backfill subbase layer

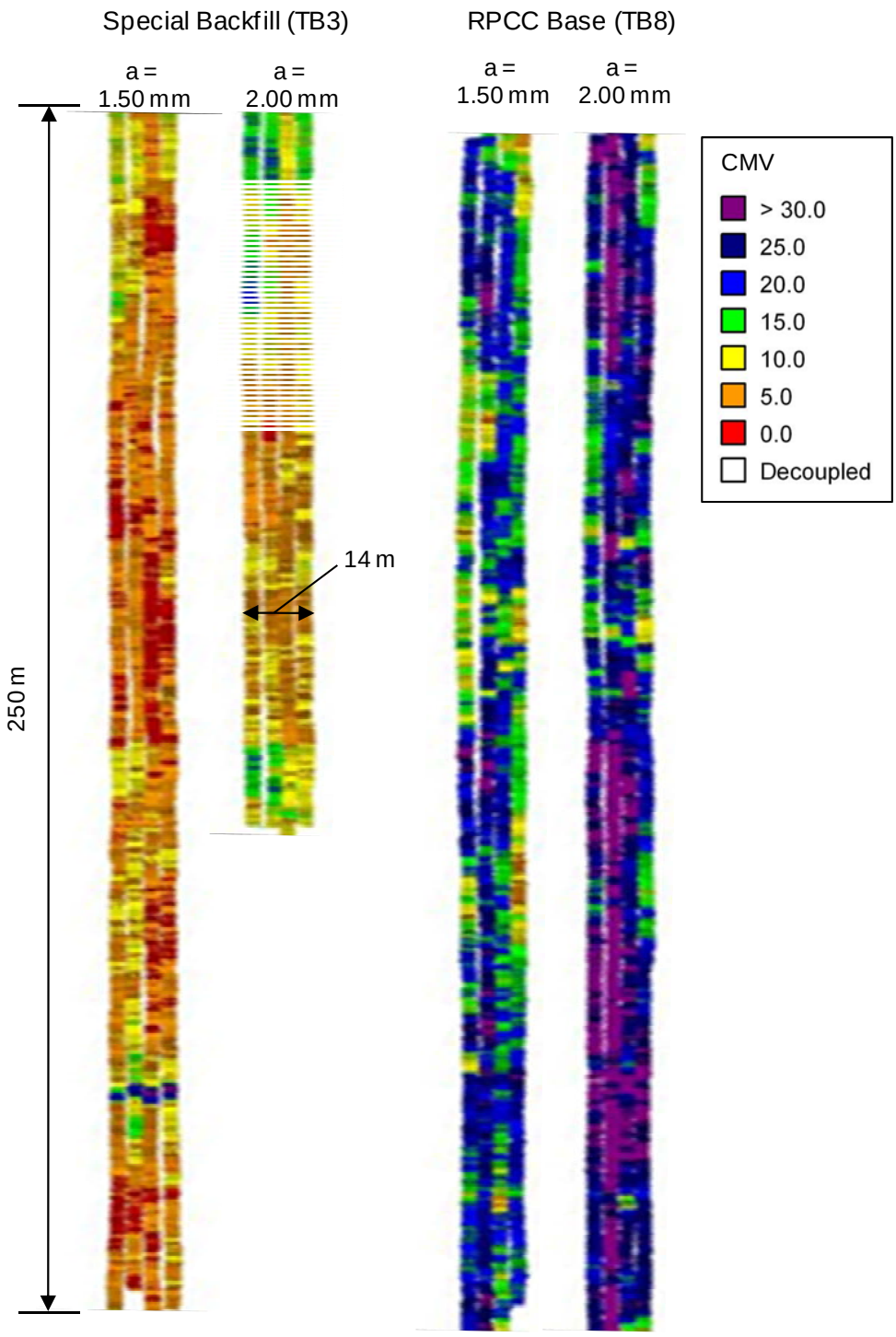

Figure 84. CMV map screenshots from Sitevision software for TB3 HMA special backfill subbase layer and overlying TB8 RPCC base layer

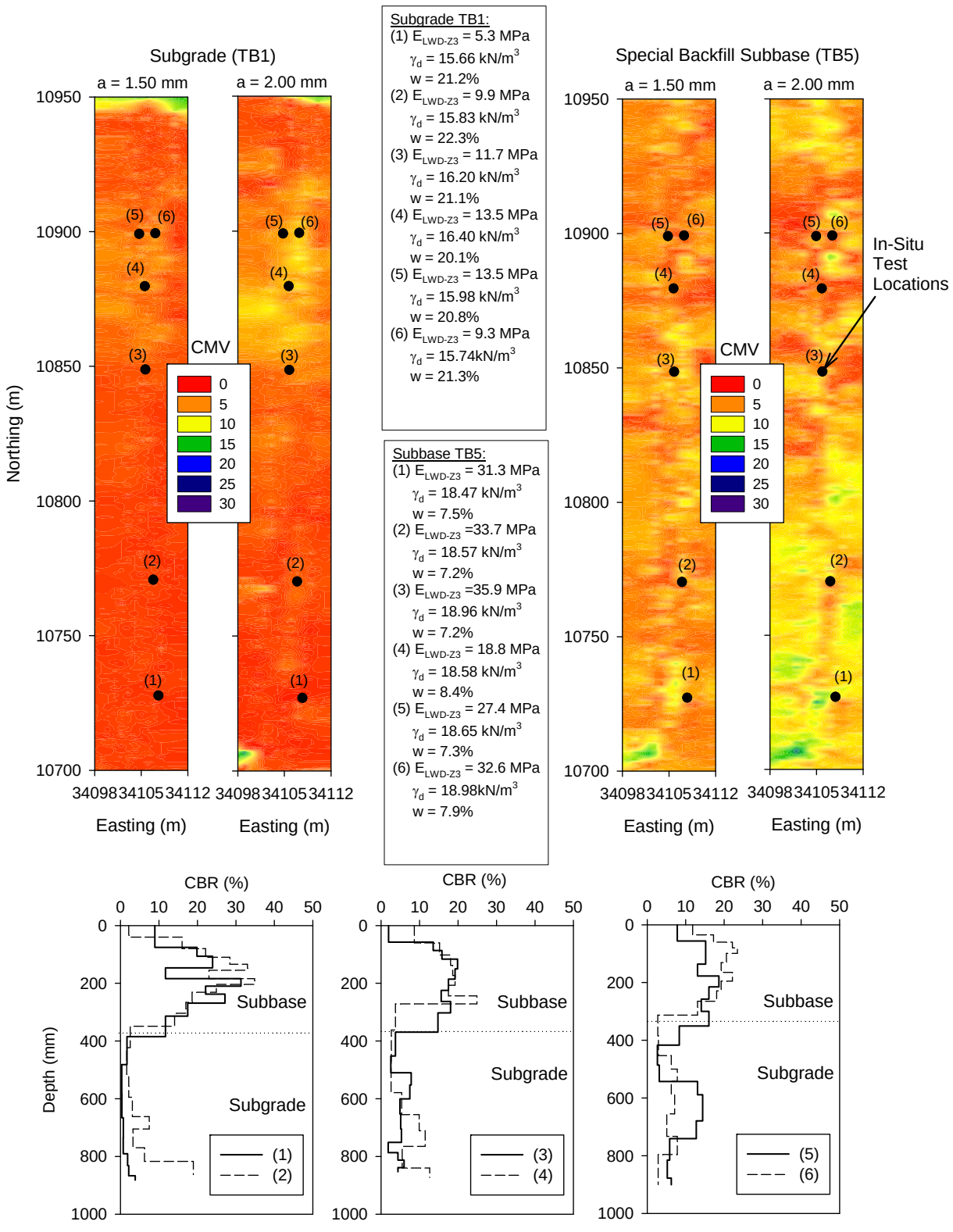

Figure 85. Spatial comparison of TB1 (subgrade layer) CMV map overlain by TB5 (recycled HMA special backfill subbase layer) CMV map, and DCP-CBR profiles at in-situ test locations

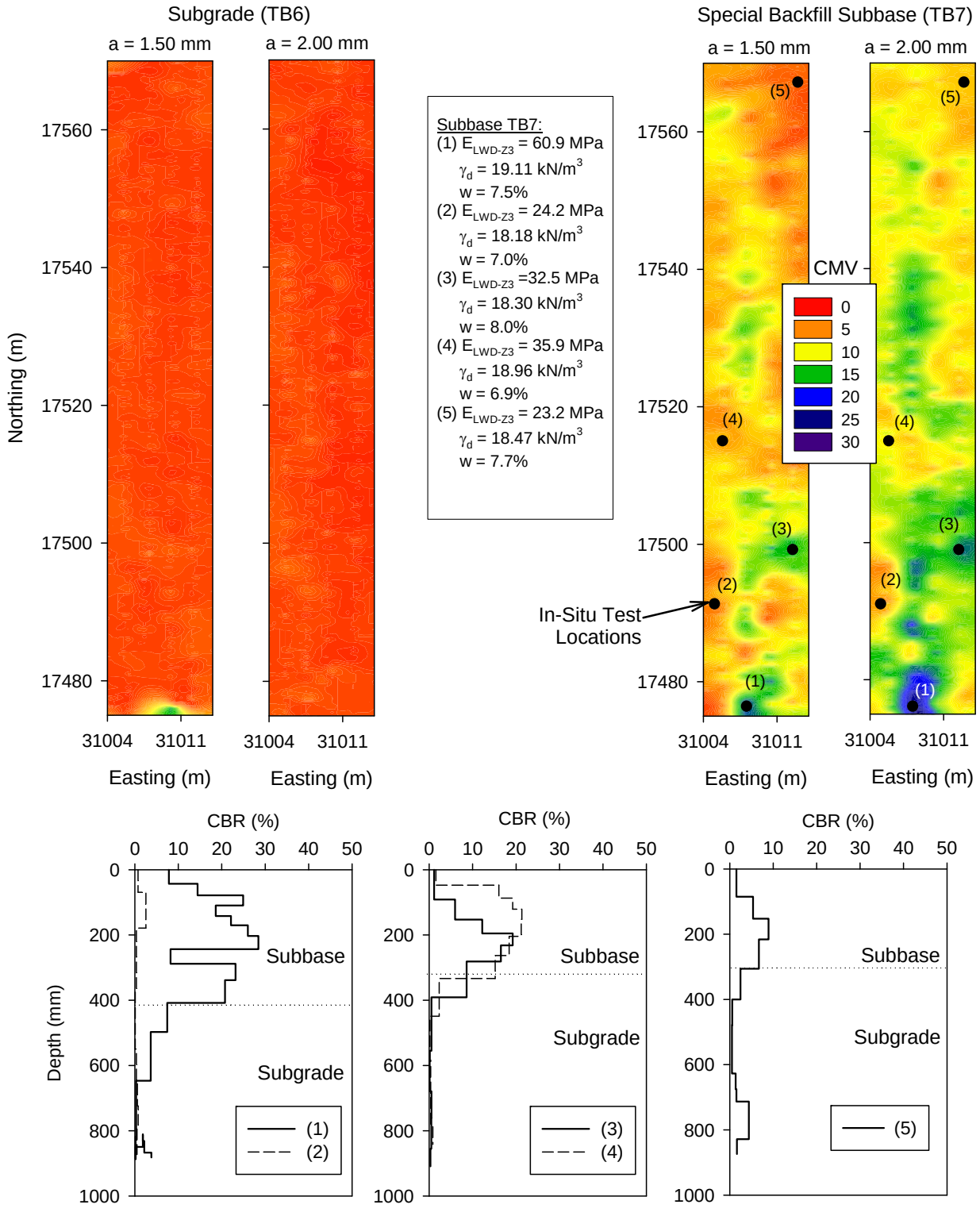

Figure 86. Spatial comparison of TB6 (subgrade layer) CMV map overlain by TB7 (recycled HMA special backfill subbase layer) CMV map, and DCP-CBR profiles at in-situ test locations

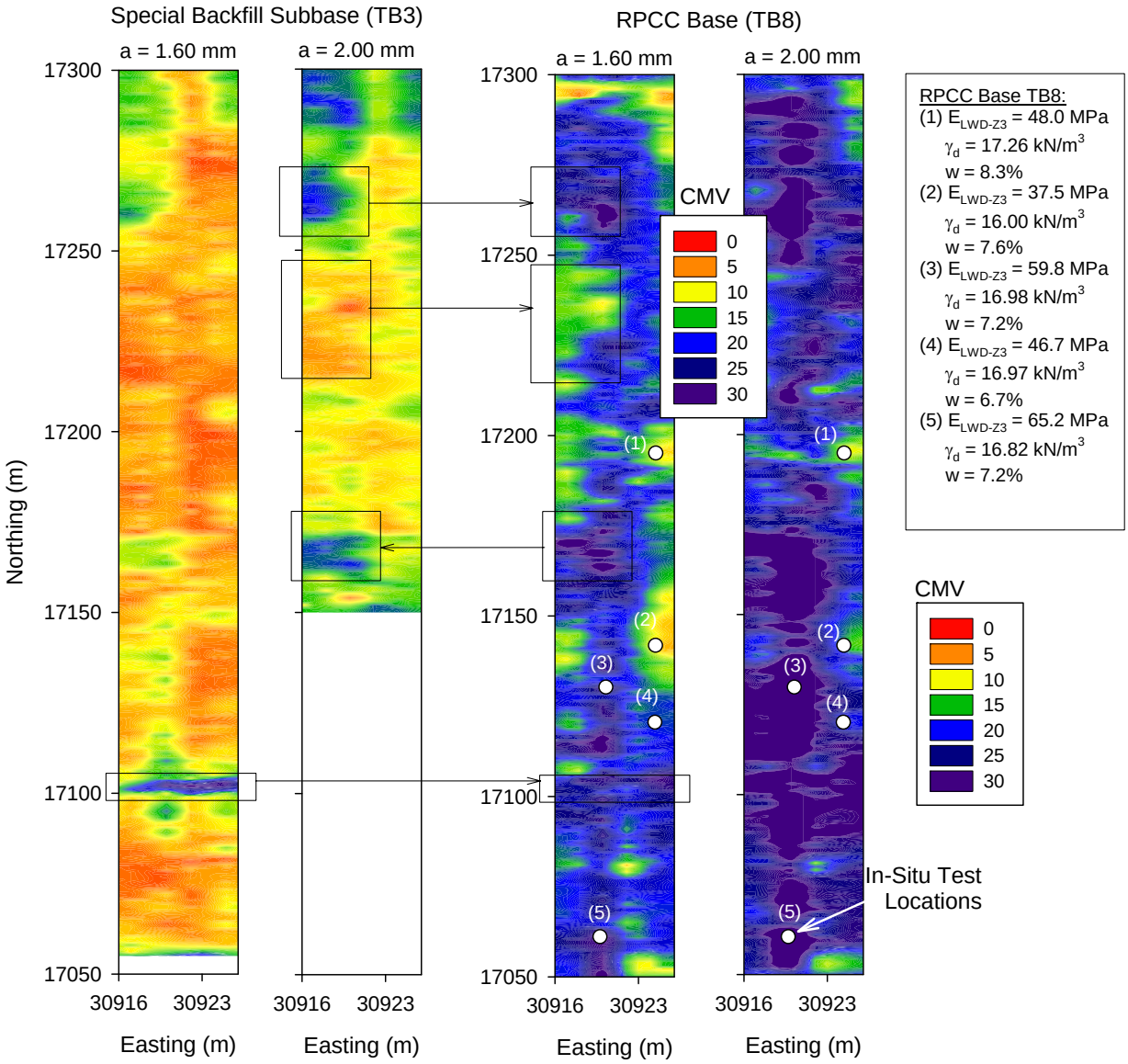

Figure 87. Spatial comparison of TB3 (recycled HMA special backfill subbase layer) CMV map overlain by TB8 (RPCC base layer) CMV map

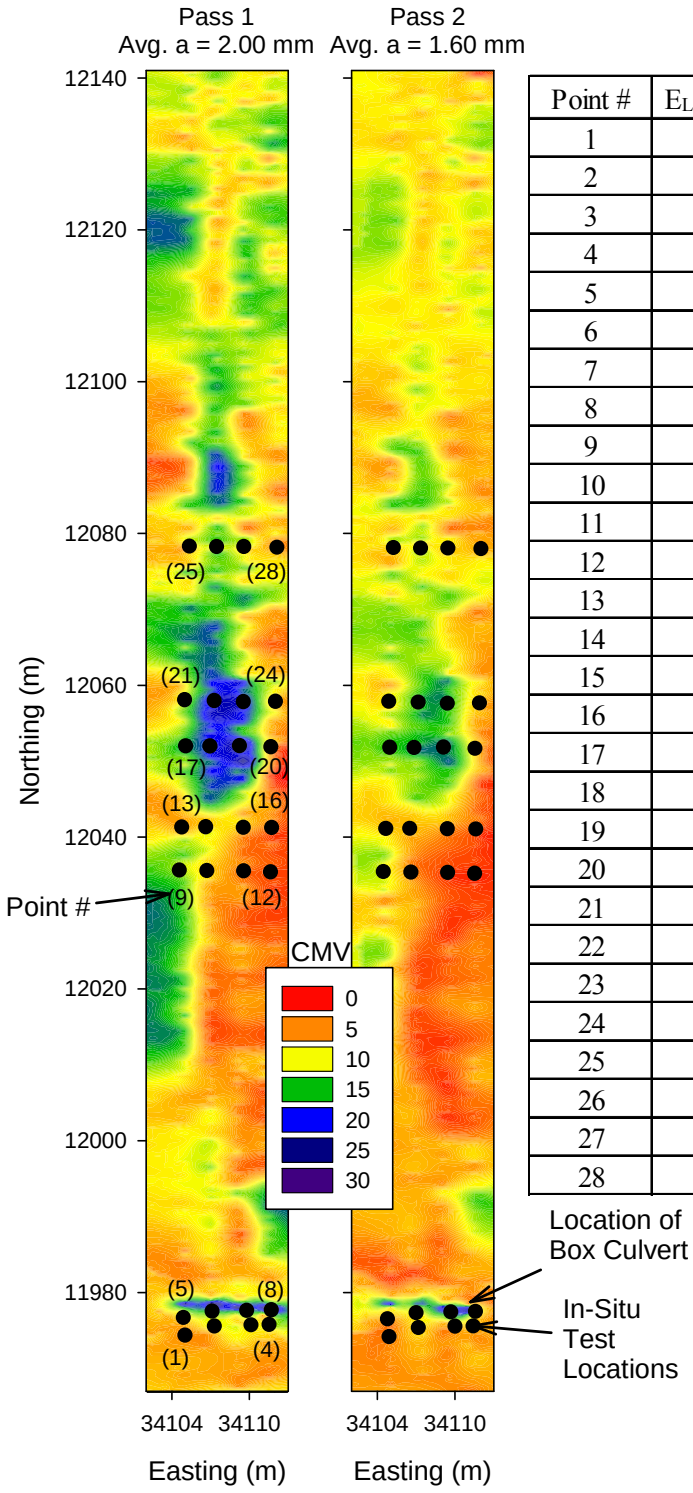

Point #	E_{LWD-Z3} (MPa)	γ_d (kN/m^3)	w (%)	CBR (%)
1	28.7	21.47	4.2	6.7
2	31.9	21.43	7.1	15.5
3	20.1	20.69	5.9	7.1
4	20.1	20.23	6.8	4.2
5	35.9	21.18	5	12.5
6	35.5	21.13	6.3	16.5
7	36.7	21.60	4.8	18.3
8	42.6	21.91	5.4	16.9
9	36.7	20.86	5.2	--
10	36.7	21.05	5.4	--
11	22.1	21.02	4.6	--
12	22.1	21.27	4.6	--
13	35.2	20.89	5.5	--
14	28.4	20.74	5.6	--
15	29.1	21.14	4.3	--
16	20.5	20.53	5.4	--
17	48.7	21.24	4.4	--
18	52.5	20.81	5.6	--
19	48.7	21.27	4.7	--
20	40.6	20.94	5.1	--
21	42.6	20.80	4.8	--
22	47.4	21.11	5.2	--
23	46.7	20.85	6.4	--
24	36.7	20.67	5.5	--
25	32.8	20.89	4.6	--
26	33.8	21.18	5.4	--
27	24.2	20.58	6.9	--
28	28.4	20.26	6.1	--

Figure 88. Spatial comparison of CMV maps obtained on TB11 (virgin special backfill subbase layer) using low and high amplitude settings and summary of in-situ point measurements

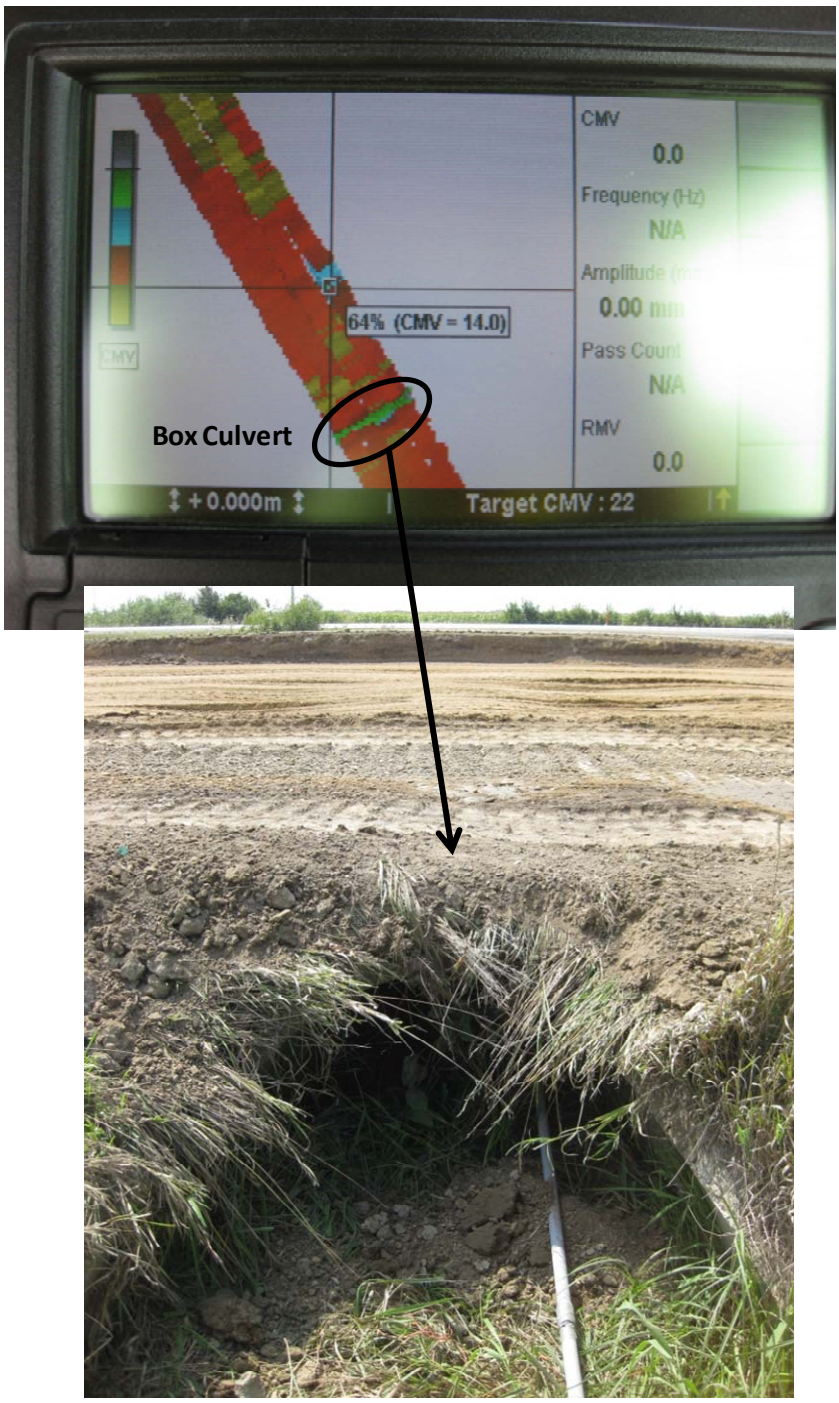

Figure 89. Box culvert location highlighted on AccuGrade display CMV map – TB11 RPCC base

Combined Regression Analysis

Data presented above captured IC-MVs and corresponding point-MVs over a wide measurement range. The data from multiple test beds are combined in this section to develop site wide correlation results. As discussed above, results from calibration test beds represented a narrow range of measurement values when data from each test bed is analyzed separately. Combining results should provide a perspective on more general trends and associated variability.

Relationships between CMV obtained in low amplitude setting (a = 1.60 mm) and point-MVs are presented in Figure 90. Relationships between CMV obtained in high amplitude setting (a = 1.60 mm) and point-MVs are presented in Figure 91. Non-linear exponential relationships showed the best fit for CMV vs. $E_{LWD\text{-}Z3}$ MVs with R^2 = 0.66 to 86. Relatively weak regression relationships with R^2 = 0.12 to 0.18 was observed for CMV vs. CBR. No statistically significant relationship was found for CMV vs. γ_d.

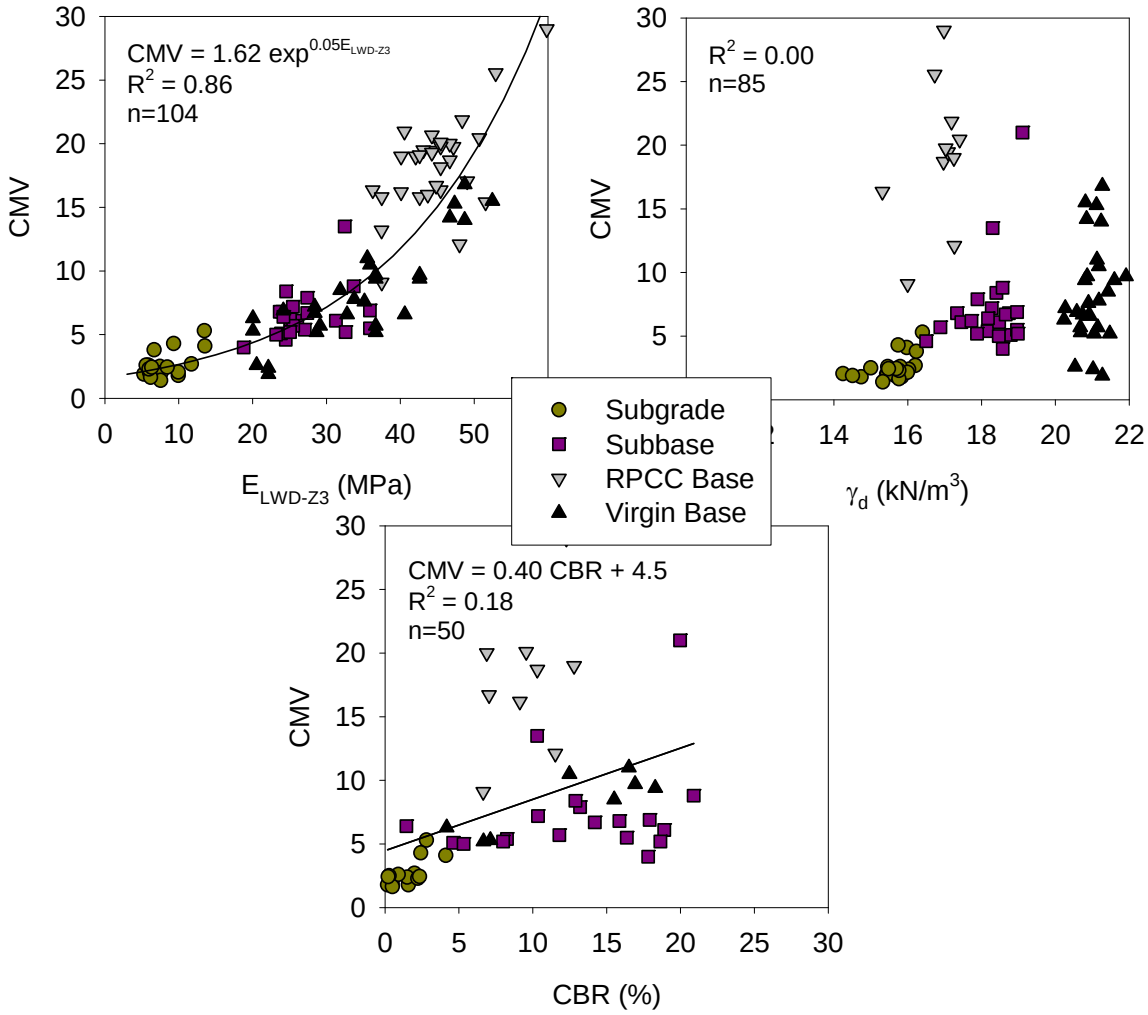

Figure 90. Empirical correlations between CMV and in-situ point measurements (a = 1.60 mm)

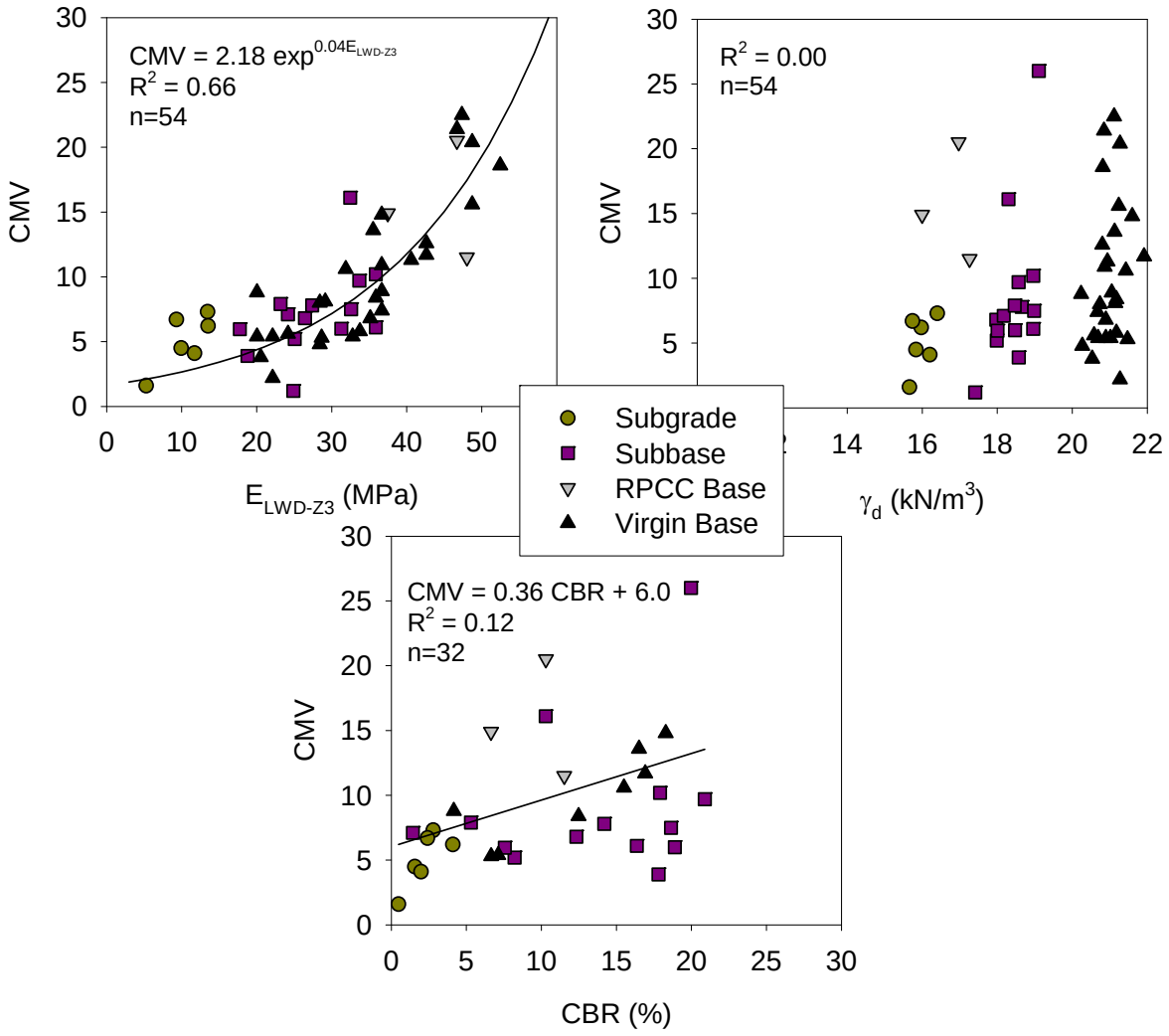

Figure 91. Empirical correlations between CMV and in-situ point measurements (a = 2.00 mm)

Repeatability Analysis

Error associated with repeatability of IC-MVs is believed to be one source of scatter in relationships with in-situ point-MVs. Repeatability measurement error refers to variation observed in the measurement values obtained over a test area from consecutive passes under identical operating conditions (i.e., using same operator, amplitude, speed, direction of travel, etc.). The repeatability measurement error is quantified in this section for CMV IC-MVs.

One challenge with evaluating repeatability of roller measurement values is that the data points obtained from different passes are not collected at the exact same location. To overcome this problem, the data was processed in such a way that an average data is assigned to a preset grid point along the roller path. The grid point was set at 0.3 m along the roller path which represented an average of IC-MVs that falls within a window of size 0.15 m in forward and backward directions (the actual data was reported every 0.15 to 0.3 m). This approach has been validated in previous case studies (see White et al. 2007, 2009). Following the same procedure,

roller data used for the analysis were filtered and organized using a customized VB program called as *IC-REPEAT* developed at Iowa State University.

Repeatability analysis was performed on measurements obtained from compaction passes subgrade (TB2), subbase (TB4), and base layer (TB9) test beds under identical operating conditions (i.e., same amplitude, nominal speed, and direction). Data filtered following the approach described above for selected roller passes is presented in Figure 92 to Figure 94. To account for change in soil properties with each pass, the effect of pass on CMV was considered in the analysis. This was accomplished by performing two-way analysis of variance (ANOVA), by taking both pass and measurement location as random effects (Vardeman and Jobe1999). The parameter of interest from this analysis is the root mean squared error ($\sqrt{MSE}$) which represents the measurement error. Detailed procedure for calculating the repeatability measurement error is provided in White et al. (2009). The CMV measurement error was about ≤ 1.1 for low amplitude settings at a nominal operation speed of about 4 km/h.

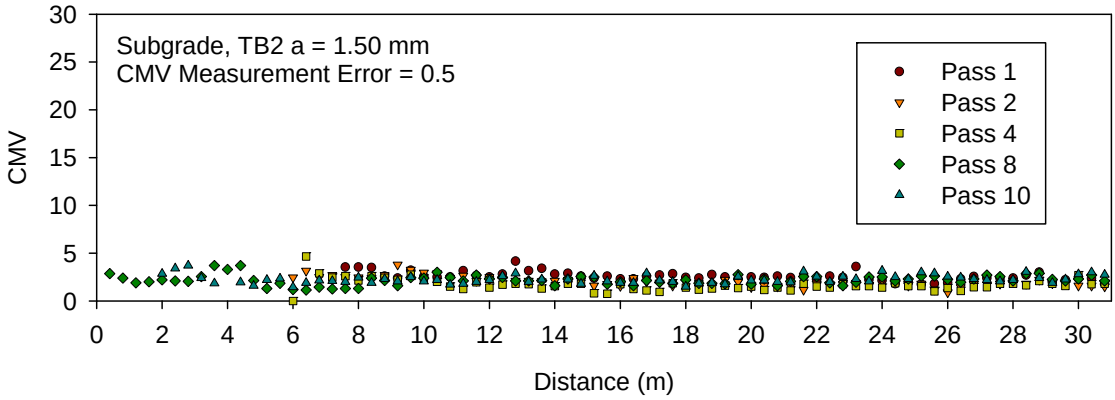

Figure 92. CMV measurements from multiple passes on TB2 subgrade

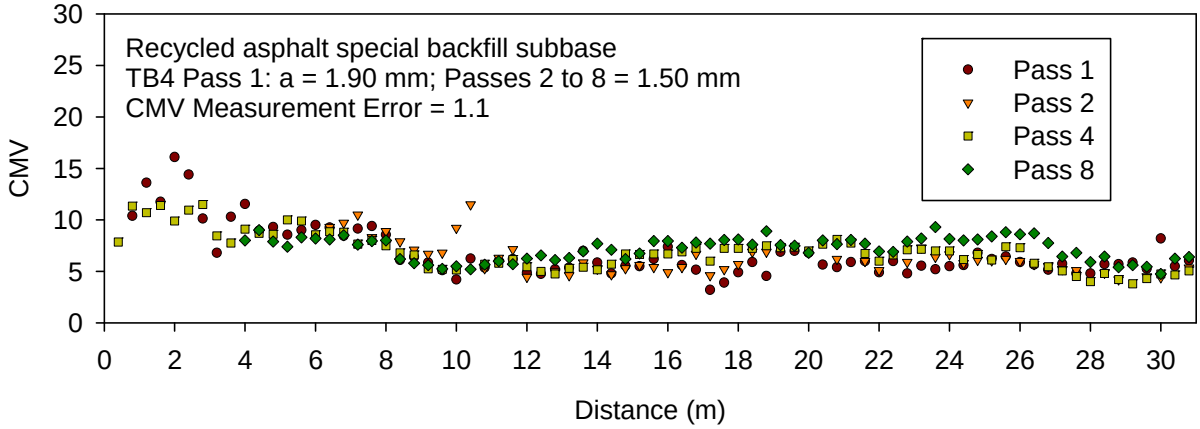

Figure 93. CMV measurements from multiple passes on TB4 subbase (note only passes 2 to 8 were used in the analysis - pass 1 was not included due to different amplitude setting)

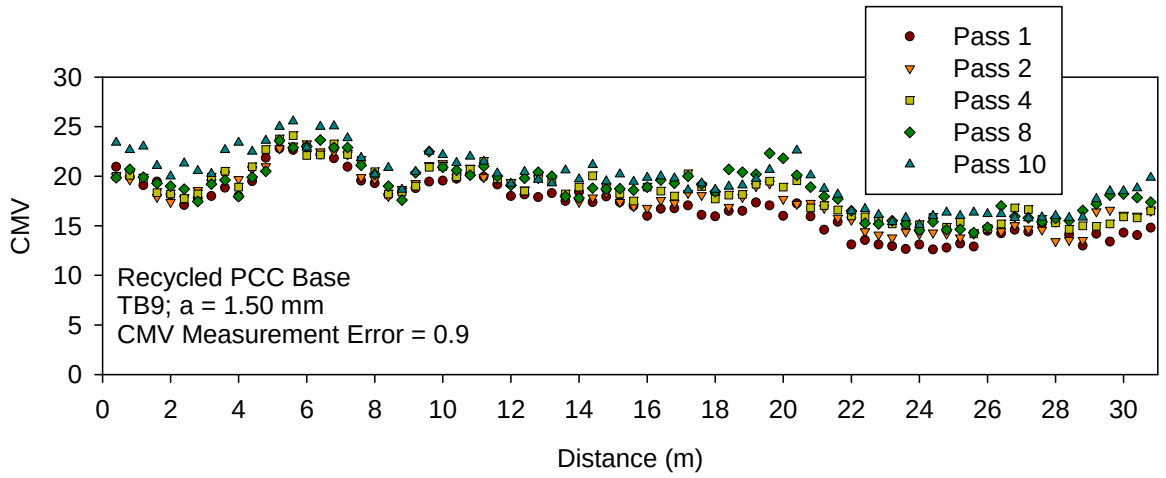

Figure 94. CMV measurements from multiple passes on TB9 base

Summary of Key Findings

Experimental test results and field observations from a demonstration project conducted on I-29 in Monona County, using a Volvo IC vibratory smooth drum roller equipped with CMV measurement system are presented above. The project involved construction of three calibration test beds and eight production area test beds. In summary, calibration test beds involved performing multiple roller passes over a one-dimensional test strip and obtaining in-situ point-MVs after intermediate passes to develop CMV and point-MV compaction curves, and data for correlation analysis. Production test beds involved mapping compacted subgrade, subbase, and base layer areas using low and high amplitude settings, and obtaining in-situ point-MVs at locations selected based on the CMV map on the on-board display. Data obtained from the production areas were used to assess the influence of amplitude on the CMV measurements and the correlations between CMV and point-MVs. Production area maps were obtained on subgrade and subbase layers in the same areas, and subbase and base layers in the same areas to assess the influence of the underlying layers on the surface layer CMV measurements. Multiple pass data obtained from the calibration test strips was used to assess the repeatability of the CMV IC-MVs. Following are some of the key findings from this project:

- Data from calibration strips indicated that the CMV, $E_{LWD\text{-}Z3}$, CBR, and γ_d measurements on the recycled HMA subbase layer were relatively higher than on the subgrade layer. The CMV and $E_{LWD\text{-}Z3}$ values on the RPCC base layer were higher than on the subbase layer. The γ_d measurements were slightly lower on the RPCC base layer than on the recycled HMA subbase layer.
- The average CMV values did not change much with increasing pass number on the subgrade (varied from 2 to 3) and recycled HMA subbase layers (varied from 6 to 8), but showed a slight increase (from about 17 to 20) on the RPCC base layer.
- The average $E_{LWD\text{-}Z3}$ values on the subgrade and subbase layers increased from pass 0 to 2 and then remained constant up to the final compaction pass. The average $E_{LWD\text{-}Z3}$ on the base layer increased from pass 0 to 1, remained constant up to pass 4, and then increased up to pass 10. The average γ_d on all three layers increased from pass 0 to 1 and then generally remained at the same level up to the final compaction pass.

- Correlations between CMV IC-MVs and point-MVs on calibration test strips generally showed weak correlations ($R^2 < 0.4$). The primary reason for weak correlations is the narrow range over which the measurements were obtained in each calibration test strip. Correlations developed by combining data from multiple test beds yielded non-linear exponential relationships between CMV and $E_{LWD\text{-}Z3}$ with $R^2 = 0.66$ and 0.86 for low and high amplitude settings, respectively. Relatively weak regression relationships with $R^2 < 0.2$ was observed between CMV and CBR. No statistically significant relationship was found between CMV and γ_d.
- Comparison of CMV IC-MV production area maps with in-situ point MVs obtained at selected locations generally indicate that relatively low, medium, and high CMV locations match with relatively low, medium, and high $E_{LWD\text{-}Z3}$ point-MVs and in some cases with CBR point-MVs. CMV maps obtained on special backfill subbase and the overlaid RPCC base layers indicate that "soft" and "stiff" zones in the subbase layer maps are reflected on the RPCC base layer maps.
- CMV maps were able to effectively delineate "soft" and "stiff" zones effectively. This was verified in a case of subbase layer over a concrete box culvert where CMV and in-situ point-MVs ($E_{LWD\text{-}Z3}$, CBR, and γ_d) were all relatively higher compared to measurements along the edge of the culvert with "soft" conditions.
- CMV measurements on the subgrade, subbase, and base layers were on average about 1.1 to 1.5 times greater in high amplitude setting (i.e., $a = 2.00$ mm) than in low amplitude setting (i.e., $a = 1.50$ mm). This is likely due to potential differences in the magnitude of stresses applied on the materials by the roller drum under different amplitude settings (Vennapusa et al. 2010b).
- The CMV measurement error was about ≤ 1.1 for low amplitude settings at a nominal operation speed of about 4 km/h.

CHAPTER 8: SUMMARY AND CONCLUSIONS

Results from three field demonstration projects conducted to evaluate three different IC measurement technologies (MDP, CMV, and CCV) on earthwork and HMA construction projects are presented in this report. Summary of key findings from each project are as follows:

US30 – Cohesive Fill Compaction Demonstration Project

Experimental test results and field observations from a demonstration project conducted on US30 near Colo, Iowa using Caterpillar IC padfoot roller equipped with MDP_{40} measurement system is presented above. The project involved construction and testing of on calibration test strip, two spatial areas, and one production test bed with multiple lifts wherein IC-MVs and in-situ point-MVs were obtained. Data obtained from each test bed was analyzed separately to develop correlations. In the end, data obtained from all the test beds were combined to develop site wide correlations over a wide measurement range. Following are some of the key findings from the analysis presented above.

- The moisture content of the subgrade materials was generally wet of optimum (about 5% wet of w_{opt}) and the relative compaction of the materials varied on average (per test bed) from 90% to 97% of standard Proctor γ_{dmax}. The material was in wet conditions due to frequent rain events at the time of project demonstration.
- MDP_{40} IC-MV compaction curves are affected by roller "off-tracking", i.e., roller operator not maintaining the same track as the previous pass.
- Spatial visualization of MDP_{40} IC-MV maps from multiple lifts in a production area (TB3) indicated that a "soft" zone with relatively low MDP_{40} values (< 70) on lift 1 reflected through the successive lifts 2, 3, 4, and 5 with similarly low MDP_{40} values in that zone. Geostatistical semivariogram analysis on MDP_{40} measurements on lifts 1 to 5 indicated that the variability reduced and the spatial continuity of the measurements improved from lifts 1 to 5 as demonstrated by a decrease in the sill and an increase in the range values.
- Regression analysis results indicated better correlations between MDP_{40} and $E_{LWD\text{-}Z3}$ and CBR_{300} point-MVs compared to γ_d measurements. Combining data from all test beds, MDP_{40} vs. $E_{LWD\text{-}Z3}$ and CBR_{300} yielded a non-linear power relationship with $R^2 > 0.50$. MDP vs. γ_d did not yield a statistically significant relationship. MDP_{40} measurements were somewhat sensitive to moisture content (MDP_{40} decreased with increasing w). Correlation between MDP_{40} and w yielded a linear relationship with $R^2 = 0.20$.
- Multivariate non-linear regression analysis was performed to assess the influence of including a moisture content parameter in predicting MDP_{40} from $E_{LWD\text{-}Z3}$ measurements. This analysis showed $R^2 = 0.71$, which is a slight improvement over the simple regression model without the moisture content parameter ($R^2 = 0.63$). Similar analysis was performed to predict MDP_{40} from CBR_{300} measurements, but it did not show any improvement in the R^2 value. MDP-γ_d dataset combined with moisture content did not show a statistically significant relationship.

IA218 – HMA Overlay Construction Demonstration Project

Experimental test results and field observations from a IC-HMA demonstration project on Highway 218 south of I-80 near Coralville, Iowa using a Sakai dual drum IC roller are presented above. The project involved compaction of HMA overlay over the existing PCC layer. The Sakai IC roller was used for HMA break down rolling along with another Sakai conventional break down roller. Main objectives of testing and data analysis on this project were to: (1) evaluate the impact of using real-time pass coverage information to the roller operator on the uniformity of the pass coverage achieved during compaction; (2) develop correlations between CCV IC-MVs and asphalt density (RC) and modulus ($E_{FWD\text{-}K3}$) point-MVs; and (3) evaluate the influence of temperature measurements on the correlations. Objective (1) was achieved by conducting a blind study on day 1 where the IC monitoring system was switched on but the on-board monitor was closed for viewing by the operator, and by allowing the operator to use the on-board monitor on days 2 and 3 to aid in uniform pass coverage. Objective (2) was achieved by obtaining spatially referenced (with GPS measurements) RC and $E_{FWD\text{-}K3}$ point-MVs at 50 test locations and pairing them with spatially nearest CCV IC-MVs to develop correlations. Objective (3) was achieved by obtaining temperature measurements at each in-situ point-MV location and conducting statistical analysis. Following are the key findings from the results and data analysis from this project:

- Univariate statistics (mean and standard deviation) of pass count information on each day did not reveal any differences between day 1 (blind study) and days 2 and 3. Geostatistical semivariogram analysis of pass count information revealed quantitative evidence of improved uniformity in pass coverage on day 3 compared to on day 1.
- The temperature of HMA on the shoulder lane was on average about 19^{o}F warmer than the temperature of the HMA on the mainline. The RC of the HMA layer was on average about 6% lower on the shoulder compared to the mainline. These differences in temperature and RC measurements are attributed to greater HMA layer thickness on the shoulder lane than on the mainline.
- $E_{FWD\text{-}K3}$ point-MVs and CCV IC-MVs obtained over a stretch of about 1.3 km showed that the measurements on the shoulder lane were lower than on the mainline. This is likely because of potentially weaker support conditions under the shoulder lane compared to the mainline.
- Correlation between CCV and $E_{FWD\text{-}K3}$ showed a relatively strong linear regression relationship with $R^2 = 0.8$ compared to correlation between CCV and RC with $R^2 = 0.4$. This should be expected as CCV is a result of drum response under loading which is a measure of material stiffness and not necessarily related to the density of the material. The regression relationships are influenced by differences in underlying support conditions as it was clearly reflected with data groupings (with separate groups for shoulder lane and mainline measurements) in the correlations. Data analysis indicated that the CCV, RC, and $E_{FWD\text{-}K3}$ measurements are influenced by temperature.

I-29 – Pavement Foundation Layer Construction Demonstration Project

Experimental test results and field observations from a demonstration project conducted on I-29 in Monona County, using Volvo IC vibratory smooth drum roller equipped with CMV

measurement system are presented above. The project involved construction of three calibration test beds and eight production area test beds. Data from calibration test beds was used to develop CMV and point-MV compaction curves and correlation analysis. Data obtained from the production areas were used to assess the influence of amplitude and underlying layer support conditions on the CMV measurements and the correlations between CMV and point-MVs. Multiple pass data obtained from the calibration test strips was used to assess the repeatability of the CMV IC-MVs. Following are some of the key findings from this project:

- Data from calibration strips indicated that the CMV, $E_{LWD\text{-}Z3}$, CBR, and γ_d measurements on the recycled HMA subbase layer were relatively higher than on the subgrade layer. The CMV and $E_{LWD\text{-}Z3}$ values on the RPCC base layer were relatively higher than on the subbase layer. The γ_d measurements were slightly lower on the RPCC base layer than on the recycled HMA subbase layer.
- The average CMV values did not change much with increasing pass number on the subgrade (varied from 2 to 3) and recycled HMA subbase layers (varied from 6 to 8), but showed a slight increase (from about 17 to 20) on the RPCC base layer.
- The average $E_{LWD\text{-}Z3}$ values on the subgrade and subbase layers increased from pass 0 to 2 and then remained constant up to the final compaction pass. The average $E_{LWD\text{-}Z3}$ on the base layer increased from pass 0 to 1, remained constant up to pass 4, and then increased up to pass 10. The average γ_d on all three layers increased from pass 0 to 1 and then generally remained at the same level up to the compaction pass.
- Correlations between CMV IC-MVs and point-MVs on calibration test strips generally showed weak correlations ($R^2 < 0.4$). Primary reason for such weak correlations is the narrow range over which the measurements were obtained in each calibration test strip. Correlations developed by combining data from multiple test beds yielded non-linear exponential relationships between CMV and $E_{LWD\text{-}Z3}$ with $R^2 = 0.66$ and 0.86 for low and high amplitude settings, respectively. Relatively weak regression relationships with $R^2 < 0.2$ was observed between CMV and CBR. No statistically significant relationship was found between CMV and γ_d.
- Comparison of CMV IC-MV production area maps with in-situ point MVs obtained at selected locations generally indicate that relatively low, medium, and high CMV locations match with relatively low, medium, and high $E_{LWD\text{-}Z3}$ point-MVs and in some cases with CBR point-MVs. CMV maps obtained on special backfill subbase and the overlaid RPCC base layers indicate that "soft" and "stiff" zones in the subbase layer maps are reflected on the RPCC base layer maps.
- CMV maps were able to effectively delineate "soft" and "stiff" zones effectively. This was verified in a case of subbase layer over a concrete box culvert where CMV and in-situ point-MVs ($E_{LWD\text{-}Z3}$, CBR, and γ_d) were all relatively higher compared to measurements along the edge of the culvert with "soft" conditions.
- CMV measurements on the subgrade, subbase, and base layers were on average about 1.1 to 1.5 times greater in high amplitude setting (i.e., $a = 2.00$ mm) than in low amplitude setting (i.e., $a = 1.50$ mm). This is likely due to potential differences in the magnitude of stresses applied on the materials by the roller drum under different amplitude settings (Vennapusa et al. 2010b).
- The CMV measurement error was about ≤ 1.1 for low amplitude settings at a nominal operation speed of about 4 km/h.

REFERENCES

ASTM D6951. (2003). "Standard test method for use of the dynamic cone penetrometer in shallow pavement application." American Standards for Testing Methods (ASTM), West Conshohocken, Pennsylvania.

ATB Väg. (2004). "Kapitel E - Obundna material VV Publikation 2004:111," *General technical construction specification for roads,* Road and Traffic Division, Sweden.

Brandl, H., and Adam, D. (1997). "Sophisticated continuous compaction control of soils and granular materials." *Proc. 14th Intl. Conf. Soil Mech. and Found. Engrg.*, Hamburg, Germany, 1–6.

Clark, I., and Harper, W. (2002). *Practical geostatistics 2000*. 3rd reprint, Ecosse North America Llc, Columbus, Ohio.

Floss, R., Gruber, N., Obermayer, J. (1983). "A dynamical test method for continuous compaction control." *Proc. 8th European Conf. on Soil Mech. and Found. Engg,* H.G. Rathmayer and K. Saari, eds., May, Helsinki, 25-30.

Humboldt. (2006). *Humboldt radiation safety training class.* Humboldt Scientific, Inc., Raleigh, NC.

Isaaks, E. H., and Srivastava, R. M. (1989). *An introduction to applied geostatistics*. Oxford University Press, New York.

ISSMGE. (2005). *Roller-Integrated continuous compaction control (CCC): Technical Contractual Provisions, Recommendations*, TC3: Geotechnics for Pavements in Transportation Infrastructure. International Society for Soil Mechanics and Geotechnical Engineering.

Mn/DOT. (2007a). *Excavation and embankment – (QC/QA) IC quality compaction (2105) pilot specification for granular treatment S.P.0301-47*. Minnesota Department of Transportation, St. Paul, Mn.

Mn/DOT. (2007b). *Excavation and embankment – (QC/QA) IC quality compaction (2105) pilot specification for non-granular soils S.P.6211-81*. Minnesota Department of Transportation, St. Paul, Mn.

Newman, K., and White, D. (2008). "Rapid assessment of cement/fiber stabilized soil using roller-integrated compaction monitoring." *Transportation Research Record*, 2059, 95-102.

RVS 8S.02.6. (1999). "Continuous compactor integrated compaction – Proof (proof of compaction)," *Technical Contract Stipulations RVS 8S.02.6 – Earthworks,* Federal Ministry for Economic Affairs, Vienna.

Samaras, A.A., Lamm, R., Treiterer, J. (1991). "Application of continuous dynamic compaction control for earthworks in railroad construction." *Transp. Res. Rec.,* 1309, Journal of the Transportation Research Board, Washington, D.C., 42–46.
Sandström, Å. (1994). *Numerical simulation of a vibratory roller on cohesionless soil,* Internal Report, Geodynamik, Stockholm, Sweden.

Sandström Å., and Pettersson, C. B., (2004). "Intelligent systems for QA/QC in soil compaction", *Proc. TRB 2004 Annual Meeting* (CD-ROM), Transportation Research Board, Washington, D. C.

Scherocman, J., Rakowski, S., and Uchiyama, K. (2007). "Intelligent compaction, does it exist?" 2007 *Canadian Technical Asphalt Association (CTAA) Conference,* Victoria, BC, July.

Thurner, H. and Sandström, Å. (1980) "A new device for instant compaction control," *Proc., International Conference on Compaction*, Vol II, 611–614, Paris.

Thompson, M., and White, D. (2008). "Estimating compaction of cohesive soils from machine drive power." *J. of Geotech. and Geoenv. Engrg.,* ASCE, 134(12), 1771-1777.

Vennapusa, P., and White, D. J. (2009). "Comparison of light weight deflectometer measurements for pavement foundation materials." *Geotech.Test. J.*, ASTM, 32(3), 239-251.

Vennapusa, P., White, D.J., Morris, M. (2010a). "Geostatistical analysis for spatially referenced roller-integrated compaction measurements, *J. of Geotech. and Geoenv. Engrg.,* ASCE, 136 (6), 813-821.

Vennapusa, P., White, D.J., Siekmeier, J., Embacher, R. (2010b). "In situ mechanistic characterizations of granular pavement foundation layers." *Intl. J. of Pavement Engineering* (in review).

White, D.J. (2008). *Report of the workshop on intelligent compaction for soils and HMA.* Earthworks Engineering Research Center, Iowa State University, Ames, Iowa, 2-4 April.

White, D.J., and Thompson, M. (2008). Relationships between in situ and roller-integrated compaction measurements for granular soils. *J. of Geotech. and Geoenv. Engrg.,* ASCE, 134(2), 1763-1770.

White, D.J., and Vennapusa, P. (2009). R*eport of the Workshop on Intelligent Technologies for Earthworks*, EERC Publication ER09-02, Earthworks Engineering Research Center, Iowa State University, Ames, Iowa.

White, D.J., and Vennapusa, P. (2010). R*eport of the Workshop on Intelligent Technologies for Earthworks*, EERC Publication ER09-02, Earthworks Engineering Research Center, Iowa State University, Ames, Iowa.

White, D. J., Jaselskis, E., Schaefer, V., Cackler, T. (2005). "Real-time compaction monitoring in cohesive soils from machine response." *Transp. Res. Rec., 1936*, Journal of the Transportation Research Board, Washington D.C., 173–180.

White, D.J, Thompson, M., Vennapusa, P. (2007). *Field study of compaction monitoring systems: self-propelled non-vibratory 825G and vibratory smooth drum CS-533 E rollers,* Final Report, Center of Transportation Research and Education, Iowa State University, Ames, Ia.

White, D., Vennapusa, P., Gieselman, H. (2008). "Roller-integrated compaction monitoring technology: Field evaluation, spatial visualization, and specifications." *Proc., 12th Intl. Conf. of Intl. Assoc. for Computer Methods and Advances in Geomechanics (IACMAG),* 1-6 October, Goa, India.

White, D.J., Vennapusa, P., Zhang, J., Gieselman, H., Morris, M. (2009). *Implementation of Intelligent Compaction Performance Based Specifications in Minnesota*, EERC Publication ER09-03, MN/RC 2009-14, Minnesota Department of Transportation, St. Paul, Minnesota, March.

Zorn, G. (2003). *Operating manual: Light drop-weight tester ZFG2000*, Zorn Stendal, Germany.

ZTVE-StB. (1994). "Flächendeckende dynamische Prüfung der Verdichtung, " *Technische Prüfvorschriften für Boden und Fels im Straßenbau*, FGSV-Nr 599, FGSV Verlag GmbH, Köln (in German).